Syracuse University
SURFACE at Syracuse University

Dissertations - ALL | SURFACE at Syracuse University

Summer 7-16-2021

Eccentricity of Merging Neutron Star Binaries: Searches, Parameter Estimation, and Future Prospects

Amber Kiana Lenon
Syracuse University

Follow this and additional works at: https://surface.syr.edu/etd

 Part of the Astrophysics and Astronomy Commons, and the Physics Commons

Recommended Citation

Lenon, Amber Kiana, "Eccentricity of Merging Neutron Star Binaries: Searches, Parameter Estimation, and Future Prospects" (2021). *Dissertations - ALL*. 1463.
https://surface.syr.edu/etd/1463

This Dissertation is brought to you for free and open access by the SURFACE at Syracuse University at SURFACE at Syracuse University. It has been accepted for inclusion in Dissertations - ALL by an authorized administrator of SURFACE at Syracuse University. For more information, please contact surface@syr.edu.

ABSTRACT

Since the start of the first observing run the Advanced Laser Interferometer Gravitational-Wave Observatory (LIGO) and the Advanced Virgo observatory have detected 48 binary black hole mergers and two binary neutron star mergers. Knowledge about the properties of the binary can be gained from the gravitational-wave observations. Binary neutron star systems can form with significant orbital eccentricity. Gravitational radiation efficiently removes this eccentricity from the binary's orbit as the star's inspiral together. This thesis describes a search for neutron star binaries that have an eccentric orbits when their gravitational waves enter the sensitive band of Advanced LIGO and Virgo. For the detected binary neutron star mergers GW170817 and GW190425, Bayesian parameters estomation is used to constrain the binary's orbital eccentricity. Finally, we consider the prospects of Cosmic Explorer, a planned third-generation gravitational-wave observatory, to detected eccentric binary neutron stars and measure their eccentricity. This analysis has important implications for the computational cost of the search for binaries in quasi-circular orbits with Cosmic Explorer.

ECCENTRICITY OF MERGING NEUTRON STAR BINARIES: SEARCHES, PARAMETER ESTIMATION, AND FUTURE PROSPECTS

By

Amber K. Lenon

BSc., Syracuse University, Syracuse, New York
MSc., West Virginia University, Morgantown, West Virginia

Dissertation
Submitted in Partial Fulfillment of the Requirements
for the degree of
Doctor of Philosophy in Physics

Syracuse University
July 2021

Copyright © Amber K. Lenon 2021
All rights reserved.

ACKNOWLEDGEMENTS

I would like to express my heartfelt thanks to Duncan Brown–I am incredibly lucky to have met an advisor like him. He has been a huge source of inspiration in both my undergraduate and graduate years, as an amazing scientist and an excellent mentor. I have benefited tremendously from his advice as well as his extensive knowledge about gravitational-wave astronomy. Under his guidance I have learned how to become an independent researcher and how to manage my off time when I'm not doing research. I am grateful to have had an advisor like Duncan.

I am fortunate and grateful to have had the opportunity to collaborate with Alex Nitz on the work presented in Chapters 3–5. His knowledge is invaluable and I am thankful that I was able to learn so much from him.

While I wasn't able to be at Syracuse in person I thank everyone in the gravitational-wave group for making my experience welcoming and engaging. I am thankful to have learned so much about other aspects of the research being conducted in the group. Thank you to Daniel Finstad, Erick Leon, and Soumi De for the help and contributions that have been vital to my research.

To my friends–Sam Usman, Belinda Cheeseboro, Dave Caron, Jaysin Lord, Esraa Ahmad, and Greg Walsh–thank you for all of the support and fun. I would like to thank Sam Usman for the hours long phone calls and amazing advice. I would like to thank Belinda Cheeseboro for being there for me at each road block and for all the laughs. I would like to thank Dave Caron for letting me spend countless hours in his office working. I would like to thank Jaysin Lord and Greg Walsh for their continuous support and belief in me. I would like to thank Esraa Ahmad for being there for me and comforting me when things got tough.

Thanks to the West Virginia University friends for all of your support, laughs, and fun chats. Thank you to Cindy Ramsey, Jim Adams, and the Mountaineer United Soccer Club for your support and for reintroducing me to soccer. I really appreciate the outlet for my stress and the joy that I experience when I play. Thank you to the VanguardSTEM team for all of your amazing advice, support, encouraging me, and giving me a space for me to be unapologetically me. The community that I gained through VanguardSTEM has continuously inspired me throughout my journey.

I would like to thank my defense committee members–Duncan Brown, Stefan Ballmer, Lisa Manning, Jay Hubisz, Alex Nitz, and Natalie Russo–for taking the time to review and critique this dissertation. For my graduate school research, I would thankfully like to acknowledge support from the NSF award AST-1559694 and the Chancellor's Scholars Program.

Finally, I would like to thank my family–my mom and brothers–to whom this dissertation is dedicated. I thank my brothers, Collin and Jace, and cousin, Zach for our countless hours of DnD, video games, and joking my graduate career to decompress from weeks of hard work.

Contents

List of Tables

List of Figures

Preface

Chapter 3 is based on material from:
Alexander H. Nitz, *Amber Lenon*, Duncan A. Brown, "Search for Eccentric Binary Neutron Star Mergers in the first and second observing runs of Advanced LIGO," **The Astrophysical Journal, Volume 890, Number 1 (2019)**
https://iopscience.iop.org/article/10.3847/1538-4357/ab6611

Chapter 4 is based on material from:
Amber Lenon, Alexander H. Nitz, Duncan A. Brown, "Measuring the Eccentricity of GW170817 and GW190425" **Monthly Notices of the Royal Astronomical Society, Volume 497, Issue 2, September 2020, Pages 1966–1971**
https://doi.org/10.1093/mnras/staa2120.

Chapter 5 is based on material from:
Amber Lenon, Duncan A. Brown, Alexander H. Nitz, "Eccentric Binary Neutron Star Search Prospects for Cosmic Explorer" (2021). This work has been submitted for publication in the *American Physical Society Physical Review D*. A pre-print is available online at https://arxiv.org/abs/2103.14088.

To Mom, Collin, & Jace

Chapter 1

Introduction

In 1915 Albert Einstein published the theory of general relativity which describes gravity as the curvature of four-dimensional spacetime. General relativity predicts the existence of gravitational radiation. Gravitational waves travel at the speed of light, carrying energy and information about the sources that generate them. Sources of gravitational waves include: core collapse supernova, compact-object binary inspirals, the gravitational-wave stochastic background, and isolated neutron stars. In this thesis we will focus on gravitational waves from binary neutron stars. As the neutron stars orbit around each other, they lose energy due to gravitational-wave emission causing their orbit to shrink and the neutron stars to merge. The Hulse-Taylor binary [6] indirectly confirmed the existence of gravitational waves. In 1988, Driever, Weiss, and Thorne proposed the construction of the Laser Interferometer Gravitational-wave Observatort (LIGO), a ground-based interferometer to directly detect gravitational waves, test Einstein's theory, and study the properties of gravitational-wave sources. The first-generation LIGO [7] detectors began searching for gravitational waves in 2002. The second-generation Advanced LIGO [8] and Advanced Virgo [9] detectors made the first direct detection of gravitational waves in 2015, the first detection of a binary neutron star merger in 2017, and to date have completed three observing runs and detected fifty gravitational wave signals from the merger of compact-object binaries. Planning is underway for the construction of a third-generation U.S. gravitational-wave observatory known as Cosmic Explorer; this detector will have an order of magnitude better sensitivity that Advanced LIGO and will see binary black holes to the edge of the visible universe.

Advanced LIGO detected the first gravitational wave signal from a binary black hole merger, GW150914 [10], during its first observing run. Two more binary black hole mergers were detected soon after in the same observing run [11, 12]. The first binary neutron star inspiral, GW170817 [4], was detected during the second observing run. In addition to the gravitational-wave detection, the merger was observed across the full electromagnetic spectrum [13], making it the first multi-messenger gravitational-wave detection and contributed to answering outstanding questions in physics such as the origin of short gamma-ray bursts, the nature of kilonovae, and the creation of the r-process elements. Seven binary black hole detections were also made in the second observing run on top of the binary neutron star detection [14, 15, 16, 17]. In the third observing run 39 additional detections were confirmed [18] with one binary neutron star merger [19], 36 binary black hole mergers [18, 20, 21], and the first black hole compact object merger, where the compact object could be a highest mass neutron star or a lowest mass black hole ever discovered [22]. With the gravitational-wave detections being made by Advanced LIGO and Virgo becoming regular, we have the ability to answer exciting questions about binary physics and the formation of these compact object binaries. In this thesis we study the detection and measurement of eccentric binary neutron stars and the use of eccentricity to make inferences the formation channel of the binary.

1.1 Eccentricity

The Hulse-Taylor binary was discovered in 1974 [6] and is composed of a neutron star and a pulsar with an eccentricity of $e = 0.615$ and a period of 7.75 hours. It was the first binary pulsar discovered and led to a Nobel prize for Hulse and Taylor [23]. As a binary emits gravitational waves orbital energy is lost which causes a decrease in the binary's orbital period [24, 25]. After thirty years of observations the decay in orbital period of the Hulse-Taylor binary was measured and found to be consistent with the emission of gravitational waves [26]. Sixteen additional double neutron star systems have been observed through radio surveys of the Milky Way field [27, 28, 29, 30, 31] with eccentricities varying from 0.06 to 0.828 [32, 33]. As the orbit of a binary neutron star evolves, the orbital eccentricity of the binary will decrease [25]. Eccentricity is radiated away very efficiently causing the binary to circularize. Given

the significant time to merger of the binary like the Hulse-Taylor pulsar, by the time that the gravitational waves enter the LIGO-Virgo band, the binary's orbit will have circularized. However, formation channels have been proposed in which binaries may still have residual eccentricity when they enter the LIGO-Virgo band.

Eccentricity describes how much an object's orbit deviates from a circle as seen in Fig. 1. The shape and motion of an object in an elliptical orbit can be described by Kepler's first law

$$r(\theta) = \frac{a(1-e^2)}{1-e\cos(\theta)}, \tag{1.1}$$

where $r(\theta)$ is the position of a particle in the orbit assuming the origin is at one foci of the ellipse, a is the semimajor axis, e is the eccentricity, and θ is the true anomaly. The true anomaly is an angular parameter that defines the position of a particle moving along a Keplerian orbit. The angle defined is the angle between the closest point to the body that is being orbited and the current position of the particle in its orbit.

In the Newtonian description of gravity, a stars have closed orbits around their center of mass with the motion described by Kepler's laws. This Newtonian description is valid in the slow motion and weak gravitational-field limit. For example, it does not accurately describe the perihelion precession of Mercury. Einstein's theory of general relativity, however, accurately predicts the precession of Mercury and also predicts the orbital decay of a binary as it radiates gravitational waves.

As compact objects orbit around each other they emit gravitational waves. Binaries without eccentricity evolve in a sequence of circular orbits where the frequency and amplitude are monotonically increasing as the stars inspiral together. However, binaries with eccentricity have weaker gravitational wave emission when the compact objects are far apart and a stronger emission when the compact objects are close. This emission of gravitational waves in binaries with eccentricity will cause the orbit of the binary to become smaller and more circular. In most cases as gravitational waves are emitted the binary the binary loses energy and angular momentum. In the case of eccentric binaries, the semi-major axis and eccentricity also decay over time. The orbital decay for an eccentric binary system is described in Sec. 2.1 and in Refs. [24, 25].

Gravitational waves can be detected in searches with ground based detectors. For

systems that have circularized eccentricity can be neglected. However, this means that binaries with residual eccentricity may be missed. Even though a binary system may be detected by a search that neglects eccentricity, the system may have residual eccentricity that can be measured. Parameter estimation can be used to measure or place an upper limit on the eccentricity of the binary. The Hulse-Taylor binary had a significant amount of eccentricity $e = 0.615$ and a short orbital period [6] during its discovery. As a results of the high eccentricity and short orbital period suggestions about the formation of the binary have been made [34, 35]. Depending on the detected or measured eccentricity of the binary we can gain knowledge about the formation of the binary.

1.2 Gravitational-wave Detectors

Advanced LIGO [8] and Advanced Virgo [9] are gravitational-wave detectors with 4 km long arms in a worldwide detector network. The Advanced LIGO detectors are located in Hanford, Washington and Livingston, Louisiana, while the Virgo detector is located in Pisa, Italy. These detectors are Michelson interferometers with a Fabry-Perot cavity in each arm to build up the phase introduced by a change in the length of the arms. When a gravitational-wave passes through the detectors, there will be a small change in the light travel time in the arms. The change in the arms is measured as a phase difference over a period of time and from that a gravitational-wave signal can be measured. The lower frequency sensitivity limit on the Advanced LIGO and Virgo detectors are 10 Hz and the detectors are sensitive to sources in the 10-1000 Hz band of the gravitational-wave spectrum.

The strain sensitivity of the detectors is the strain, h, a source must have at a specific frequency to detectable. As a gravitational wave travels away from the binary system it will cause space-time to be stretched and squeezed. A gravitational wave with stain amplitude, h, will change the length of the arms ΔL as it passes through a detector with arms of length, L, and can be written as

$$h \sim \frac{\Delta L}{L}. \tag{1.2}$$

The sensitivity of the detectors or noise floor is determined by environmental, thermal, quantum, and other noise sources [36]. Environmental noise included seismic motion

and acoustic and magnetic noises. The thermal noise is determined by set parameters in the interferometer, such as beam size and material properties. The quantum noise is dependent on the input laser power and the signal recycling mirror transmission. The signal recycling mirror reflects the light back into the detector [37]. The next stage of proposed detector upgrades to Advanced LIGO is referred to as A+ which will further increase the sensitivity of the LIGO detectors [38].

Future gravitational-wave detectors, like Cosmic Explorer [2] and Einstein Telescope [1], have been proposed. We will focus on Cosmic Explorer in this thesis. Cosmic Explorer is a two-stage ground based gravitational-wave detector with 40 km arms that improves on the Advanced LIGO design. Since the arms of Cosmic Explorer are 10 times as long as that of Advanced LIGO and Advanced Virgo, the detector will be 10 times more sensitivity as shown by Eq. 1.2 In the first stage (CE1) the detector will scale up current Advanced LIGO technology to create a detector with arms that are close to the wavelength of a gravitational-wave signal. The second stage (CE2) upgrades the optics of the detector achieve an order of magnitude sensitivity beyond that of Advanced LIGO [39]. The low-frequency sensitivity limit of Cosmic Explorer is expected to be a factor of two smaller than that of Advanced LIGO, pushing the limit from 10 Hz to 5 Hz as can be seen in Fig. 2. Cosmic Explorer will also be sensitive to sources in the 5-4000 Hz band of the gravitational-wave spectrum.

The last stage of detector upgrades, A+, is expected to be able to detect binary neutron star mergers out to a distance of 330 Mpc and Virgo is expected to have a distance of $150 - 260$ Mpc at design sensitivity [40]. Cosmic Explorer is expected to be able to detect binary neutron star mergers out to a distance of ~ 2 Gpc. The addition of another detector to the detector network would significantly improve the ability to determine a location of a detection in the sky.

1.3 Formation of Compact Object Binary Sources

The compact object mergers that Advanced LIGO and Virgo observe are the last stage in the evolution of massive compact object binary systems. Unfortunately the formation of these binaries is difficult to discern. Typically binaries form either in the plane of the galaxy, or field, [41, 42, 43, 44, 45, 46, 47, 33, 48, 49, 28, 50], where two stars that are born together and their evolution is solely dependent on the interactions

between the components, or in dynamical environments [51, 52, 53, 54, 55, 56, 57, 58, 59, 60, 61, 62, 63], where the interactions in dense stellar environments are crucial to the evolution of the binary. Most binaries are expected to have formed in the field and will have eccentricity $e \leq 10^{-4}$ by the time they merge [25, 64, 49] making them detectable by matched-filter searches that neglect eccentricity [65, 66, 67, 68]. However, binaries formed in dynamical environments may retain residual eccentricity $e \geq 0.1$ when they enter the LIGO-Virgo band [57, 51, 59, 60, 61, 62, 63].

Binaries in the field typically decrease the separation of their orbit due to the common envelope phase [69] in the evolution of the binary. When a binary undergoes the common envelope phase, the more massive star, primary star, leaves the main sequence phase and rapidly expands. Once the radius crosses the Roche Lobe radius it transfers mass to the less massive star, secondary star, that is still in the main sequence phase. Once mass transfer ends the massive star loses its hydrogen envelope, turns into a helium burning core and eventually goes through a core-collapse supernova explosion to end up a compact object, either a black hole or neutron star. Once the primary star has become a compact object, the secondary star eventually leaves its main sequence phase and the secondary star goes through the same process as the primary. The mass transfer of the secondary star is unstable, which results in the two stars evolving in a shared envelope. This causes the compact object to spiral into the dense stellar environment shrinking the orbit of the binary [69, 70]. There are two usual outcomes after the inspiral phase of the binary. The envelope could get ejected due to a deposit of orbital energy which would leave a binary composed of the secondary star and a compact object. Once the secondary star undergoes a supernova explosion it will collapse to a black hole. If the system survives the explosion a close compact object binary is formed which emits gravitational waves in the LIGO-Virgo band and merges within the lifetime of the universe. If the envelope is not ejected, the compact object and companion star could merge and become a single compact object.

Binaries that form dynamically interact with stars or compact objects in dense stellar environments, like globular clusters or galactic nuclei. One such method is when binaries shrink their orbits and merge due to three or four-body interactions with other stars, typically called gravitational-wave captures. During the three or four-body interactions there is a release of strong gravitational-wave emission that

brings the orbit closer to merger. A specific example of a three-body interaction is called an exchange encounter [71, 53]. In an exchange encounter an existing binary will undergo interactions with a third star or compact object. The interactions will cause one of the components in the binary to be thrown out and replaced by third star or object [72]. These binaries may still have significant residual eccentricity when their gravitational waves enter the LIGO-Virgo band. Measurements of the eccentricity of the two binary neutron star mergers, GW170817 and GW190425, were made. Based on the upper limit estimates of their eccentricity the binaries were most likely formed in the field (see Sec. 4 for detail).

In Chapter 3, we describe the results of a search for eccentric binary neutron star mergers. We used matched filtering methods and waveforms that model the gravitational waves from low eccentricity systems to detect potential gravitational-wave signals in the first and second observing runs of Advanced LIGO and Virgo. We use the results of search to place an upper limit on the binary neutron star merger rate and determine how many years of data would be needed to constrain current binary neutron star merger rates. In Chapter 4, we use Bayesian parameter estimation in the PyCBC Inference [73] toolkit to measure parameters of interest of the two binary neutron star mergers from the first and second observing runs. This study concentrated on measuring the eccentricity of the two detections using full parameter estimation and compared that with similar work done for a binary neutron star detection. In Chapter 5, we determine Cosmic Explorer's ability to detect and measure the eccentricity of eccentric gravitational-wave signals. We non-eccentric and eccentric template banks as well as simulations of eccentric signals to determine the eccentricity that Cosmic Explorer will be sensitive to in searches and parameter estimation. We also determine the computational cost of a search in Cosmic Explorer compared to previous searches.

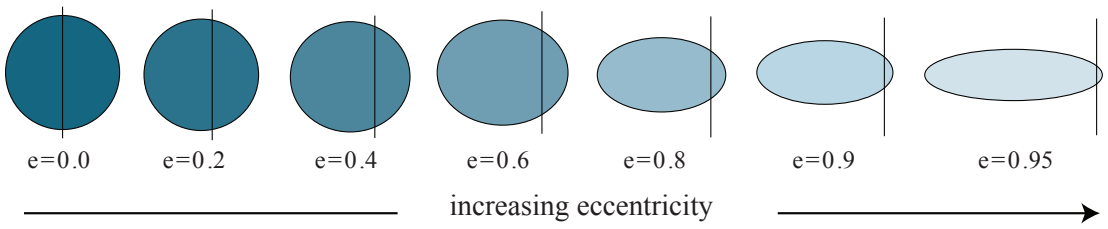

Figure 1: The shape of an orbit at a given eccentricity shown from $e = 0$ and increasing to the right up to $e = 0.95$. The Hulse-Taylor binary whose eccentricity is $e = 0.615$ has an eccentricity close to the depicted $e = 0.6$. The eccentric gravitational waveforms currently available publicly are valid up to an eccentricity of $e = 0.4$. The orbit of the Earth also has a small amount of eccentricity, 0.017. We can see that an eccentricity of $e = 0.2$ is close to circular, so the orbit of the Earth is essentially circular.

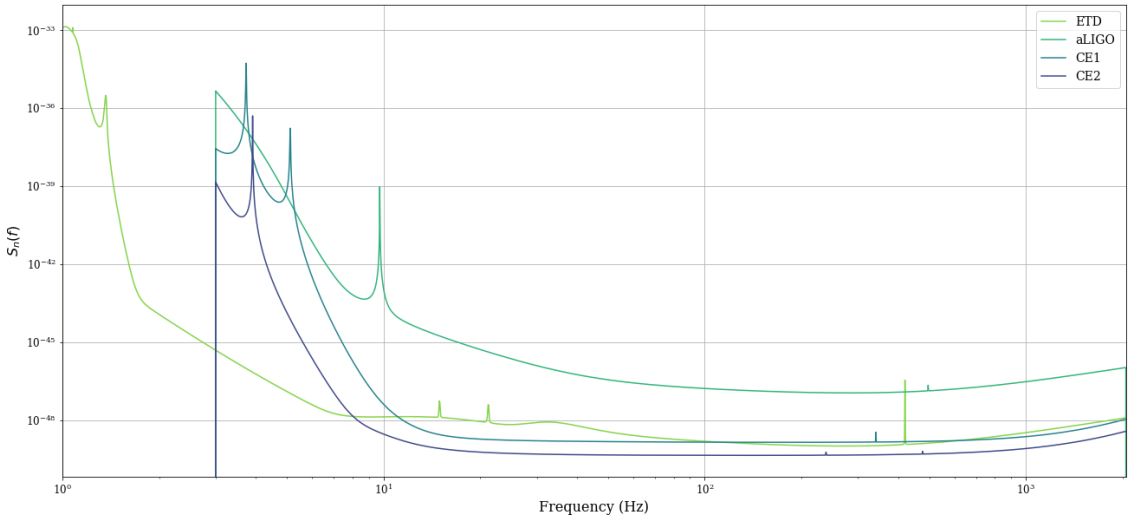

Figure 2: The detector noise power spectral density (noise curve) for Einstein Telescope (ETD) [1], Advanced LIGO (aLIGO), and Cosmic Explorer (CE1/CE2) [2] plotted as a function of frequency. The lower frequency limit of Einstein Telescope is 1 Hz. CE1 and CE2 correspond to the first and second stages of upgrades to Cosmic Explorer. Cosmic Explorer is an order of magnitude more sensitive than Advanced LIGO. The second stage of Cosmic Explorer will further increase the sensitivity.

Chapter 2

Methods

Gravitational waves provide valuable insight into the formation and physics of compact objects. It is important to accurately detect and measure their parameters, specifically eccentricity in our case. In this chapter we review existing literature that underlies the results of this thesis. First, we describe eccentricity and the derivation of equations describing the decrease in energy, angular momentum, semimajor axis, and eccentricity due to gravitational radiation. Next, we describe the methods and algorithms used to detect gravitational-waves and determine their significance. Finally, we describe the Bayesian methods and algorithms used to measure the parameters of detected gravitational-wave signals.

2.1 Gravitational Waves from Eccentric Binary Inspiral

Circular binary systems that consist of two neutron stars with mass m_1, m_2, separated by a distance, d with eccentricity, $e = 0$ have been considered in Refs. [74, 75]. Here we consider a similar case with non-zero eccentricity, $e \neq 0$. Eccentricity describes how much an object's orbit deviates from a circle. As gravitational radiation is emitted, there is a loss of energy and angular momentum. However, unlike in the circular case, in the case of non-zero eccentricity as gravitational waves are emitted there is a decrease in the eccentricity and semi-major axis.

In 1918, Albert Einstein derived formula that described gravitational radiation, known as the quadrupole formula, which are written as [74, 24, 25]

$$\frac{dE}{dt} = -\frac{G}{5c^5}\left(\frac{d^3Q_{ij}^{TT}}{dt^3}\frac{d^3Q_{ij}^{TT}}{dt^3} - \frac{1}{3}\frac{d^3Q_{ii}^{TT}}{dt^3}\frac{d^3Q_{jj}^{TT}}{dt^3}\right), \tag{2.1}$$

$$\frac{dL}{dt} = -\frac{2G}{5c^5}\left(\frac{d^2Q_{ij}^{TT}}{dt^2}\frac{d^3Q_{ij}^{TT}}{dt^3}\right), \tag{2.2}$$

where Q_{ij}^{TT} is the transverse traceless component of Q_{ij} and Q_{ij} is given by

$$Q_{ij} = \int \rho(\boldsymbol{x}) x_i x_j d^3x. \tag{2.3}$$

These equations describe the energy and angular momentum carried away by gravitational radiation.

To further reduce these equations, we can solve for each component of Q_{ij} and substitute into Eqs. 2.1 and 2.2. First we define the Cartesian coordinates of a binary with component masses m_1 and m_2 as $(d_1\cos\psi, d_1\sin\psi)$ and $(d_2\cos\psi, d_2\sin\psi)$ in the xy plane with the rotation aligned along the z axis. If the origin is at the center of mass of the binary, the mass distribution of the binary, in the point mass approximation. is given by

$$\rho(\boldsymbol{x}) = m_1[\delta(x - d_1\cos\psi)\delta(y - d_1\sin\psi)\delta(z)] \tag{2.4}$$

$$+\ m_2[\delta(x - d_2\cos\psi)\delta(y - d_2\sin\psi)\delta(z)], \tag{2.5}$$

where

$$d_1 = \left(\frac{m_2}{m_1 + m_2}\right) d, \tag{2.6}$$

$$d_2 = \left(\frac{m_1}{m_1 + m_2}\right) d, \tag{2.7}$$

and the angular velocity, ψ is given by

$$\psi = \frac{[G(m_1 + m_2)a(1 - e^2)]^{1/2}}{d^2}. \tag{2.8}$$

Using Keplerian motion, we can define the orbit equation as

$$d = \frac{a(1 - e^2)}{1 + e\cos\psi}, \tag{2.9}$$

where a is the semimajor axis and e is the eccentricity.

To calculate the loss of energy and angular momentum due to gravitational radiation, we first calculate the quadrupole moment of the mass distribution Q_{jk}. The

non-zero components are Q_{xx}, Q_{yy}, and $Q_{xy} = Q_{yx}$. The derivation of Q_{xx} from Eq. 2.3 gives

$$\begin{aligned} Q_{xx} &= \int m_1[\delta(x - d_1\cos\psi)\delta(y - d_1\sin\psi)\delta(z)] \\ &\quad + \ m_2[\delta(x - d_2\cos\psi)\delta(y - d_2\sin\psi)\delta(z)]x^2 d^3x \\ &= (m_1 d_1^2 + m_2 d_2^2)\cos^2\psi \\ &= \left[m_1\left(\frac{m_2}{m_1+m_2}\right)^2 + m_2\left(\frac{m_1}{m_1+m_2}\right)^2\right] d^2\cos^2\psi \\ &= \left[\frac{m_1 m_2^2 + m_2 m_1^2}{(m_1+m_2)^2}\right] d^2\cos^2\psi \\ &= \left[\frac{m_1 m_2(m_1+m_2)}{(m_1+m_2)^2}\right] d^2\cos^2\psi \\ &= \mu d^2\cos^2\psi \end{aligned} \tag{2.10}$$

where

$$\begin{aligned} \int \delta(x - x_0) f(x) d^3x = f(x_0), \\ \int \delta(x) d^3x = 1, \end{aligned} \tag{2.11}$$

and μ, the reduced mass, is given by

$$\mu = \frac{m_1 m_2}{m_1 + m_2}. \tag{2.12}$$

The other components, Q_{yy} and $Q_{xy} = Q_{yx}$, are derived in a similar way to give

$$\begin{aligned} Q_{yy} &= \mu d^2\sin^2\psi, \\ Q_{xy} &= Qyx = \mu d^2\sin\psi\cos\psi. \end{aligned} \tag{2.13}$$

In the case of a circular binary, the orbital angular velocity can be described as

$$\Omega = \sqrt{\frac{GM}{d^3}}. \tag{2.14}$$

This means that the quadupole moments Q_{xx}, Q_{yy}, and $Q_{xy} = Q_{yx}$ are derived to be

$$
\begin{aligned}
Q_{xx} &= \frac{1}{2}\mu d^2(1+\cos 2\Omega t),\\
Q_{yy} &= \frac{1}{2}\mu d^2(1-\cos 2\Omega t),\\
Q_{xy} &= Qyx = \frac{1}{2}\mu d^2 \sin 2\Omega t.
\end{aligned}
\tag{2.15}
$$

Derivatives of Eq. 2.15 are easily calculated as μ and Ω are not dependent on time. Unlike the orbit of a circular binary, which can be described using Newtonian gravity, the orbit of an eccentric binary includes two time dependent parameters that are necessary to describe the orbit: the semimajor axis, a, and the eccentricity, e. This makes derivatives of the quadrupole moment difficult to calculate.

The third derivatives of the quadrupole moment from Eqs. 2.10 and 2.13 in the frame of the binary are [24]

$$
\begin{aligned}
\frac{d^3Q_{xx}}{dt^3} &= \beta(1+e\cos\psi)^2(2\sin 2\psi + 3e\sin\psi\cos\psi),\\
\frac{d^3Q_{yy}}{dt^3} &= -\beta(1+e\cos\psi)^2[2\sin 2\psi + e\sin\psi(1+3\cos^2\psi)],\\
\frac{d^3Q_{xy}}{dt^3} &= \frac{d^3Q_{yx}}{dt^3} = -\beta(1+e\cos\psi)^2[2\cos 2\psi - e\cos\psi(1-3\cos^2\psi)],
\end{aligned}
\tag{2.16}
$$

where β is defined as

$$
\beta = \frac{4G^3m_1^2m_2^2(m_1+m_2)}{a^5(1-e^2)^5}. \tag{2.17}
$$

Substituting the calculated Q_{ij}^{TT} into Eqs. 2.1 and 2.2 and taking a time average, the equations for the loss of energy and angular moment are

$$
\frac{dE}{dt} = -\frac{32}{5}\frac{G^4m_1^2m_2^2(m_1+m_2)}{c^5a^5(1-e^2)^{7/2}}\left(1+\frac{73}{24}e^2+\frac{37}{96}e^4\right), \tag{2.18}
$$

$$
\frac{dL}{dt} = -\frac{32}{5}\frac{G^{7/2}m_1^2m_2^2(m_1+m_2)^{1/2}}{c^5a^{7/2}(1-e^2)^2}\left(1+\frac{7}{8}e^2\right). \tag{2.19}
$$

For a system with non-zero eccentricity we know that the semimajor axis, a and eccentricity, e are dependent on time. To find an equation for da/dt and de/dt we need to relate the semimajor axis and eccentricity to energy and angular momentum. The relations are given by

$$a = -Gm_1m_2/2E, \tag{2.20}$$

$$L^2 = Gm_1^2m_2^2(m_1+m_2)^{-1}a(1-e^2). \tag{2.21}$$

Using Eqs. 2.20 and 2.18 we can derive an equation for the change in semimajor axis over time as

$$\frac{da}{dt} = -\frac{64}{5}\frac{G^3m_1m_2(m_1+m_2)}{c^5a^3(1-e^2)^{7/2}}\left(1+\frac{73}{24}e^2+\frac{37}{96}e^4\right). \tag{2.22}$$

Similarly using Eqs. 2.21, 2.19, and 2.22, we can also derive an equation for the change in eccentricity

$$\frac{de}{dt} = -\frac{304}{15}e\frac{G^3m_1m_2(m_1+m_2)}{c^5a^4(1-e^2)^{5/2}}\left(1+\frac{121}{304}e^2\right) \tag{2.23}$$

In the case of a circular binary where $e = 0$, the equations for the change in total energy and the change in semimajor axis, Eqs. 2.18 and 2.22 respectively, are reduced to

$$\frac{dE}{dt} = -\frac{32}{5}\frac{G^4m_1^2m_2^2(m_1+m_2)}{c^5a^5} = -\frac{32G^4}{5c^5}\frac{M^3\mu^2}{a^5}, \tag{2.24}$$

$$\frac{da}{dt} = -\frac{64}{5}\frac{G^3m_1m_2(m_1+m_2)}{c^5a^3} = -\frac{64G^3}{5c^5}\frac{\mu M^2}{a^3}, \tag{2.25}$$

where $M = m_1 + m_2$ and μ is given by Eq. 2.12.

As the system loses energy to gravitational radiation, we can write an equation for the decay relating a and e

$$\frac{da}{de} = \frac{da/dt}{de/dt} = \frac{12}{19}\frac{a[1+(73/24)e^2+(37/96)e^4]}{e(1-e^2)[1+(121/304)e^2]}. \tag{2.26}$$

With given initial parameters, a_0 and e_0 we can uniquely determine $a(t)$ and $e(t)$ for a binary using Eqs. 2.22 and 2.23. The eccentricity of the binary depends on at what frequency the eccentricity is defined at. $e(t)$ can be converted to the frequency domain using a Fourier transform given by

$$\tilde{e}(f) = \int_{-\infty}^{\infty} e(t)e^{-2\pi ift}dt. \tag{2.27}$$

The eccentricity of the binary decreases as gravitational waves are emitted so at lower frequencies the eccentricity will be larger than at higher frequencies. For a circular binary we can set $e_0 = 0$ and derive and equation for $a(t)$

$$a(t) = (a_0^4 - 4\xi t)^{1/4}, \tag{2.28}$$

where

$$\xi = \frac{64}{5}\frac{G^3 m_1 m_2 (m_1 + m_2)}{c^5}. \tag{2.29}$$

The system will decay in a finite time T_c for a circular binary given by

$$T_c = \frac{a_0^4}{4\xi}. \tag{2.30}$$

To determine the decay time for a binary with $e_0 \neq 0$, we need to solve Eqs. 2.22 and 2.23 to get $a(t)$ and $e(t)$. We can integrate Eq. 2.26 to calculate $a(e)$

$$a(e) = \frac{c_0 e^{12/19}}{(1-e^2)}\left[1 + \frac{121}{304}e^2\right]^{870/2299}, \tag{2.31}$$

where c_0 is determined by the initial conditions $a = a_0$ when $e = e_0$. In the case of small e, Eq. 2.31 reduces to

$$a(e) \approx c_0 e^{12/19}, \quad e^2 \ll 1, \tag{2.32}$$

and for e close to 1, this becomes

$$a(e) \approx c_1/(1-e^2), \quad (1-e^2) \ll 1, \tag{2.33}$$

where $c_1 = c_0(425/304)^{870/2299} \approx 1.137 c_0$. If we neglect the complicated factor in c_1, $a(e)$ is given by

$$a(e) \approx c_0 e^{12/19}/(1-e^2). \tag{2.34}$$

Using Eqs. 2.23 and 2.31 we can write an equation for the decay time of an eccentric binary system. We can use $e(t)$ instead of $a(t)$ in calculating the decay time $T(a_0, e_0)$, since $e \to 0$ as $a \to 0$. The equation for de/dt in terms of $a(e)$ is given by

$$\frac{de}{dt} = -\frac{19}{12}\frac{\xi}{c_0^4}\frac{e^{-29/19}(1-e^2)^{3/2}}{[1 + (121/304)e^2]^{1181/2299}}. \tag{2.35}$$

The lifetime of the system $T(a_0, e_0)$ is then given by the integral

$$T(a_0, e_0) = \frac{12}{19}\frac{c_0^4}{\xi}\int_0^{e_0} \frac{de e^{29/19}[1 + (121/304)e^2]^{1181/2299}}{(1-e^2)^{3/2}}. \tag{2.36}$$

For small e_0, this reduces to

$$T(a_0, e_0) \approx \frac{12}{19}\frac{c_0^4}{\xi}\int_0^{e_0} dee^{29/19} = \frac{c_0^4}{4\xi}e_0^{48/19}. \tag{2.37}$$

This is approximately agrees with Eq. 2.30 where $T_c = a_0^4/4\xi$. For e_0 close to 1, Eq. 2.36 becomes

$$T(a_0, e_0) \approx (768/425)T_c(a_0)(1-e^2)^{7/2}. \tag{2.38}$$

We can introduce an orthonormal triad, $\boldsymbol{p}, \boldsymbol{q}, \boldsymbol{N}$ to define the relative separation of the binary $\boldsymbol{x}$ with magnitude r as

$$\boldsymbol{x} = \boldsymbol{p}r\cos\phi + (\boldsymbol{q}\cos i + \boldsymbol{N}\sin i)r\sin\phi, \tag{2.39}$$

where i is the inclination angle of the binary and ϕ is the true anomaly, which defines the position of an object along a Keplerian orbit. $\boldsymbol{p}$ points towards a suitable ascending node, $\boldsymbol{N}$ points from the observer to the source, and $\boldsymbol{q} = \boldsymbol{N} \times \boldsymbol{p}$. The two gravitational wave polarizations states, h_+ and $h_\times$, generated from an binary system due to gravitational radiation can generally be written as [76] as [76]

$$\begin{aligned} h_+^{\mathrm{N}} &= -\frac{G\mu}{c^4 D}\Bigg\{ \left(1+C^2\right)\left[\left(\frac{M}{r} + r^2\dot{\phi}^2 - \dot{r}^2\right)\cos 2\phi + 2\dot{r}r\dot{\phi}\sin 2\phi\right] \\ &\quad + S^2\left[\frac{M}{r} - r^2\dot{\phi}^2 - \dot{r}^2\right] + O(v)\Bigg\}, \\ h_\times^{\mathrm{N}} &= -2\frac{G\mu C}{c^4 D}\left[\left(\frac{M}{r} + r^2\dot{\phi}^2 - \dot{r}^2\right)\sin 2\phi + 2\dot{r}r\dot{\phi}\cos 2\phi + O(v)\right], \end{aligned} \tag{2.40}$$

where D is the distance to the binary, μ is the reduced mass in 2.12, $C \equiv \cos i$, and $S \equiv \sin i$. Gravitational waves from eccentric sources have been accurately modeled [77, 78, 79, 80, 81, 82, 83, 84].

In this thesis we model the gravitational-wave signals using waveform models, EccentricFD [77] and TaylorF2Ecc [79]. EccentricFD is an inspiral-only enhanced post-circular waveform model that extends the post-circular analysis of Ref. [85] to a 3.5PN Fourier-domain to produce an eccentric, compact binary inspiral waveform in the small eccentricity approximation, $e < 0.4$ and total mass $\leq 12\mathrm{M}_\odot$. In the zero eccentricity limit this model reproduces the non-eccentric model, TaylorF2, and in the small eccentricity limit this model will reproduce the PC model to leading order. TaylorF2Ecc is an inspiral-only TaylorF2 post-Netwonian model with eccentric

corrections accurate for $e \leq 0.1$. The waveforms are plotted in Fig. 4 for $e = 0.1$ with the non-eccentric waveform TaylorF2. For eccentricities ≥ 0.4 other methods for searching, like burst searches, might be necessary.

2.2 Matched Filter Search Algorithms

Models of gravitational waves like the ones mentioned in Sec. 2.1 can be used to detect gravitational waves in observations using a process called matched-filtering. We describe the methods and algorithms used in the PyCBC search pipeline [86, 87, 88, 89, 90] to detect gravitational-wave signals and to provide a measure of their significance.

Since the parameters of the gravitational-wave signal are unknown before a search is conducted, we can construct a template bank that covers the parameter space. Methods of template bank construction for non-spinning and aligned spin waveforms for a given parameter space have been extensively explored in literature [91, 92, 93, 94, 95, 96, 97]. We will focus on the method of stochastic template placement in Refs. [95, 96] as we consider the eccentricity of a signal. The stochastic method places templates at random and then removes the templates that it deems too close together. The stochastic template bank is created according to the algorithm defined in Ref. [95].

The density of the templates in the parameter space depends on the bandwidth of the detectors. In a PyCBC search, we use stochastic placement to generate a template bank covering a five dimensional parameter space of mass and spin of the component objects and eccentricity of the binary. A single template bank is used for all detectors or for the entire duration of the search, this allows for the requirement that a coincident event be observed by the same template in all detectors. The PyCBC search is a coherent search over i where the data is defined as

$$d_i(t) = \begin{cases} n_i(t), & \text{if signal not present,} \\ n_i(t) + s_i(t) & \text{if signal is present,} \end{cases} \tag{2.41}$$

where i is the i-th detector in the network.

Unfortunately, transient noise may appear in the detectors' data stream can produce triggers with high signal-to-noise ratio, even if they do not resemble templates.

Data quality investigations and vetoes [98, 99] may remove many, but not all, of these loud transients that have the potential to affect the sensitivity of the search. Loud noise transients, or glitches [100], that survive data quality investigations are suppressed by the chi-squared test, but can still reduce the sensitivity of the search through: dead time as a result of the clustering algorithm and ringing of the matched filter. Both of these reductions in sensitivity are related to the impulse response of the matched filter.

The impulse response can be considered a delta function glitch in the data defined as $s(t) = \delta(t - t_g)$, where t_g is the time of the noise transient. Though not all glitches are like this, loud transients can be approximated well as $s(t) = n(t) + \delta(t - t_g)$. The impulse response of the matched filter tend to dominate the matched filter signal-to-noise ratio. To make sure that the impulse response is of limited duration, the inverse of the power spectral density is truncated to a 16 second duration in the time domain before a filter is applied [86]. Loud transient glitches tend to be sharply peaked and the truncation of the inverse power spectral density smears out the sharp features in the power spectral density.

The process of identifying and removing loud noise transients from the data is called gating. To remove short-duration noise transients, first the input data, $s(t)$, around it is multiplied by a window function centered at the time of the peak of the noise transient before matched filtering. This is done to set the data to zero. Then a Tukey window is applied to evenly set the data to zero and prevent discontinuities in the input data. Since gating is usually done for short-duration transients, longer duration transients, identified by data quality investigations, are typically removed prior to analysis by the PyCBC search pipeline. One such case of the gating of a noise transient, or glitch, was during the detection of GW170817 [4].

The noise power spectral density averaged over both the time and detectors must be computed to generate an appropriate template bank. This is done using the harmonic mean, where the noise power spectral density is measured every 2048 seconds over an observation period independent of each detector [86]. By averaging each of the frequency bins, f_k, we can generate a harmonic mean power spectral density for a single detector given by

$$S_n^{\text{harmonic}}(f_k) = \frac{N_s}{\sum_{i=1}^{N_s} \frac{1}{S_n^i(f_k)}}. \tag{2.42}$$

We then obtain N_s power spectrum, S_n, for each detector in the network. This method is repeated to calculate the harmonic mean power spectral density from each detector in the network. The power spectral density estimate or bank will only need to be regenerated if there is a drastic change detector's noise power spectral density. This is usually the case when there are significant physical changes to the detectors. The use of a single power spectral density estimate allows for productive use of template banks that contain eccentricity as is demonstrated in Chapter 3.

Waveforms of target signals are well modeled so the PyCBC search pipeline uses matched filtering to search for these signals in the noise of the detectors. If we assume the noise, $n(t)$ is stationary and Gaussian with a one-sided power spectral density, $S_n(f)$ we can define it as

$$\langle \tilde{n}(f)\tilde{n}^*(f')\rangle = \frac{1}{2}S_n(|f|)\delta(f-f'). \tag{2.43}$$

The matched-filter signal-to-noise ratio calculate in the PyCBC search pipeline is based on the FindChirp algorithm which was developed for use in Initial LIGO/Virgo searches for gravitational waves [86]. The waveforms of the matched filter have additional unknown parameters: phase and amplitude. These depend on the sky localization and the orientation of the binary. The phase and amplitude are maximized over when a matched filter is constructed by projecting the data against two orthogonal phases of the template, $h(t)$ given by h_{cos} and h_{sin} [86]. The phases are related by $h_{sin} = ih_{cos}$. The matched-filter signal-to-noise ratio, $\rho(t)$ can be described by a weighted inner product in the frequency domain given by [90]

$$\rho^2(t) = \frac{\langle s|h_{cos}\rangle^2}{\langle h_{cos}|h_{cos}\rangle} + \frac{\langle s|h_{sin}\rangle^2}{\langle h_{sin}|h_{sin}\rangle} = \frac{|\langle s|h\rangle|^2}{\langle h|h\rangle}, \tag{2.44}$$

where the inner product, $\langle s|h\rangle$ is given by

$$\langle s|h(t)\rangle = 4\Re\int_{\mathrm{f_{lower}}}^{\mathrm{f_{high}}} \frac{\tilde{s}(f)\tilde{h}^*(f)}{S_n^(f)} e^{2\pi i f t}\mathrm{d}f. \tag{2.45}$$

We define the Fourier transformed detector data, $\tilde{s}(f)$ as

$$\tilde{s}(f) = \int_{-\infty}^{\infty} s(t)e^{-2\pi i f t}dt \tag{2.46}$$

and $\tilde{h}(f)$ is the Fourier transformation of the template waveform. The frequency limits, $\mathrm{f_{low}}$ and $\mathrm{f_{high}}$ of the inner product in Eq. 2.45 decided by the bandwidth of the detector's data.

The pipeline uses discretely sampled quantities like $s_j \equiv s(t_j)$ where s_j represents the input strain data, s(t), at a particular time, t_j. The noise power spectral density can be represented a similar way where $S_n(f_k)$ is the noise power spectral density at a discrete frequency, f_k. A fixed sampling interval, $\delta t = 1/4096$ seconds, is used to discretely sample the input strain data. Fourier transforms are then calculated using the Fast Fourier Transform algorithm in intervals of $T_B = 265$ seconds. The number of discretely sampled data points, N in the input data is $N = T_B/\delta t = 256 \times 4096 = 2^{20}$. The discrete Fourier transform of s_j is given by

$$\tilde{s_k} = \sum_{j=0}^{N-1} e^{-2\pi i j k/N}, \tag{2.47}$$

where $k = f_k/(N\delta t)$. The frequency resolution of this quantity is given by $\delta f = 1/N\delta t$.

The final step after the matched-filter signal-to-noise ratio time series, ρ_j^2, has been calculated is to generate the maxima where the signal-to-noise ratio time series exceeds a chosen threshold value. There are called triggers. The PyCBC search pipeline uses a time-clustering algorithm to keep the local maxima that exceed the threshold set for the signal-to-noise ratio time series as a real signal with have a single narrow peak in the time series. The time-clustering is done by dividing the time series into equal 1-second windows and then determining the maximum in each window. To ensure that the it is a local maximum in the time series, the candidate trigger is only kept if it has a higher signal-to-noise ratio than the window before and after it.

To distinguish between possible signal candidates and noise a chi-squared signal consistency test is introduced [86, 90]. The chi-squared test is a time-frequency decomposition ensures that the power in the data is consistent with the power in the matching waveform template [87]. To calculate the chi-squared value, the template waveform is first split into p frequency bins which a constructed such that each bin contributes an equal amount of power to the total matched-filter signal-to-noise ratio. The matched-filter signal-to-noise ratio, ρ_i, is then calculated for each bin, p, such that in the presence of a real signal, ρ_i will contain $1/p$ of the total power. The χ^2 statistic correlates the expected power to the measure power in each bin and is defined by

$$\chi^2 = p \sum_{i=1}^{p} \left[\left(\frac{\rho_{\text{cos}}^2}{p} - \rho_{\text{cos},i}^2 \right)^2 + \left(\frac{\rho_{\text{sin}}^2}{p} - \rho_{\text{sin},i}^2 \right)^2 \right] \tag{2.48}$$

where ρ^2_{cos} and ρ^2_{sin} are the signal-to-noise ratios of the two orthogonal phases of the matched filter. The reduced chi-squared, $\chi^2_r = \chi^2/(2p-2)$ should be near unity for a signal. Large χ^2 values suggest a high probability of being a noise transient than a signal. To suppress triggers from noise transients the matched filter signal-to-noise ratio is re-weighted using ρ and the reduced chi-squared, χ^2_r, [101] according to

$$\hat{\rho} = \begin{cases} \rho/[1+(\chi^2_r)^3]^{1/6}, & \text{if } \chi^2_r\, 1, \\ \rho, & \text{if } \chi^2_r \leq 1. \end{cases} \tag{2.49}$$

Using the re-weighted signal-to-noise ratio, the PyCBC search pipeline discards the triggers that are below a predetermined re-weighted signal-to-noise ratio threshold.

For a trigger to be considered a candidate the search requires that the parameters are consistent in the detector network. To make sure this is a the case a coincidence test is conducted on the triggers. If they survive the coincidence tests these triggers are considered coincident events. Before the test is executed, triggers that occur during instrumental or environmental artifacts are discarded. A trigger must survive both the time and parameter coincidence test to be considered a candidate event. The time coincidence test is when the trigger is observed with difference of arrival time less than or equal to the gravitational-wave travel time between the detectors, 10 ms, with an additional 5 ms window to account for uncertainty in measurements of the arrival time. The parameter coincidence test ensures that the triggers are observed in both detectors with the same waveform template, called exact-match coincidence. Exact-match coincidence requires that the intrinsic parameters of the system (i.e. masses and spins) of the triggers match exactly in each of the detectors. Coincident events, or candidates, are ranked by the quadrature sum of the re-weighted signal-to-noise ratio in each detector. This re-weighting is is called the detection statistic, $\hat{\rho}_c$ and is given by

$$\hat{\rho}_c = \sqrt{\hat{\rho}^2_1 + \hat{\rho}^2_2 + \ldots + \hat{\rho}^2_i}, \tag{2.50}$$

where i is the i-th detector in the network.

The detection statistic ranks the likelihood that a trigger is due to a gravitational-wave signal. Statistical significance is assigned to the candidates by measuring the false-alarm rate of the search as a function of detection statistic, $\hat{\rho}_c$. The false-alarm rate of the search is measured by time shifting the triggers from one detector

relative to another. This is done since the detector noise is non-stationary and non-Gaussian and it is impossible to directly measure the detector noise without signals. After the triggers have been shifted in time, the coincidence test is recalculated to create background data that does not contain coincident signals. This is repeated a multitude of times to create a large sample of false coincidences that are then used to estimate the false-alarm rate of the search as a function of detection statistic, $\hat{\rho}_c$. This is a sufficient approximation of the background assuming that transient noise artifacts in the data are not correlated between detectors and there are few gravitational-wave signals in the data.

The significance of each candidate is measured using a p-value, p_b. The p-value of a candidate event with detection statistic, $\hat{\rho}_c$ is the probability that there are one or more coincident noise events, or false alarms, that have a detection statistic $\geq \hat{\rho}_c$. The p-values are calculated under the null hypothesis that all triggers observed are due to noise. A low p-value indicate less support for the null hypothesis. Using the coincident events from the time shifts, we can calculate how many background noise events, n_b are louder than a given candidate event. The probability of one or more noise events being as long as a candidate event with a detection statistic $\hat{\rho}_c^*$ occurs in the search is given by

$$p\left(\geq 1 \text{ above } \hat{\rho}_c^* \mid T, T_b\right)_0 = 1 - \exp\left[\frac{-T\left(1 + n_b\left(\hat{\rho}_c^*\right)\right)}{T_b}\right], \tag{2.51}$$

where T is the duration of the observing time, T_b is the amount of background time from the time shifts, and $n_b(\hat{\rho}_c^*)$ is the number of background events with a detection statistic value greater than $\hat{\rho}_c$.

In Chapter 3 we search for eccentric binary neutron star signals in Advanced LIGO's first and second observing runs. We describe the search methodology used and place on upper limit on the rate of eccentric binary neutron star mergers. In Chapter 5 we generate non-eccentric and eccentric template banks and inject eccentric signals to determine the match of the waveforms. We use the results of our simulations to determine Cosmic Explorer's ability to detect eccentric binary signals.

2.3 Estimation of Binary Parameters

We can use Bayesian inference to ascertain a signal model that best fits the observations and obtain posterior probability densities for a model's parameters. This will tells us the best parameters for a signal that best fit the data. We discuss the Bayesian inference methods implemented in PyCBC Inference [73].

We consider the data, $d(t)$ which represents the output of a detector or the observations. The data is comprised of noise, $n(t)$ and if a signal is present a signal component, $s(t)$. In our case $d(t)$ is the data from a gravitational-wave detector where a signal has been identified in a search. The PyCBC inference implementation assumes that the noise, $n(t)$ each detector produces is stationary and Gaussian.

We can use Bayes' theorem

$$p(A|B) = \frac{p(B|A)p(A)}{p(B)}, \tag{2.52}$$

where $p(A|B)$ is the probability of event A given event B. In the case of a gravitational-wave detection to determine the probability of an event given a hypothesis, H, we can define this as

$$p(\boldsymbol{\theta}|\boldsymbol{d}(t), H) = \frac{p(\boldsymbol{\theta}|H)p(\boldsymbol{d}(t)|\boldsymbol{\theta}, H)}{p(\boldsymbol{d}(t)|H)}, \tag{2.53}$$

where H is a model of the gravitational-wave signal and $\boldsymbol{\theta}$ denotes the parameters of the model. Both H and $\boldsymbol{\theta}$ describe the properties of the source of the gravitational waves. The posterior probability density, $p(\boldsymbol{\theta}|\boldsymbol{d}(t), H)$, in Eq. 2.53, is the probability that the probability that the signal has parameters $\boldsymbol{\theta}$ given the observation $\boldsymbol{d}(t)$ and the waveform model, H. The prior probability density, $p(\boldsymbol{\theta}|H)$, is the prior distribution on the signal parameters and expresses the parameters of the model before observing the data, $\boldsymbol{d}(t)$. The likelihood, $p(\boldsymbol{d}(t)|\boldsymbol{\theta}, H)$ is the probability of obtaining the observation, $\boldsymbol{d}(t)$, given the signal parameters $\boldsymbol{\theta}$ and waveform model, H. The denominator in Eq. 2.53, $p(\boldsymbol{d}(t)|H)$, is a normalization constant and can be obtained by marginalizing over the parameters, $\boldsymbol{\theta}$.

In a binary's source frame, the gravitational-wave signal is described by the component masses, $m_{1,2}$, the three-dimensional spin vector of the component objects, $\boldsymbol{s}_{1,2}$ [102], and the eccentricity of the binary, e [25]. A phase of the binary can be described by ϕ and the tidal deformabilities of neutron star binaries are described by $\Lambda_{1,2}$ [103, 104]. The waveform observed by a detector on Earth is dependent on

the time of arrival of the signal, t_c, the luminosity distance of the system, d_L, and the angles that describe the transformation from the binary's frame to the the detector frame: the inclination angle, ι, polarization angle, Ψ, right ascension, α, and declination, δ [105]. The inclination angle describes the angle between the angular momentum axis of the binary and the line of sight. In PyCBC the conventions for inclination angle, ι are defined as $\iota = 0$ for a binary whose line of sight is parallel to the binary angular momentum ("face-on"), $\iota = \pi/2$ for a binary whose line of sight is perpendicular to the binary angular momentum ("edge-on"), and $\iota = \pi$ for a binary whose line of sight is anti-parallel to the binary angular momentum ("face-off").

Since the dimensionality of the parameter space is extensive this presents challenges for Bayesian inference. Correlations between signal parameters also adds to the difficulty. However, the size of the parameter space can be reduced depending on the problem of interest. Assumptions can be made about the spins of the binary to further reduce the dimensionality of the parameter space. Since we are considering eccentricity, we do not neglect eccentricity in the waveform models. A variety of waveform models are available through PyCBC implementation or calls to the LIGO Algorithm Library [106]. As we are exploring the eccentricity of a system, we choose gravitational waveform models, H that contain eccentricity, EccentricFD [77] and TaylorF2Ecc [79]. Both waveforms reduce to TaylorF2 in the zero eccentricity limit and since we expect binary neutron star mergers to have low mass, spin, and eccentricity these waveforms are acceptable for our analyses.

The data, $\boldsymbol{d}(t)$, is introduced to the posterior probability density function in the likelihood. For a multi-detector network, this data is modeled as $d_i(t) = n_i(t) + s_i(t)$, where $s_i(t)$ is the signal or gravitational-waveform in the i-th detector. Since the detectors are not identical or in the same location, the signals observed in each detector are slightly different due to different sky locations and polarizations [105]. The likelihood models the noise, $n_i(t)$ in the detector as stationary Gaussian noise and depends upon a noise-weighted inner product between the gravitational waveform and gravitational-wave data, $\boldsymbol{d}(t)$ and is given by [107]

$$
\begin{aligned}
p(\boldsymbol{d}(t) \mid \boldsymbol{\theta}, H) &= \exp\left[-\frac{1}{2}\sum_{i=1}^{N}\langle \tilde{n}_i(f) \mid \tilde{n}_i(f)\rangle\right] \\
&= \exp\left[-\frac{1}{2}\sum_{i=1}^{N}\left\langle \tilde{d}_i(f) - \tilde{s}_i(f,\boldsymbol{\theta}) \mid \tilde{d}_i(f) - \tilde{s}_i(f,\boldsymbol{\theta})\right\rangle\right],
\end{aligned}
\tag{2.54}
$$

where N is the number of detectors in the network. The inner product, $\langle \tilde{a}|\tilde{b}\rangle$ is

$$
\left\langle \tilde{a}_i(f) \mid \tilde{b}_i(f)\right\rangle = 4\Re\int_0^\infty \frac{\tilde{a}_i(f)\tilde{b}_i(f)}{S_n^{(i)}(f)}\mathrm{d}f, \tag{2.55}
$$

where $S_n^{(i)}(f)$ is the power spectral density of the i-th detector's noise and $\tilde{d}_i(f)$ and $\tilde{n}_i(f)$ are the data and noise in the frequency domain obtained from the Fourier transformation of $d_i(t)$ and $n_i(t)$, respectively. Here, $\tilde{s}_i(f,\boldsymbol{\theta})$ is the model waveform and can be generated in the frequency domain or in the time domain and then Fourier transformed to the frequency domain. Several of these operations, Fourier transform, noise power spectral density estimation, and inner products, are common in the computation of the matched-filter signal-to-noise ratio in Sec. 2.2 and are used in PyCBC Inference as they currently exists in PyCBC [86, 90, 88].

Markov Chain Monte Carlo (MCMC) techniques can be used to marginalize over the parameters to obtain the posterior probabilities [108]. Ensemble MCMC algorithms sample the parameter space using multiple Markov chains. A set of parameters, $\boldsymbol{\theta}_1^{(k)}$, can be drawn from the probability density function to initiate the k-th Markov chain in the ensemble. The k-th Markov chain has the set of parameters, $\boldsymbol{\theta}_l^{(k)}$ at iteration, l. The sampling algorithm then proposes another set of parameters, $\boldsymbol{\theta}_{l'}^{(k)}$ with probability $Q(\boldsymbol{\theta}_l^{(k)}, \boldsymbol{\theta}_{l'}^{(k)})$. The sampler computes an acceptance probability, γ, when a new set of parameters is proposed. This determines if the Markov chain should move to the new proposed parameter set, $\boldsymbol{\theta}_{l'}^{(k)}$. If the new parameter set is accepted $\boldsymbol{\theta}_{l+1}^{(k)} = \boldsymbol{\theta}_{l'}^{(k)}$ and if it is rejected $\boldsymbol{\theta}_{l+1}^{(k)} = \boldsymbol{\theta}_{l}^{(k)}$. Once an adequate number of iterations have been obtained, the ensemble converges to a distribution that is proportional to a sampling of the posterior probability density function. Different ensemble samplers make different choices for the probability, $Q(\boldsymbol{\theta}_l^{(k)}, \boldsymbol{\theta}_{l'}^{(k)})$, and acceptance probability, γ.

Currently PyCBC inference supports the open source ensemble sampler, `emcee` [109],

the parallel-tempered *emcee* sampler, `emcee_pt` [109, 110], a more robust parallel-tempered *emcee* sampler, `PTEmcee` [109, 110], a multi-purpose sampler, and `dynesty` [111]. In Chapter 4, we use the parallel-tempered *emcee* sampler, `emcee_pt` to measure the eccentricity of GW170817 and GW190425 and will focus on discussing that sampler.

The `emcee_pt` sampler is a parallel-tempered sampler that uses several Markov chains to explore the probability density function at different tempering or "temperatures". The probability density function at a particular temperature, T, is

$$p_T(\boldsymbol{\theta}|\boldsymbol{d}(t), H) = \frac{p(\boldsymbol{\theta}|H)p(\boldsymbol{d}(t)|\boldsymbol{\theta}, H)^{1/T}}{p(\boldsymbol{d}(t)|H)}. \tag{2.56}$$

The `emcee_pt` sampler uses several temperatures in parallel, where each chain explores the probability density function, and then the positions of the Markov chains are swapped based on acceptance criteria stated in Ref. [110]. The exchanging of positions between chains from different temperatures makes parallel-tempered samplers suitable for sampling from posterior probability density functions with widely separated modes in the parameter space [110].

The output of the sampling algorithms are Markov chains. However, these consecutive states of the chains are not independent since the Markov processes depend on the previous state [112]. To determine the number of iterations to produce independent samples of the posterior probability density function we consider the autocorrelation length, τ_K of a Markov chain [113]. For the k-th Markov chain $X_l^{(k)} = \{\boldsymbol{\theta}_g^{(k)}; 1 < g < l\}$ of length, l, the autocorrelation length obtained form the sampling algorithm is given by

$$\tau_K = 1 + 2\sum_{i=1}^{K} \hat{R}_i, \tag{2.57}$$

where K is the first iteration of the Markov chain where the condition $m\tau_K \leqslant K$ is true [113]. m is a parameter that is set to 5 in PyCBC Inference. The autocorrelation function, $\hat{R}_i$ is defined as [113]

$$\hat{R}_i = \frac{1}{l\sigma^2}\sum_{t=1}^{l-i}(X_t - \mu)(X_{t+i} - \mu) \tag{2.58}$$

where μ and σ are the mean and variance of X_t, respectively, X_t are the samples of the Markov chain, $X_l^{(k)}$ between the 0-th and t-th iteration, and X_{t+1} are the samples of the Markov chain, $X_l^{(k)}$ between the 0-th and $(t+1)$-th iteration.

The "burn-in" period is the length of the Markov chains before they are considered to have lost any memory their initial positions. Since the initial positions of the Markov chains influence their subsequent positions, it is common to discard samples from the burn-in period to prevent any biases. PyCBC Inference has several methods to determine when the chains are past the burn-in period, but we will focus on `n_acl` test as it works well with the `emcee_pt` sampler. If the length of the chains is 10 times the autocorrelation length, then the `n_acl` test assumes the sampler is past the burn-in period. The autocorrelation length is calculated from samples in the second half of the Markov chains. The sampler is assumed to be past the burn-in period at the halfway point of the Markov chains, if the test is fulfilled.

The samples to estimate the posterior probability density function need to be independent so correlations between nearby samples are removed by drawing samples from the Markov chains in an interval of the autocorrelation length after the burn-in period [112]. The number of independent samples for our posterior probability density function is equivalent to the number of Markov chains in our ensemble times the number of iterations after hte burn-in period times the autocorrelation length, τ_K.

The measurement of a parameter from the independent samples is given using a credible interval. A credible interval is the interval in which a parameter has a given probability. For example, the $x\%$ credible interval is an interval where the true parameter lies with a probability of $x\%$. PyCBC Inference has the ability to calculate credible intervals based on percentile values. The values for an $x\%$ credible interval are usually written as A^{+B}_{-C} where A is the median (50th percentile) of the marginalized histograms and the $A+B$ and $A-C$ values are the upper and lower bounds of the $x\%$ credible interval and are calculated as $(50+x/2)$-th and $(50-x/2)$-th percentiles respectively.

In Chapter 4, we use parameter estimation to measure the parameter of interest of the two binary neutron star gravitational-wave detections, GW170817 and GW190425. This study focused on using full parameter estimation to measure the eccentricity of the two binary neutron star detections and if the measured eccentricity provides insight to the formation of the binary.

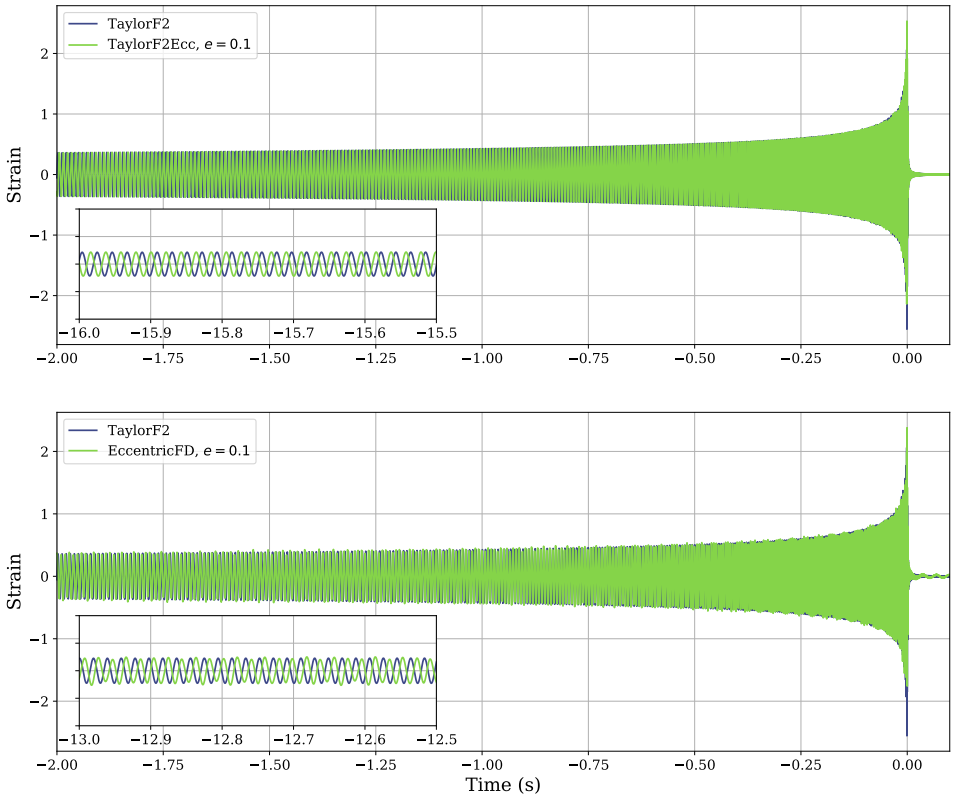

Figure 3: The scaled strain as a function of time for two eccentric gravitational waveform models. TaylorF2Ecc (top) EccentricFD (bottom) gravitational waveforms generated at a dominant-mode gravitational-wave reference frequency of 10Hz with component masses of $1.4M_{\odot}$ at an eccentricity of $e = 0.1$ compared with the non-eccentric TaylorF2 waveform that show merging binary neutron stars up to the time of merger. The inset plot shows a zoomed-in depiction of the the phase difference in the non-eccentric (violet) and eccentric (green) waveforms.

Chapter 3

Search for Eccentric Binary Neutron Star Mergers in the first and second observing runs of Advanced LIGO

We present a search for gravitational waves from merging binary neutron stars which have non-negligible eccentricity as they enter the LIGO observing band. We use the public Advanced LIGO data which covers the period from 2015 through 2017 and contains $\sim$ 164 days of LIGO-Hanford and LIGO-Livingston coincident observing time. The search was conducted using matched-filtering using the PyCBC toolkit. We find no significant binary neutron star candidates beyond GW170817, which has previously been reported by searches for binaries in circular orbits. We place a 90 % upper limit of $\sim$ 1700 mergers $\mathrm{Gpc}^{-3}\mathrm{Yr}^{-1}$ for eccentricities $\lesssim$ 0.43 at a dominant-mode gravitational-wave frequency of 10 Hz. The absence of a detection with these data is consistent with theoretical predictions of eccentric binary neutron star merger rates. Using our measured rate we estimate the sensitive volume of future gravitational-wave detectors and compare this to theoretical rate predictions. We find that, in the absence of a prior detection, the rate limits set by six months of Cosmic Explorer observations would constrain all current plausible models of eccentric binary neutron star formation.

3.1 Introduction

With the detections made by the Advanced LIGO (Laser Interferometer Gravitational Wave Observatory) [8] and Virgo observatories [9], we have entered the age of gravitational-wave astronomy. During their first (O1) and second (O2) observing runs, the LIGO and Virgo collaborations detected ten binary black hole mergers and one binary neutron star merger [17]. Independent groups have since verified these events and detected several additional binary black hole mergers [114, 115, 12, 116]. One possible channel for the formation of merging binaries is through dynamical interaction in dense stellar environments such as globular clusters [55, 56, 52] or galactic nuclei [57, 58]. Unlike binaries formed in the field which can radiate away their eccentricity [25, 64], dynamically formed binaries may still have significant residual eccentricity when their gravitational waves enter the LIGO-Virgo band. The observation of a binary with measurable eccentricity would confirm the existence of a dynamical formation channel. The existing LIGO-Virgo binary black hole candidates are consistent with non-eccentric binary mergers [117]. The third LIGO-Virgo observing run is currently underway and is expected to produce dozens more events [40].

A search for eccentric binary black hole mergers in O1 and O2 data using methods which do not use models of the gravitational waveform [118, 119, 120] reported no eccentric merger candidates [121]. The sensitivity of gravitational-wave searches can be improved by the use of matched-filtering, if a model of the target waveform is available. Existing matched-filter searches were designed for the detection of circular binaries [122, 90, 114]. It is possible that compact binaries with measurable eccentricity may have been missed by these initial searches [67, 68]. For binary black hole mergers, highly accurate models with the full inspiral-merger-ringdown, along with support for both a large range of eccentricity and spin do not yet exist, though development is rapidly progressing and there are models which satisfy some of these constraints [123, 81, 124, 82, 125].

In this paper, we search for eccentric binary neutron star mergers. There are several models of the gravitational waveform suitable for this task which include EccentricFD [77] and TaylorF2e [126, 84]. These waveform models do not currently support compact-object spin. However, neutron star binaries formed by dynamical capture in globular clusters may have non-negligible spin if they follow the observed

distribution of millisecond pulsars (MSPs). Even if large spins are supported, we may expect the effective spin $\chi_{\rm eff} = (\chi_{1z} m_1 + \chi_{2z} m_2)/(m_1 + m_2)$ to peak around zero if the individual neutron stars orientations are isotropic. Searches which do not account for spin still have significant sensitivity to sources with low effective spin $\chi_{\rm eff} < 0.1$, though there will be significantly reduced sensitivity in the case where both component neutron stars are consistent with the fastest observed MSP [127] and their respective spins are aligned with the orbital angular momentum [128].

Using these waveforms, we perform a matched-filtering based analysis by extending the methods used by Ref. [12] to include eccentric binaries. We find that our search is effective at detecting eccentric binary neutron star mergers up to an eccentricity $e \sim 0.43$ at a dominant-mode gravitational-wave frequency of 10 Hz. Using a representative sample of the O1 and O2 dataset, we find that a non-eccentric search starts losing significant sensitivity relative to the eccentric search starting at $e \sim 0.07$, in agreement with the results of [68, 129].

We find no individually significant eccentric binary neutron star merger candidates using the public O1 and O2 datasets [130]. The only significant event is the previously reported merger GW170817 [4] since our search is also sensitive to circular binaries. In the absence of a new detection, we place a 90% upper limit on the merger rate of ~ 1700 Gpc^{-3}Yr^{-1} for binaries whose eccentricity is $e \lesssim 0.43$ at the 10 Hz reference frequency. While we do not detect any individually significant mergers, it is possible that follow-up could uncover sub-threshold sources, and so we make available our full population of sub-threshold candidates [131].

We can compare our measured rate to predictions for the proposed channels for eccentric binary neutron star formation. Ref. [132] predict a binary neutron star merger rate of 30 Gpc^{-3}Yr^{-1} at z=0 from binaries formed by the tidal capture and collision of neutron stars in globular clusters. Ref. [133] predict a merger rate of ~ 0.02Gpc^{-3}Yr^{-1} from binaries formed by dynamical interactions in globular clusters. Given these predicted rates, it is unsurprising that our search did not observe a signal. Future detectors like A+ [40] and Cosmic Explorer [2], will observe a large volume of the universe and have a higher probability of observing eccentric binary neutron star mergers. Using our measured rate and the expected sensitivity of A+ and Cosmic Explorer, we estimate the time it would take for observed rates to impinge on the predicted rates. Using the A+ expected sensitivity distance of 330 Mpc [40], we find

the most optimistic predictions [132] require half a year of data for the measurement to be comparable to the predictions. The most pessimistic predictions [133] require $\sim$ 775 years of data before the measured rate limits are comparable with the prediction. However, the proposed third-generation detector Cosmic Explorer would need at most half a year of data to achieve a rate limit comparable to the most pessimistic models, although a serendipitous detection is always a possibility with current detectors.

3.2 Search Methodology

We use a matched-filtering search for compact-object binaries using the PyCBC toolkit [134]. We use gravitational waveforms that model mergers with elliptical orbits, but otherwise employ the same configuration as used by Ref. [12] for their search for gravitational waves from compact binary mergers.

Of the available waveform models, we employ two waveform models that contain eccentricity, EccentricFD and TaylorF2e. EccentricFD [77] extends the post-circular (PC) analysis of [85] to obtain a 3.5PN Fourier-domain enhanced PC gravitational-wave model that produces an eccentric, compact binary inspiral waveform in the small eccentricity approximation. In the zero eccentricity limit this model reproduces the non-eccentric model, TaylorF2, and in the small eccentricity limit this model will reproduce the PC model to leading order. Figure 4 shows two waveforms generated using EccentricFD with a non-eccentric waveform shown in blue and an eccentric waveform shown in orange. TaylorF2e is a 3PN Fourier-domain, eccentric waveform model, valid for larger initial eccentricities, defined by the stationary phase approximation (SPA) of a harmonically-decomposed time-domain signal. While both models expand the amplitude coefficients in small eccentricity, the TaylorF2e model does not invert the dependence of orbital frequency on eccentricity and numerically solves the stationary phase condition [126, 84, 129].

We find that a template bank generated by straightforward stochastic placement of EccentricFD waveforms starting at a gravitational-wave frequency of 30 Hz is sufficient to recover binary neutron star signals with eccentricity as modelled by either EccentricFD or TaylorF2e. In addition to the component masses of the binary neutron star, our bank adds a parameter for the eccentricity, e_{30}, along with an additional

binary orientation parameter. Our template bank is designed to detect binary neutron star mergers where the component masses range from $1.1 - 1.6\mathrm{M}_{\odot}$ [135] and eccentricities up to 0.2 at a reference of 30 Hz. This corresponds to ~ 0.43 at a reference frequency of 10 Hz. Fig. 5 shows the distribution of templates in both chirp mass and eccentricity. The density of templates increases rapidly with eccentricity. Adding the additional degrees of freedom increases the size of the template bank by a factor of 160 relative to a non-eccentric, non-spinning bank that would cover the same region. Due to the inherent degeneracy between the component masses, the template bank will have significant sensitivity outside this parameter space in regions where the chirp mass $\mathcal{M} = (m_1 m_2)^{3/5}/(m_1 + m_2)^{1/5}$ is otherwise consistent i.e. a $1.2 - 2.0\mathrm{M}_{\odot}$ merger.

Matched-filtering is used to calculate the signal-to-noise (SNR) time series using our bank of template waveforms independently for each observatory [86]. Peaks in the SNR time series are followed up by a series of signal consistency tests [136, 87] and combined into multi-detector candidates [90, 88]. We assign each candidate a ranking statistic, $\tilde{\rho}_c$, using the same methods employed in the 1-OGC catalog [12]. The ranking statistic, $\tilde{\rho}_c$, accounts for the signal-to-noise (SNR) of each candidate, the consistency of its morphology and signal properties with an astrophysical source, and the rate of background for candidates arising from similar templates.

3.3 Observational Results

We search the public LIGO O1 and O2 dataset which contains $\sim$ 164 days of coincident LIGO-Hanford and LIGO-Livingston data after removal of data which has been flagged as potentially containing instrumental artefacts [137, 138, 130]. Data when only a single observatory was operating was not considered, nor was data from the Virgo observatory which operated only in the last month of O2. In this search, we neglect data from the Virgo detector as it only provides a marginal senstivity improvement [116]. Future analyses will incorporate data from the full network.

The most significant candidates are listed in Table 1. As our search is also sensitive to circular binaries, it is not surprising that GW170817—first detected by the LIGO-Virgo search for circular binaries—was observed as a high-significance event. The remaining candidates are consistent with the rate of false alarms expected for the

amount of data analyzed. However, we cannot rule out a sub-threshold population which may be uncovered by correlation with non-GW datasets (GRBs, Kilonovae, etc) such as performed in Ref. [139].

3.4 Upper Limits

As our search did detect any significant individual eccentric binary neutron star merger candidates, we place an upper limit on the rate of eccentric mergers as a function of their eccentricity. We determined a 90% confidence upper limit on the rate of mergers using the method introduced in Ref. [140]. The upper limit on the merger rate R_{90} is

$$R_{90} = 2.303\,[TV(\mathcal{F}^*)]^{-1} \tag{3.1}$$

where T is the total observation time and $V(\mathcal{F}^*)$ is the average volume the search is sensitive to at the false alarm rate of the loudest observed candidate. Under the assumption that GW170817 is a non-eccentric merger, we exclude it from our analysis. The sensitivity is measured using a simulated population of sources distributed uniform in volume and isotropic in orientation. We have primarily used the EccentricFD model for our simulated population, however, we have confirmed our results are consistent with a smaller sample using the TaylorF2e model. Fig. 6 shows the upper limit on the merger rate as a function of the binary eccentricity as well as the average sensitive distance of the search over the observation period. We find that up to an eccentricity of ~ 0.43 at a reference frequency of 10 Hz, we can place a 90% upper limit at $\sim$1700 mergers per cubic Gpc per year.

Under the assumption that eccentric signals will not have been detected, we can determine the observation time required by future detectors to constrain the binary neutron star merger rates predicted by Ref. [132] and Ref. [133] by scaling the upper limit from our search. We find that the Advanced LIGO observatories had an average range, D_{O1+O2}, of 90 Mpc during O1 and O2 for a fiducial $1.4 - 1.4\mathrm{M}_\odot$ merger by taking the weighted-average of their noise curves. Similarly, using their respective noise curves, we find an average range, D_{A+}, of 330 Mpc for A+ [40] and D_{CE} of 7130 Mpc for Cosmic Explorer[1]. The observation time required, $T_{CE,A+}$, to match

[1] https://cosmicexplorer.org/researchers.html

the predicted rates, $R_{Ye,Lee}$, is given as

$$T_{CE,A+|Ye,Lee} = T_{O1+O2} \frac{R_{O1+O2}}{R_{Ye,Lee}} \left(\frac{D_{O1+O2}}{D_{CE,A+}} \right)^3 , \tag{3.2}$$

where T_{O1+O2} is the total observation time of O1 and O2 and R_{O1+O2} is the upper limit achieved by our current search. We find that with the increased sensitivity of A+ the most optimistic predictions [132] would require half a year of data and the most pessimistic predictions [133] would require $\sim$ 775 years. Cosmic Explorer would need at most half a year of data to constrain current binary neutron star merger rate models. Understanding the constraints that future observational limits place on eccentric binary formation channels will require computation of the rate as a function of eccentricity from population synthesis.

3.5 Conclusions

We have developed a search that is effective at detecting binary neutron star mergers with orbital eccentricity $\lesssim 0.43$ at 10 Hz. Our search uses the public PyCBC toolkit [134] based on a standard matched filtering approach [12, 90]. We have found that straightforward stochastic placement algorithms are sufficient to tackle the construction of template banks for eccentric binary merger waveforms. As broadly applicable and highly accurate eccentric waveform models are developed which include corrections for component-object spin, the full inspiral-merger-ringdown, and support for large values of eccentricity it will be possible to apply the same methods demonstrated here to the detection of binary black hole mergers.

To aid in further analysis of our results, we make available our full sub-threshold catalog of eccentric binary neutron star candidates. For each candidate we provide the false alarm rate, parameters of the associated template waveform, and signal parameters such as the signal-to-noise and results of our signal consistency tests [131][2].

While the detection of a single binary neutron star or binary black hole eccentric merger would immediately demonstrate the existence of dynamical formation, current estimates of the rate of binary neutron star mergers imply that a single observation would be rare for the current generation of ground based observatories. Future observatories such as Cosmic Explorer will be able to probe current models.

[2] www.github.com/gwastro/eccentric-bns-search

Date designation	GPS time	FAR^{-1} (y)	$\tilde{\rho}_c$	ρ_H	ρ_L	m_1	m_2	e_{30}
170817+12:41:04UTC	1187008882.45	> 10000	27.86	18.41	23.60	1.48	1.28	0.02
151127+02:24:56UTC	1132626313.67	.57	8.60	7.28	5.73	1.23	1.55	0.16
151130+22:40:53UTC	1132958470.76	.54	8.60	6.76	5.89	1.29	1.22	0.19
170705+12:02:50UTC	1183291388.00	.31	8.54	7.29	5.56	1.48	1.57	0.16
151227+13:12:35UTC	1135257172.28	.14	8.42	6.33	6.21	1.42	1.37	0.10
170618+15:35:01UTC	1181835319.00	.08	8.40	7.30	5.35	1.22	1.19	0.15
170812+20:07:43UTC	1186603681.67	.07	8.35	6.92	5.47	1.21	1.13	0.17
170302+22:45:10UTC	1172529928.62	.07	8.42	6.93	5.46	1.23	1.17	0.12
161222+07:49:11UTC	1166428168.98	.06	8.39	6.33	6.14	1.50	1.12	0.18
170328+07:26:40UTC	1174721218.74	.05	8.38	5.11	7.26	1.11	1.22	0.12

Table 1: Binary neutron star candidates from the search of O1 and O2 LIGO data sorted by the rate of false alarms with a detection statistic at least as large as the candidate. The mass and eccentricity parameters of the template associated with each candidate are listed. Note the eccentricity is given at the 30 Hz gravitational-wave frequency reference used to generate the template bank. The values associated with a candidate can be considered point estimates and may differ significantly from the results of full Bayesian parameter estimation. Masses are quoted in the detector frame.

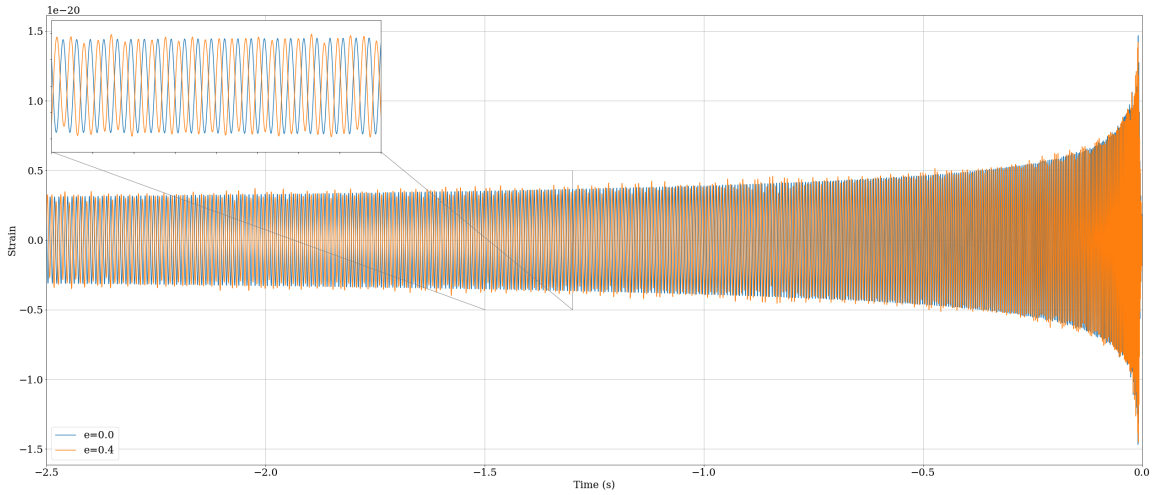

Figure 4: EccentricFD gravitational waveforms generated at a dominant-mode gravitational-wave reference frequency of 10Hz with component masses of $1.3M_{\odot}$ for a non-eccentric, e=0.0, (blue) and eccentric, e=0.4, (orange) merging binary neutron star up to the time of merger. Though the waveforms look similar they overlap by $\sim 16\%$. The inset plot shows a zoomed-in depiction of the the phase difference in the non-eccentric (blue) and eccentric (orange) waveforms from -9.0 to -8.7s.

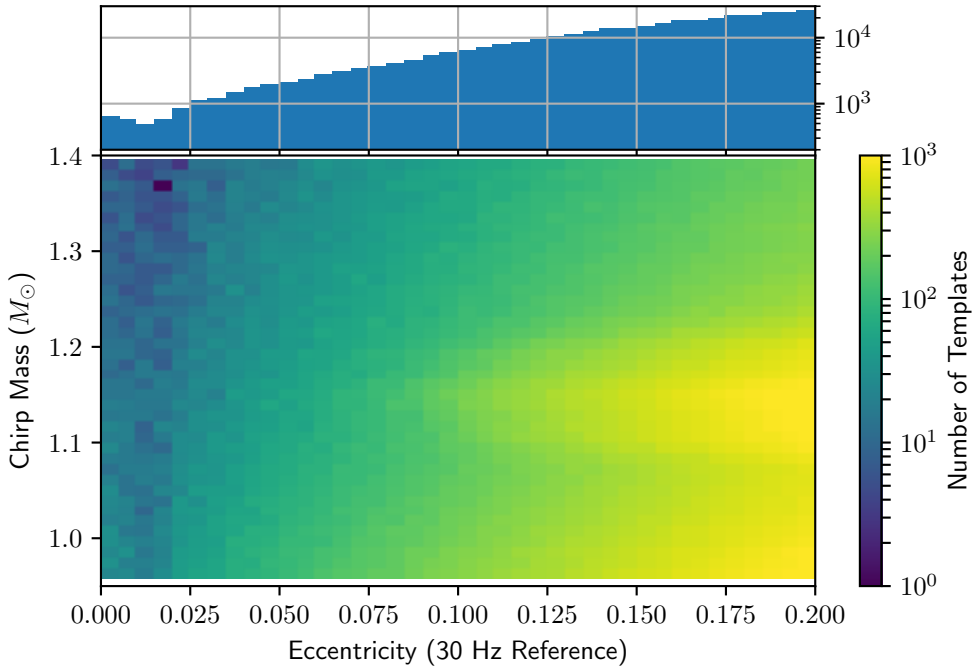

Figure 5: This distribution of templates in our eccentric binary neutron star bank. Note that the eccentricity is given at a dominant-mode gravitational-wave reference frequency of 30 Hz as opposed to 10 Hz used elsewhere in this paper.

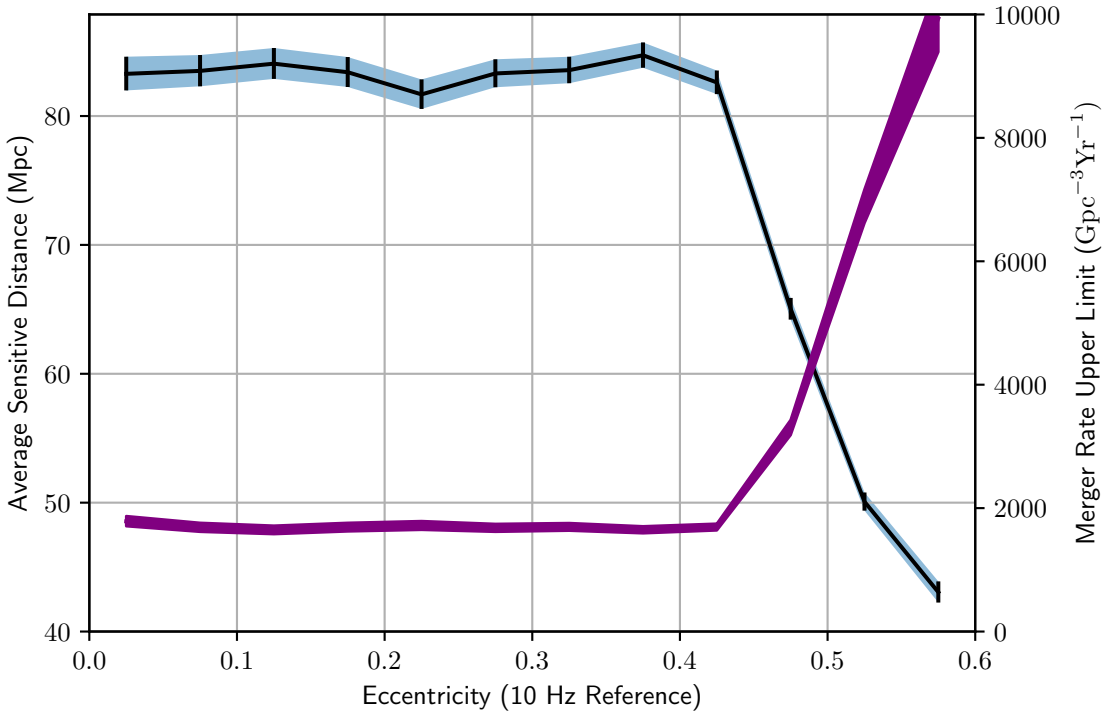

Figure 6: The average sensitive distance of the search (blue/left scale) and the 90% upper limit on the rate of eccentric binary neutron star mergers (purple/right scale) as a function of eccentricity at a reference frequency of 10 Hz. The average sensitivity is nearly flat up to an eccentricity of 0.43, where we begin to see sharp drop-off in sensitive range. This corresponds to the edge of our template bank.

Chapter 4

Measuring the Eccentricity of GW170817 and GW190425

Two binary neutron star mergers, GW170817 and GW190425, have been detected by Advanced LIGO and Virgo. These signals were detected by matched-filter searches that assume the star's orbit has circularized by the time their gravitational-wave emission is observable. This suggests that their eccentricity is low, but full parameter estimation of their eccentricity has not yet been performed. We use gravitational-wave observations to measure the eccentricity of GW170817 and GW190425. We find that the eccentricity at a gravitational-wave frequency of 10 Hz is $e \leq 0.024$ and $e \leq 0.048$ for GW170817 and GW190425, respectively (90% confidence). This is consistent with the binaries being formed in the field, as such systems are expected to have circularized to $e \leq 10^{-4}$ by the time they reach the LIGO-Virgo band. Our constraint is a factor of two smaller that an estimate based on GW170817 being detected by searches that neglect eccentricity. However, we caution that we find significant prior dependence in our limits, suggesting that there is limited information in the signals. We note that other techniques used to constrain binary neutron star eccentricity without full parameter estimation may miss degeneracies in the waveform, and that for future signals it will be important to perform full parameter estimation with accurate waveform templates.

4.1 Introduction

The Advanced LIGO and Virgo observatories have detected two binary neutron star mergers, GW170817 [4] and GW190425 [19]. To date, 17 double neutron star systems have been observed through radio surveys of the Milky Way field [27, 28, 29, 30, 31]. Observations of binary neutron stars allow us to determine their formation channels [41, 42, 43, 69, 48, 49, 28, 44, 45, 46, 47, 33], constrain the neutron-matter equation of state [141, 142, 143, 144, 145, 146, 147, 148, 149, 150, 151], and test the strong-field regime of general relativity [152].

Although the eccentricity of double neutron stars in the Milky Way field ranges from 0.06 to 0.828 [32, 33], field binaries will circularize to eccentricity $e \leq 10^{-4}$ [25, 49], making them detectable by matched-filter searches that neglect eccentricity [65, 66, 67, 68]. GW170817 and GW190425 were detected by searches that neglect eccentricity [4, 19], suggesting that their eccentricity is $e \lesssim 0.05$ [68], however no direct measurement of their eccentricity has been made. Ref. [3] place a limit on the eccentricity of GW190425 by estimating the effect of eccentricity on the measured parameters of the signal. Here, we directly measure the eccentricity of GW170817 and GW190425 using Bayesian parameter estimation [73].

We use the observations from the Gravitational-Wave Open Science Center [4, 19], waveform templates that include eccentricity [79], and Markov Chain Monte Carlo parameter estimation [109, 73] to measure the eccentricity of the GW170817 and GW190425 when they have a gravitational-wave frequency of 10 Hz. We find that the eccentricity of GW170817 is $e \leq 0.027$ and GW190425 is $e \leq 0.052$ at 90% confidence for a uniform prior on e. Our limit on eccentricity of GW170817 is a factor of two smaller than the limit estimated by its detection with circular waveform templates. We note that when using a common prior on eccentricity, our limit on the eccentricity of GW190425 is a factor of three greater than the limit of Ref. [3]. We find that this is due to a degeneracy between the chirp mass and eccentricity that is not included in the analysis of Ref. [3]. However, this difference does not invalidate their conclusions about the formation of GW190425.

Dynamical interations may form binary neutron stars with residual eccentricity, although the rate of such mergers is expected to be small in current detectors [132, 133] and a search for eccentric binary neutron stars in the O1 and O2 observing

runs did not yield any candidates [153]. However, since eccentricity is an interesting probe of binary formation channels and eccentric binaries may produce different electromagnetic emission than circular binary neutron stars [154, 155], it is important to accurately constrain the eccentricity of binary neutron stars as the number of observed mergers increases in the coming years.

4.2 Methods

We measure the parameters of GW170817 and GW190425 using Bayseian inference [156, 157]. We use gravitational-wave data from Advanced LIGO and Virgo [158, 159], $\boldsymbol{d}(t)$, and a model of the gravitational waves, H, to calculate the posterior probability density function, $p(\boldsymbol{\theta}|\boldsymbol{d}(t), H)$, given by

$$p(\boldsymbol{\theta}|\boldsymbol{d}(t), H) = \frac{p(\boldsymbol{\theta}|H)p(\boldsymbol{d}(t)|\boldsymbol{\theta}, H)}{p(\boldsymbol{d}(t)|H)}, \tag{4.1}$$

where $\boldsymbol{\theta}$ denotes the parameters of the gravitational waveform, $p(\boldsymbol{\theta}|H)$, is the prior distribution on the signal parameters, and $p(\boldsymbol{d}(t)|\boldsymbol{\theta}, H)$, is the probability of observing the data, known as the likelihood. The likelihood models the noise in the detector as a Gaussian and depends upon a noise-weighted inner product between the gravitational waveform and gravitational-wave data, $\boldsymbol{d}(t)$. Markov Chain Monte Carlo (MCMC) techniques can be used to marginalize over the parameters to obtain the posterior probabilities [108]. Our implementation of Bayesian inferences uses the *PyCBC Inference* software package [73, 160] and the parallel-tempered *emcee* sampler, `emcee_pt` [109, 110].

For GW170817 and GW190425, the MCMC is performed over the component masses of the binary, $m_{1,2}$, the component spins aligned with the orbital angular momentum, $\chi_{1,2}$, the time of coalescence, t_c, the polarization of the GW, ψ, the inclination angle, ι, and the eccentricity, e.

We assume a uniform prior distribution on the component masses, component spins, and coalescence time around the trigger shown in Table 2. We assume an isotropic sky location for GW190425 and a prior uniform in $\sin\iota$ for the inclination angle of both detections. We fix the sky location of GW170817 to the observed EM counterpart using a Gaussian prior distribution on the distance [161]. We explore the

prior distribution on the eccentricity by running the MCMC with two prior distributions: a prior that is uniform in e and a prior uniform in $\log e$ to compare with the GW190425 results found by Ref. [3].

We use the GW strain data from the Advanced LIGO and Virgo detectors for GW170817 and GW190425, available through the LIGO Open Science Center (LOSC) [130]. The `LOSC_CLN_4_V1` data that we use for GW170817 includes post-processing noise-subtraction performed by the LIGO/Virgo Collaboration [158, 162]. The `T1700406_v3` data that we use for GW190425 includes pre-processing glitch removal performed by the LIGO/Virgo Collaboration specifically for use in parameter estimation [19, 159].

We high-pass the data using an eighth-order Butterworth filter with an attenuation of 0.1 at 15 Hz. To conserve the phase of the delay, the filter is applied forward and backwards. A low-pass finite impulse response filter is applied to the data prior to resampling. The data is decimated to 2048 Hz for the analysis. For computing the likelihood, we use Welch's method to estimate the detector's noise power spectral density (PSD). Welch's method is used with 16 second Hanning windowed segments that are overlapped by 8 seconds. The PSD is shortened to 8 seconds in the time domain [86]. The gravitational-wave data, $\boldsymbol{d}(t)$, used in the likelihood is taken from the intervals shown in Table 2. The gravitational-wave likelihood is evaluated from a low-frequency cutoff of 20 Hz to the Nyquist Frequency of 1024 Hz.

A variety of waveforms are available that model eccentricity [77, 78, 79, 80, 81, 82, 83, 84]. From what we know of binary neutron star mergers, we expect them to have low mass, spin, and eccentricity making TaylorF2Ecc a suitable waveform. The waveform model, H, is TaylorF2Ecc, a TaylorF2 post-Newtonian (pN) model with eccentric corrections. We use the LIGO Algorithm Library implementation [106] accurate to 3.5 pN order in orbital phase [163], 3.5 pN order in the spin-orbit interactions [164], 2.0 pN order in spin-spin, quadrupole-monopole, and self-interactions of individual spins [165, 166], and 3.0 pN order in eccentricity [79]. Since TaylorF2Ecc follows TaylorF2 in its construction, the waveform will terminate at twice the orbital frequency of a particle at the innermost stable circular orbit of a Schwarzschild black hole.

As a check on our analysis, we estimate the parameters of GW170817 and GW190425 using two available waveforms: the TaylorF2Ecc waveform at $e = 0$ and the TaylorF2 waveform. Our analyses are consistent with each other and with the parameters

estimated by Advanced LIGO and Virgo [4, 19].

4.3 Results

We first constrain the level of the eccentricity by using the TaylorF2Ecc waveform and a prior uniform in e. We find that the 90% credible intervals at 10 Hz for GW170817 and GW190425 are $e = 0.013^{+0.014}_{-0.011}$ and $e = 0.028^{+0.024}_{-0.024}$ respectively. A degeneracy between the chirp mass, $\mathcal{M}$, and eccentricity, e and a small correlation between the effective spin, $\chi_{\rm eff}$, and e are shown in our posterior distributions in Figure 7 and Figure 8. Since $\mathcal{M}$ and $\chi_{\rm eff}$ are correlated [167, 168], this will create a small correlation between e and $\chi_{\rm eff}$.

Ref. [3] estimated the eccentricity of GW190425 to determine if the formation channel was due to unstable BB mass transfer. They estimate the eccentricity induced by the supernova kick in this formation scenario to be between 10^{-6} and 10^{-3} at 10 Hz. To find the eccentricity of GW190425, Ref. [3] reweight the posterior samples from the parameter estimation performed using circular binaries to estimate the limit of the eccentricity using the same method used to estimate the eccentricity of binary black holes [117]. They estimate the eccentricity of GW190425 at 10 Hz to be $e \leq 0.007$ (90% confidence) using a prior uniform in $\log e$. They find no evidence for or against unstable BB mass transfer as their analysis is not able to distinguish the small residual eccentricity expected from the investigated formation channel.

To more directly compare our limit on GW190425's eccentricity, we repeat our analysis using a $\log e$ prior. In Figure 9 we can see the differences in the posterior distributions of each prior. With the $\log e$ prior we estimate the eccentricity at 10 Hz to be $e \leq 0.04$. This is a factor of three larger than interval estimated by Ref. [3]. By re-weighting the posterior samples rather than a full MCMC, the degeneracy between $\mathcal{M}$ and e is missed. We find that by excluding posterior samples with lower values of $\mathcal{M}$, we can recover the upper limit reported by Ref. [3]. Although our limit on the eccentricity is larger than that of Ref. [3], our result does not change their conclusion: indeed the strong dependence of the eccentricity posterior on the prior seen in Figure 9 agrees with their conclusion that the signal-to-noise ratio of GW190425 is not large enough to explore the eccentricities expected in BB mass transfer. We would need to be able to determine the eccentricity at lower frequencies to distinguish the formation

channel.

4.4 Conclusion

Our analysis used the gravitational-wave observations as well as a prior on the eccentricity to constrain the eccentricity of GW170817 and GW190425. Our 90% confidence limit using a uniform prior on e for GW170817, $e \leq 0.027$, and GW190425, $e \leq 0.052$, are consistent with expectations since they were found by a circular search [25]. We have constrained the eccentricity to a factor of two smaller than estimates obtained from circular searches [67, 68]. Our 90% credible intervals on the eccentricity of GW190425 are a approximately a factor of six larger than the interval estimated by [3], which used a prior uniform in $\log e$. This demonstrates the impact of prior choice, and the importance of measuring the eccentricity of signals using full parameter estimation to account for the correlation between parameters.

Unfortunately, based on current merger rate estimates the detection of an eccentric binary neutron star merger will be difficult with current observatories [132, 133, 153], but gravitational-wave capture binaries that have $e \geq 0.8$ and could form in the LIGO-Virgo band [62, 169]. However, since the eccentricity of the detections is expected to be low and negligible, $e \leq 0.02$, a circular search is effective in detecting them [67, 68].

Current waveform models are effective for detection as spin and eccentricity are assumed to be low, but that might not be the case for future gravitational-wave signals. Future signals may have high eccentricity and spin and will need further corrections to be able to detect them efficiently and produce unbiased parameter estimates. Waveforms that better model eccentric signals will need to be developed before we are able to make a detection of a merger with a high eccentricity or spin. The detection of a binary neutron star mergers with high eccentricity or spin in future observing runs and with third generation detectors will reveal more about the formation channel of eccentric binaries and the existence of a dynamical formation channel.

Parameters	**GW170817**	**GW190425**
Component Masses ($M_\odot$)	[1.0,3.0]	[1.0,3.0]
Component Spins	[-0.05,0.05]	[-0.05,0.05]
Coalescence Time (s)	[1187008882.33,1187008882.53]	[1240215502.917,1240215503.117]
Polarization	[0,2π]	[0,2π]
Inclination Angle	$\sin\iota$	$\sin\iota$
Distance (Mpc)	40.7 $\pm$ 2.36 [161]	uniform in comoving volume
RA/Dec ($^\circ$)	3.44615914, -0.40808407 [170, 171]	[$-\pi/2$,$\pi/2$]
Eccentricity	[0.0,0.1]	[0.0,0.1]
PSD Estimation Interval (s)	[1187008382,1187008918]	[1240215003,1240215543]
Likelihood Interval (s)	[1187008692,1187008892]	[1240215313,1240215513]

Table 2: Prior distributions and GPS time intervals for GW170817 and GW190425.

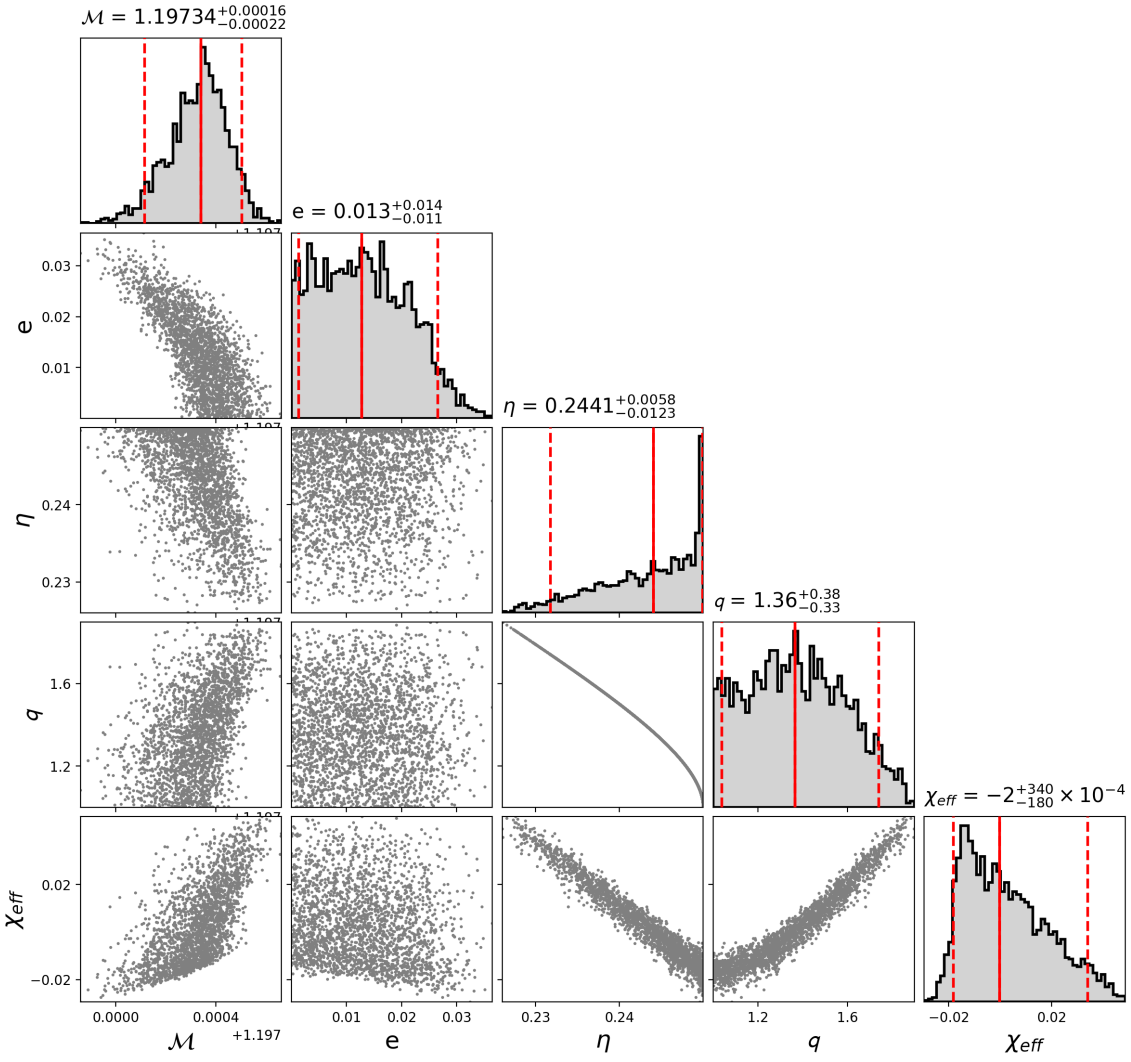

Figure 7: Posterior probability distribution of GW170817 at 10 Hz. The analysis used a prior uniform in e. Each parameter is quoted with a median value (solid red line) and a 90% credible interval (dashed red lines). The chirp mass $\mathcal{M}$ is given in the detector frame. Note the degeneracy between $\mathcal{M}$ and e.

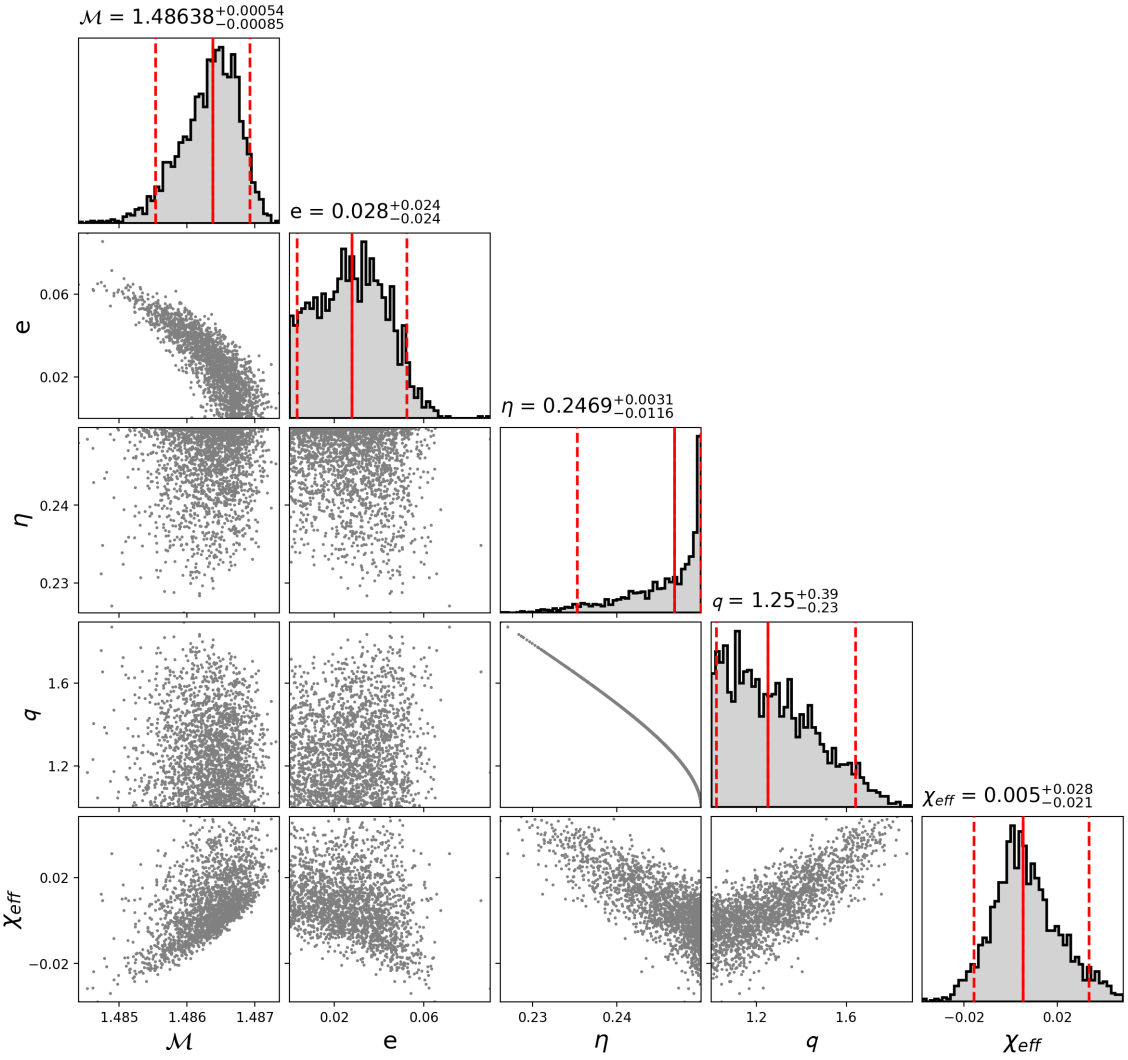

Figure 8: Posterior probability distribution of GW190425 at 10 Hz. The analysis used a prior uniform in e. Each parameter is quoted with a median value (solid red line) and a 90% credible interval (dashed red lines). The chirp mass $\mathcal{M}$ is given in the detector frame. Note the degeneracy between $\mathcal{M}$ and e.

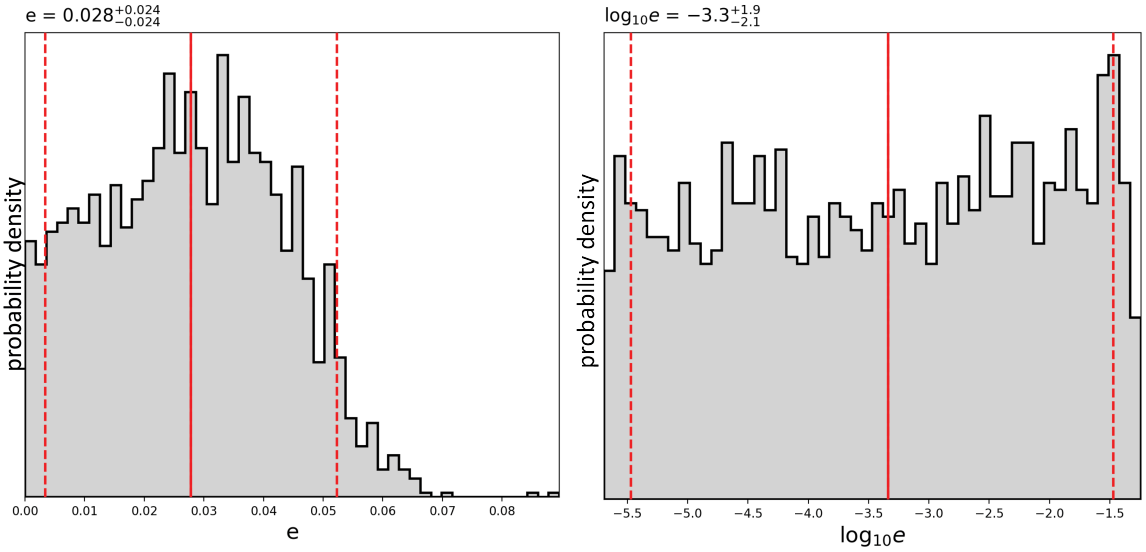

Figure 9: Eccentricity posteriors of GW190425 (solid black line) plotted against their priors (dotted line) for two choices of prior: uniform in e (left) and uniform in $\log_{10}(e)$ (right). We quote the median (solid red line) and 90% credible interval (dashed red lines) for e in each posterior. The prior uniform in $\log_{10}(e)$ has the same distribution as the prior used in the Ref. [3] analysis.

Chapter 5

Eccentric Binary Neutron Star Search Prospects for Cosmic Explorer

We determine the ability of Cosmic Explorer, a proposed third-generation gravitational-wave observatory, to detect eccentric binary neutron stars and to measure their eccentricity. We find that for a matched-filter search, template banks constructed using binaries in quasi-circular orbits are effectual for eccentric neutron star binaries with $e_7 \leq 0.004$ ($e_7 \leq 0.003$) for CE1 (CE2), where e_7 is the binary's eccentricity at a gravitational-wave frequency of 7 Hz. We show that stochastic template placement can be used to construct a matched-filter search for binaries with larger eccentricities and construct an effectual template bank for binaries with $e_7 \leq 0.05$. We show that the computational cost of both the search for binaries in quasi-circular orbits and eccentric orbits is not significantly larger for Cosmic Explorer than for Advanced LIGO and is accessible with present-day computational resources. We investigate Cosmic Explorer's ability to distinguish between circular and eccentric binaries. We estimate that for a binary with a signal-to-noise ratio of 20 (800), Cosmic Explorer can distinguish between a circular binary and a binary with eccentricity $e_7 \gtrsim 10^{-2}$ (10^{-3}) at 90% confidence.

5.1 Introduction

Cosmic Explorer is a proposed third-generation gravitational-wave observatory that will have an order of magnitude improved sensitivity beyond that of Advanced LIGO and will be able to explore gravitational-wave frequencies below 10 Hz [2]. Cosmic Explorer will be able to detect binary neutron stars with a signal-to-noise ratio of ≥ 8 out to a distance of ~ 2 Gpc [172]. Although most of the detected neutron-star binaries will be in circular orbits, measurement of eccentricity in neutron-star mergers allows us to explore their formation and to distinguish between field binaries, which are expected to be circular by the time they are observed [25], and binaries formed through other channels [41, 42, 43, 69, 48, 49, 173, 28, 174, 44, 45, 46, 47, 33].

Dynamical interactions can form binary neutron stars with eccentricity that is measurable, although the predicted rate of these mergers detectable by current gravitational-wave observatories is small [132, 133]. The two binary neutron star mergers observed by Advanced LIGO and Virgo [4, 19] were both detected with searches that use circular waveform templates [87, 86, 89, 90, 88, 175, 176, 177, 178]. Constraints have been placed on the eccentricity of these binaries. At a gravitational-wave frequency of 10 Hz, the eccentricity of GW170817 is $e_{10} \leq 0.024$ [5] and GW190425 has an eccentricity $e_{10} \leq 0.048$ [3, 5] (90% confidence). Ref. [3] considered unstable mass transfer as a formation scenario for GW190425, but the measured eccentricity limit was insufficient to confirm this hypothesis. A search for eccentric binary neutron stars in the first and second Advanced LIGO and Virgo observing runs did not yield any candidates [153].

By extrapolating the upper limit on the rate of eccentric binary neutron stars from LIGO–Virgo observations, Ref. [153] estimates that the A+ upgrade [40] of Advanced LIGO will require between half a year of observation and $\sim$ 775 years of observation before the detectable rate is comparable with the optimistic [132] and pessimistic [133] rate predictions respectively, and an observation is plausible. However, with its increased sensitivity and bandwidth, Cosmic Explorer would need at most half a year of observations to achieve a detectable rate comparable to even the pessimistic models [153].

We investigate the ability of Cosmic Explorer to detect eccentric binary neutron stars and to measure their eccentricity. We find that at an eccentricity $e_7 = 0.004$, a

matched-filter search using circular waveform templates begins to lose more than 3% of the signal-to-noise ratio due to mismatch between the circular and eccentric waveforms; this is an order of magnitude smaller than the equivalent limit for Advanced LIGO [67, 68]. We demonstrate that stochastic template placement [95, 96] can be use to construct a template bank that maintains a fitting factor greater than 97% to binaries with $e_7 \leq 0.05$. We will reference eccentricity at a reference frequency of We will use a reference frequency of 7 Hz in reference to eccentricity unless otherwise stated.

Using template banks constructed for Cosmic Explorer, we estimate the computational cost of matched-filter searches for binary neutron stars in circular and eccentric orbits and find that both are accessible with present-day computational resources. We then estimate the ability of Cosmic Explorer to measure and constrain the eccentricity of detected binary neutron star systems. For a binary neutron star with signal-to-noise ratio 8 (800), Cosmic Explorer will be able to measure eccentricities $\gtrsim 8 \times 10^{-3}$ (8×10^{-4}).

This chapter is organized as follows: In Sec. 5.2, we investigate the ability of a matched-filter search to detect eccentric binary neutron stars in Cosmic Explorer. We calculate the lower-frequency cutoff required to obtain at least 99.9% of the available signal-to-noise ratio for binary neutron stars ($m_{1,2} \in [1, 3]\,\mathrm{M}_\odot$). Using this frequency cutoff, we use geometric placement to construct a template bank using circular waveform for Cosmic Explorer that has a fitting factor of 97% and estimate the computational cost of performing a matched-filter search using this bank. In Sec. 5.3 we measure the loss in fitting factor when using a bank of circular waveform with neutron-star binaries with eccentricity $e \leq 0.05$. We use stochastic template placement to generate a bank containing circular and eccentric waveforms than has a fitting factor of 96.5% and estimate the computational cost of this eccentric binary search. In Sec. 5.4, we estimate the minimum eccentricity that can be measured by Cosmic Explorer as a function of the signal-to-noise ratio of the detected signal. We compare this to estimates of Advanced LIGO and the eccentricity constraints placed by the detection of GW170817. Finally, in Sec. 5.5, we discuss the implications our results for measurement of eccentric binaries with Cosmic Explorer and extension of our work to higher eccentricities and binary black holes.

5.2 Binary Neutron Star Searches in Cosmic Explorer

CCosmic Explorer has a two-stage design [39, 2]. The first stage of Cosmic Explorer (CE1) assumes that the detector's core technologies will be similar to those of Advanced LIGO with the sensitivity gain from increasing the detector's arm length from 4 km to 40 km. The second stage (CE2) is a technology upgrade to the CE1 detector that further increases Cosmic Explorer's sensitivity. Estimates of the detector's noise power spectral density $S_n(f)$ are available for both CE1 and CE2 [179]; we consider both detector configurations in our analysis.

Compared to the low-frequency sensitivity limit of Advanced LIGO, which lies around 10 Hz, Cosmic Explorer pushes the low-frequency limit of the detector below this limit [2]. As for Advanced LIGO, the detector noise begins to rapidly increase as the gravitational-wave frequency reaches the seismic and Newtonian noise walls at low-frequency. The length of a binary neutron star waveform has a steep power-law dependence on its starting frequency $f_{\rm lower}$, with the number of cycles between $f_{\rm lower}$ and the coalescence frequency scaling as $f_{\rm lower}^{-8/3}$. A binary neutron star waveform that starts at $f_{\rm lower} = 3$ Hz has a length of approximately 7 hours, presenting non-trivial data analysis challenges in searches and parameter estimation.

To determine the optimal starting frequency for binary neutron star searches in Cosmic Explorer, we consider the accumulation of the the signal-to-noise ratio in a matched filter search for a neutron star binary with $m_1 = m_2 = 1.4\,M_\odot$; this accumulates as $f^{-7/3}/S_n(f)$ where f is the gravitational-wave frequency [156, 86]. Fig. 10 shows the normalized signal-to-noise ratio integrand at a given frequency for Cosmic Explorer and Advanced LIGO. Advanced LIGO's most sensitive frequency lies around 40 Hz with almost no detectable signal below 10 Hz. For CE1 and CE2, the peak sensitivity of the detectors to binary neutron stars is shifted to lower frequencies, with a non-trivial amount of signal-to-noise available below 10 Hz. The fraction of signal-to-noise available drops rapidly as the frequency decreases due to the low-frequency noise wall of Cosmic Explorer.

To determine the optimal low-frequency cutoff, we consider the cumulative fraction of the total signal-to-noise ratio as a function of low-frequency cutoff, shown in Fig. 11. This is computed by comparing the ratio of the signal-to-noise obtained by integrating from 3 Hz to a fiducial low-frequency cutoff shown on the ordinate

of Fig. 11. We find that for both the CE1 and CE2 detector sensitivity curves, the matched filter accumulates 99.97% (99.53%) of the signal-to-noise above 7 Hz for CE1 (CE2). We therefore use 7 Hz as an appropriate low-frequency cutoff for our analysis. At this starting frequency, the length of a binary neutron star waveform is reduced by two orders of magnitude to 4600 s (77 minutes). For a waveform of this length, the Doppler frequency modulation due to the diurnal and orbital motion is $(\Delta f/f) \sim 10^{-8}$ and can be neglected in search algorithms. Several search algorithms already exist that can search for waveforms of this length in a computationally efficient manner [180, 175, 176]. Similarly, the time dependence of the antenna response due to the Earth's rotation can be neglected as the match between a waveform that neglected the time variation and a waveform that accounted for the variation is 98-99%. For comparison, we show the same result for the proposed E.U. third-generation detector Einstein Telescope [181]. We focus on Cosmic Explorer in this work as we have found that existing methodologies are sufficient to effectively address the challenges presented by the increased low-frequency sensitivity of the third generation observatory. Einstein Telescope has a significantly lower seismic–Newtonian-noise wall than Cosmic Explorer and so searches must be pushed to lower frequencies to accumulate all of the possible signal-to-noise ratio. For an optimal search of Einstein Telescope, this may require addressing how to best account for the time-dependent detector response.

Using a 7 Hz low-frequency cutoff, we generate a template bank that can be used to search for binary neutron star mergers with component masses $1.0\,\mathrm{M}_\odot \leq m_1, m_2 \leq 3.0\,\mathrm{M}_\odot$. We first generate a template bank for binaries with zero eccentricity and component spin using the standard hexagonal lattice method of template placement [91, 92, 93, 94]. The template bank is constructed so that it has a fitting factor of 97% [182]. We find that the number of templates required for the CE1 (CE2) sensitivity is $130,000$ $(209,000)$ to achieve a fitting factor of 97%. A template bank generated using the Advanced LIGO sensitivity and a 10 Hz low-frequency cutoff contains $77,000$ points. Since the CE1 (CE2) template banks are only a factor of 1.7 (2.8) larger than the equivalent template bank for Advanced LIGO, we do not expect significant computational challenges executing these searches. We certainly expect no obstacles to implementing real-time searches a decade or more from now when Cosmic Explorer will be operational.

Before constructing a template bank for binaries with eccentricity, we determine how effective the non-eccentric template bank is at detecting signals from eccentric binary neutron star sources. We measure the match $M = max_{\phi,t}(s|h)/(\hat{s}\hat{h})$ between a random set of eccentric gravitational-wave signals s and the templates h, where hat denotes the normalized waveform and the match is maximized over the intrinsic parameters time t and phase ϕ [156, 86]. We maximize the match for each template over the bank to obtain the bank's fitting factor to a population of eccentric signals [182]. The maximum loss in signal-to-noise ratio that the bank will incur due to its discretization is $1 - \mathcal{F}$.

To model eccentric sources, we use the LIGO Algorithm Library implementation [106] of TaylorF2Ecc, a frequency-domain post-Newtonian model with eccentric corrections. This waveform is accurate to 3.5 pN order in orbital phase [163], 3.5 pN order in the spin-orbit interactions [164], 2.0 pN order in spin-spin, quadrupole-monopole, and self-interactions of individual spins [165, 166], and 3.0 pN order in eccentricity [79]. To model non-eccentric waveforms, we use the restricted TaylorF2 approximant, accurate to the same post-Newtonian order. TaylorF2Ecc does not include the merger and ringdown signal or evolution of the argument of periapsis. Since our study is restricted to binary neutron star waveforms, the merger and ringdown occur at frequencies of order 10^3 Hz, which is significantly above the frequencies where the majority of the signal-to-noise ratio is accumulates, as shown in Fig. 10. Since we restrict our study to relatively low eccentricites, we neglect $\mathcal{O}(e)$ corrections to the waveform amplitude and oscillatory contributions to the waveform phase and hence the argument of periapsis does not enter the waveform computation Ref. [79] has demonstrated that this does not significantly affect the signal for the cases that we study here.

We test the template bank against 120,000 simulated signals that have detector-frame component masses $1.0\,\mathrm{M}_\odot \leq m_1, m_2 \leq 3.0\,\mathrm{M}_\odot$ and eccentricity $0 \leq e \leq 0.05$. The results of the simulation are shown in Fig. 12 and Fig. 13 for CE1 and CE2, respectively. If the population of neutron star binaries has eccentricity less than 0.004 (0.003) in CE1 (CE2), then the non-eccentric template banks achieve a fitting factor of 97% and are effectual. However, for sources with larger eccentricities the effectualness of the template bank begins to rapidly decline; the effectualness of a non-eccentric binary neutron star bank fails at an eccentricity an order of magnitude

lower than that of Advanced LIGO [67, 68]. To recover these signals, it is necessary to construct a template bank that captures eccentricity. We consider this in the next section.

5.3 Extension to Eccentric Template Banks

The number of templates in an eccentric bank will depend on the bandwidth of the detector and the upper eccentricity boundary of the bank. To visualize the dependency on detector bandwidth, Fig. 14 shows the eccentricity ambiguity function for a $m_1 = m_2 = 1.4\,\mathrm{M}_\odot$ binary. This shows how quickly the loss in signal-to-noise ratio (match) changes as the eccentricity increases from 0 to 0.4 (referenced to 7 Hz). Without the use of eccentric templates, the match for CE1 (CE2) decreases to 34% (30%) at $e = 0.05$. In contrast, the Advanced LIGO match decreases much more slowly, reaching 38% at $e = 0.4$. Consequently, the density of an eccentric template bank will be significantly greater for Cosmic Explorer than Advanced LIGO.

Searches for eccentric binary neutron stars in Advanced LIGO used a template bank that covers the eccentricity range $0 \leq e \leq 0.4$ (referenced to 10 Hz) [153]; this bank contained $350,000$ templates. To generate template banks of comparable density in eccentricity for Cosmic Explorer, we set the upper eccentricity of the template bank to $e = 0.05$ and keep the mass boundaries at $1.0\,\mathrm{M}_\odot \leq m_1, m_2 \leq 3.0\,\mathrm{M}_\odot$ and the lower-frequency cutoff at 7 Hz. We then generated a template bank for eccentric gravitational-wave signals in this region using the stochastic placement method [95, 96] with a fitting factor of 96.5%.

We test the eccentric template bank against $25,000$ simulated signals with detector-frame component masses uniformly distributed between $1.0\,\mathrm{M}_\odot \leq m_1, m_2 \leq 3.0\,\mathrm{M}_\odot$ and eccentricity uniformly distributed between $0 \leq e \leq 0.05$. The resulting fitting factor of these bank is shown in Fig. 15, with the fitting factor of the non-eccentric bank as reference. This result shows that the stochastic bank placement is effectual for signals with eccentricity in the target region, as all signals can be recovered with a fitting factor of $\gtrsim 95\%$ both the CE1 and CE2 banks. The number of eccentric templates generated using the CE1 (CE2) sensitivity is $1,900,000$ $(6,400,000)$, an order of magnitude larger than the non-eccentric template banks for CE and an order of magnitude larger than the the Advanced LIGO eccentric bank. We consider the

size of a template bank with $e_{max} = 0.1$ to determine the increase in templates as eccentricity increases. A template bank with $0 \leq e \leq 0.1$ has $4,500,000$ templates using the CE1 sensitivity, this is twice the size of the template bank we consider in this work. We expect that a bank of this size will present no computational challenges when Cosmic Explorer is operational in the 2030s; searches of similar magnitude are already regularly performed [183, 184].

5.4 Binary Neutron Star Parameter Estimation in Cosmic Explorer

We can use our results to estimate the constraints that Cosmic Explorer will be able to place on the eccentricity of detected binary neutron stars with parameter estimation. We express this as the signal-to-noise ratio required to distinguish between an eccentric and circular binary at 90% confidence. This can be interpreted as the minimum detectable eccentricity at a given signal-to-noise ratio, or the upper limit that can be placed on the eccentricity of a circular binary detected at a given signal-to-noise ratio.

To estimate the signal-to-noise required to distinguish between a circular binary and a binary with eccentricity e at 90% confidence, we use the method of Baird *et al.* [167]. This method relies on the fact that parameter estimation identifies regions of parameter space where a waveform is most consistent with the data. Ref. [167] uses the fact that high confidence regions in parameter estimation are associated with regions of high match between signal and template to obtain a relationship between the match and signal-to-noise ratio ρ, given by

$$M(h(\theta), h(\langle\theta\rangle)) \geq 1 - \frac{\chi_k^2(1-p)}{2\rho^2} \tag{5.1}$$

where k is the dimension of the parameter space of interest, $\chi^2(1-p)$ is the chi-square value for which there is $1-p$ probability of obtaining that value or larger. Here, we set $k = 4$ corresponding to intrinsic parameter space of an aligned spin binary neutron star merger with eccentricity $(m_1, m_2, \chi_{\rm eff}, e)$, where $\chi_{\rm eff}$ is the effective spin of the binary, and $p = 0.9$ for 90% confidence.

For Eq. (5.1) to provide a reasonable estimate of the signal-to-noise ratio, the match M must be maximized over the parameters of the signal. For eccentric binaries,

there is a known degeneracy between the chirp mass $\mathcal{M} = (m_1 m_2)^{3/5}/(m_1+m_2)^{1/5}$ of the binary and the eccentricity [65, 5]. Full parameter estimation naturally explores the likelihood and this degeneracy. Here, we use our method of eccentric template placement to place a fine grid of templates and brute-force maximize the match over this template bank to account for the chirp mass–eccentricity degeneracy.

Using this method, we estimate Cosmic Explorer's ability to constrain the eccentricity of a $m_1 = m_2 = 1.4\,\mathrm{M}_\odot$ binary as follows: Using a low frequency cutoff of 7 Hz, we generate a template bank with binary neutron star component masses $1.399\,\mathrm{M}_\odot \leq m_1, m_2 \leq 1.401\,\mathrm{M}_\odot$, eccentricity $0 \leq e \leq 0.05$, an upper-frequency cutoff of 4096 Hz, and a minimal match of 99.9999%. We measure the match between a simulated eccentric gravitational-wave signal with component masses $m_1 = m_2 = 1.4\,\mathrm{M}_\odot$ and eccentricity $0 \leq e \leq 0.05$ and maximize over the chirp mass in the template bank to get the signal-to-noise ratio. From this we determine the signal-to-noise ratio needed to reach a 90% confidence interval [167] to measure the eccentricity.

We apply the above method using the CE1, CE2, and Advanced LIGO design noise curves to obtain the signal-to-noise ratio as a function of eccentricity required to distinguish between a circular and eccentric binary. To check the accuracy of our estimation, we also compute this function using the detector noise around the time of GW170817 and compare the Baird *et al.* [167] estimate to the 90% upper limit on the eccentricity of GW170817 computed using full parameter estimation [5]. These result are shown in Fig. 16. First, we note that our method provides a reasonable approximation when comparing to GW170817 and as the eccentricity increases the signal-to-noise ratio needed to resolve the signal decreases, as expected. Our results suggest that for $e \geq 5 \times 10^{-3}$ (8×10^{-4}), a minimum signal-to-noise ratio of 20 (800) would be needed to resolve the signal at 90% confidence in CE1 and CE2. This is an order of magnitude better than expected from Advanced LIGO operating at design sensitivity.

5.5 Conclusion

Our analysis used circular and eccentric template banks to determine the ability of Cosmic Explorer to detect eccentric binary neutron stars and to measure their eccentricity. The circular template banks are effective for detecting eccentric binaries with

$e \leq 0.004$ ($e \leq 0.003$) in CE1 (CE2) at a reference frequency of 7 Hz. However, for larger eccentricities a template bank containing circular and eccentric waveform templates is required. This estimate is an order of magnitude smaller than estimates for Advanced LIGO [67, 68]. We determine the signal-to-noise ratio needed to constrain the eccentricity of a detected neutron star binary signal with 90% confidence. We also estimate that in Cosmic Explorer to measure binary neutron star with eccentricity $\gtrsim 5 \times 10^{-3}$ (8×10^{-4}) a signal-to-noise ratio of 20 (800) is needed to resolve the signal at a reference frequency of 7 Hz (90% confidence). Our method of estimation relies on the calculation of Baird *et al.* [167]; an accurate determination of this limit requires a full parameter estimation study with accurate eccentric merger waveforms, which is the subject of future work. Accurately constraining the eccentricity of the binary would provide valuable information on the formation of these mergers.

The computational cost of searches with template banks containing higher eccentricities will be challenging in Cosmic Explorer today as the density of the template bank increases with increasing eccentricity (see Fig. 2 of Ref. [153]). However, improvements in technology by the 2030s may make these searches a possibility. Along with the high computational cost, current waveform models for eccentricity break down for $e \geq 0.4$. To accurately search for higher eccentricity neutron-star binaries models that extend to high eccentricities will need to be developed or a burst search will need to be used. In this analysis, we have only considered binary neutron star signals where the measurement of eccentricity is dominated by the inspiral signal. Using an eccentric merger-ringdown waveform [77] an overlap method similar to the method used here, Ref. [185], predict that Cosmic Explorer will be able to distinguish between circular and eccentric waveforms with $e \gtrsim 2 \times 10^{-4}$ for signal-to-noise ratios of order 200. More detailed studies with full parameter estimation and accurate waveforms [78, 80, 81, 123, 82] will be required to further explore these predictions. Understanding the constraints that future observational limits place on eccentric binary formation channels will require computation of the rate as a function of eccentricity from population synthesis. As Cosmic Explorer will be able to aid in the understanding of the physics of binary neutron star mergers it is important to accurately constrain the eccentricity as the number of mergers increases.

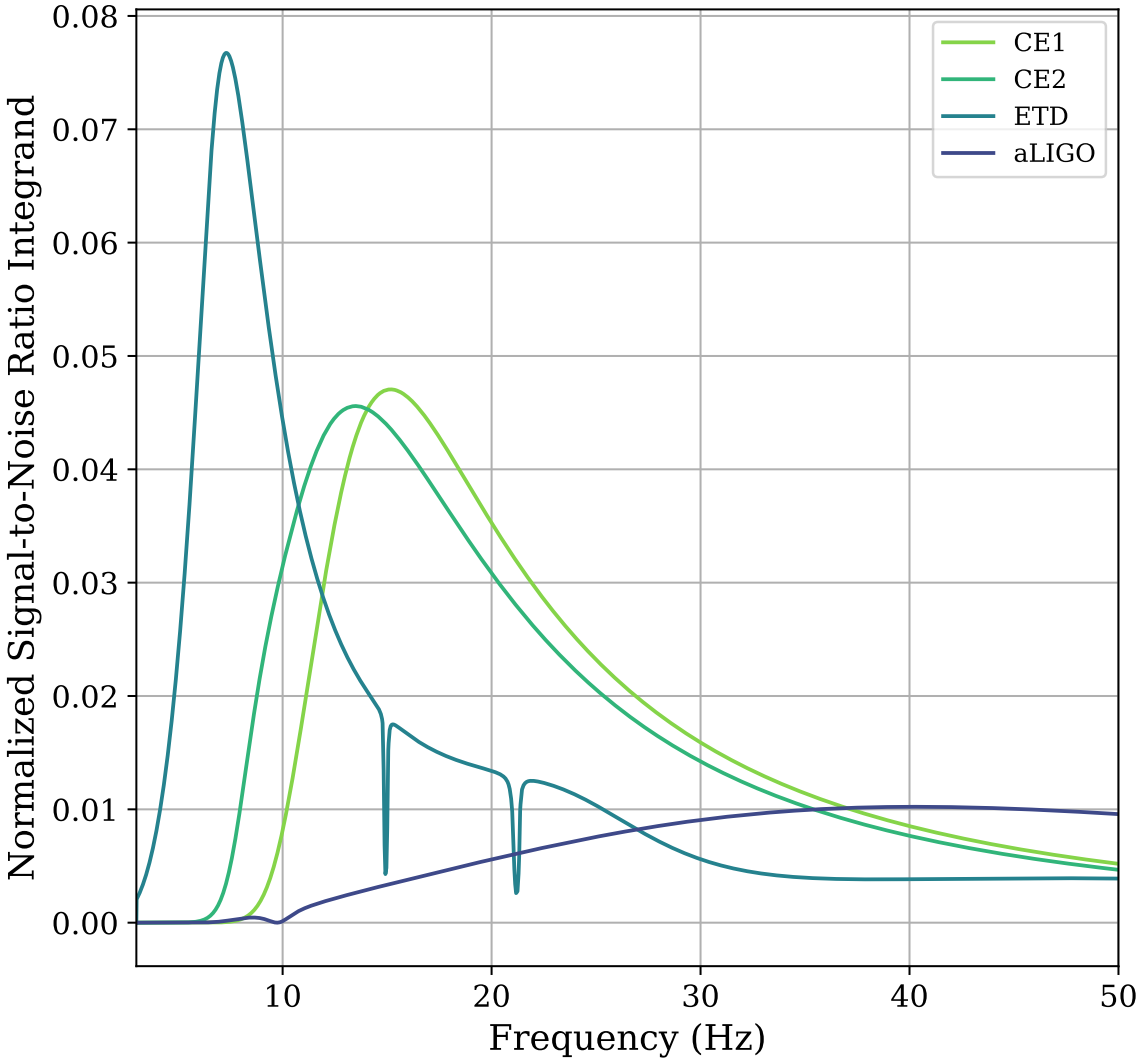

Figure 10: The normalized signal-to-noise ratio integrand as a function of frequency for Cosmic Explorer (CE1/CE2), Einstein Telescope (ETD) and Advanced LIGO (aLIGO). This gives a visual representation of what the matched filter sees when it is integrating up the signal-to-noise ratio. A majority of the signal-to-noise ratio for Cosmic Explorer and Advanced LIGO is accumulated between 10 and 50 Hz, while the signal-to-noise ratio for Einstein Telescope is accumulated below 10 Hz.

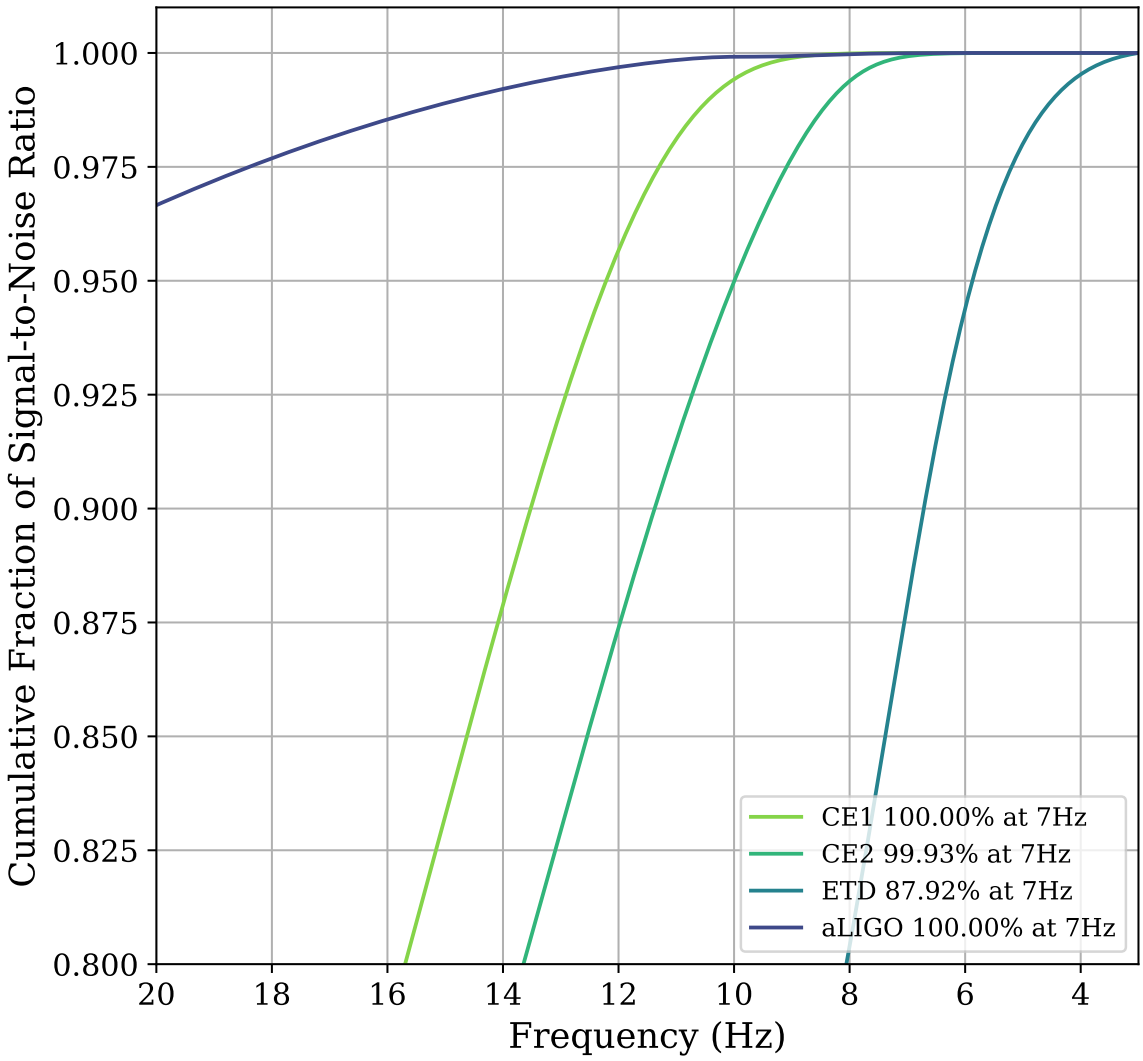

Figure 11: The cumulative fraction of signal-to-noise ratio as a function of frequency. Cosmic Explorer (CE1/CE2) and Advanced LIGO (aLIGO) have accumulated more than 99.9% of their total signal-to-noise ratio from frequencies above 7 Hz. At 7 Hz, Einstein Telescope (ETD) accumulated more than 85% of their total signal-to-noise ratio. Since more than 99.9% of the total signal-to-noise ratio is accumulated, we use a low-frequency cutoff of 7 Hz to generate the waveforms in our template banks.

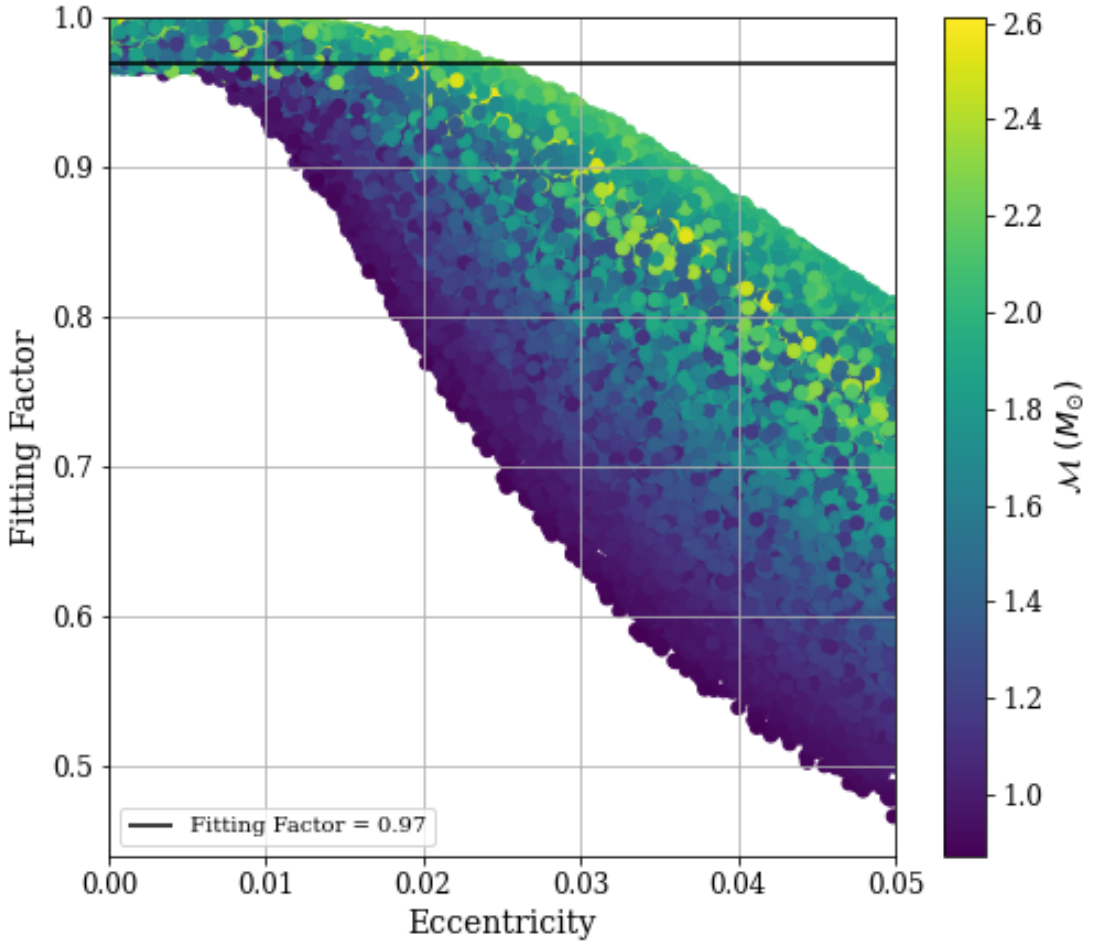

Figure 12: The fitting factor as a function of eccentricity correlated with chirp mass for CE1. A non-eccentric template bank was used to calculate the fitting factor. For Cosmic Explorer the fitting factor decreases for increasing values of eccentricity. The non-eccentric template bank is effective in detecting eccentric systems with a fitting factor greater than 97% for $e \lesssim 0.004$.

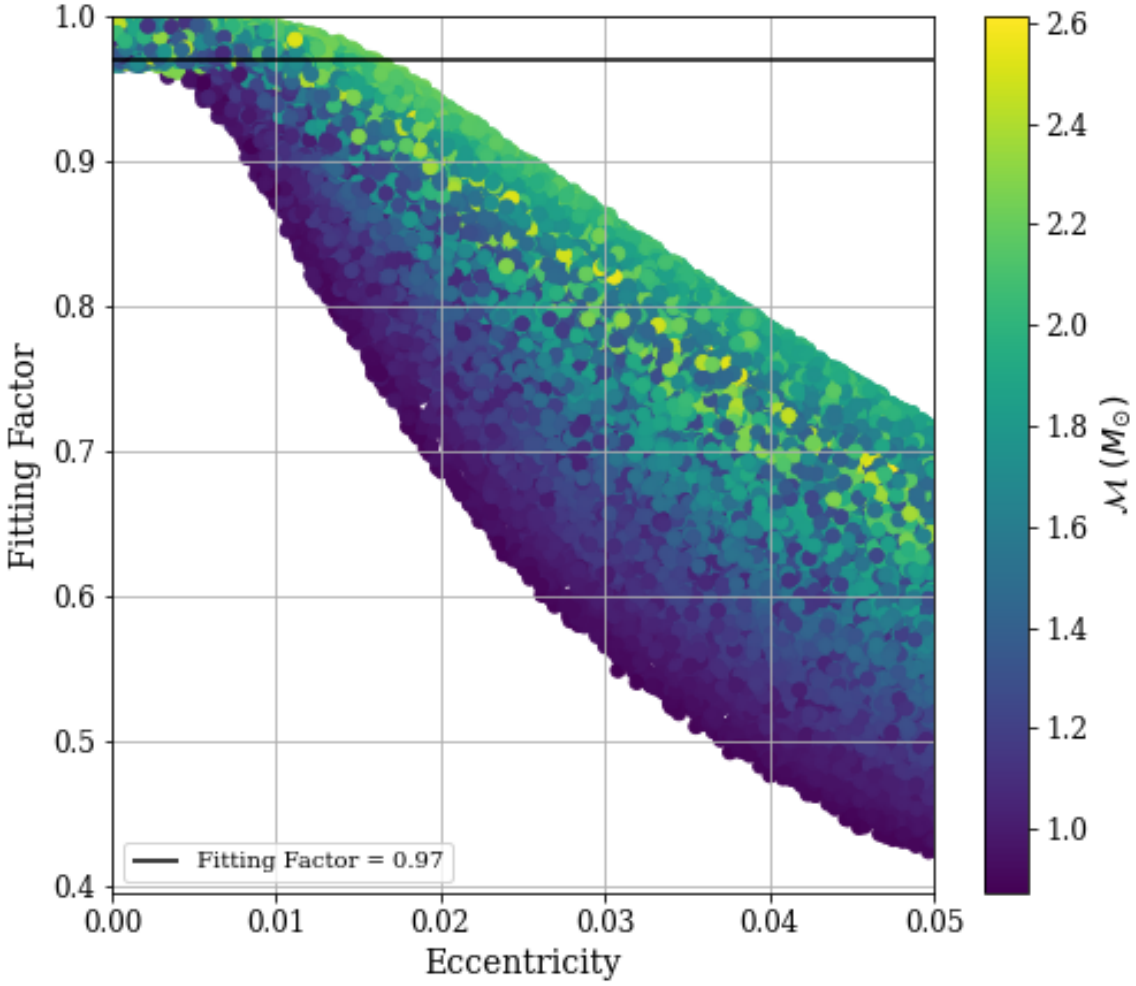

Figure 13: As in Fig. 12, but we use the CE2 noise curve. A non-eccentric template bank was used to calculate the fitting factor. The non-eccentric template bank is effective in detecting eccentric systems with a fitting factor greater than 97% for $e \lesssim 0.003$.

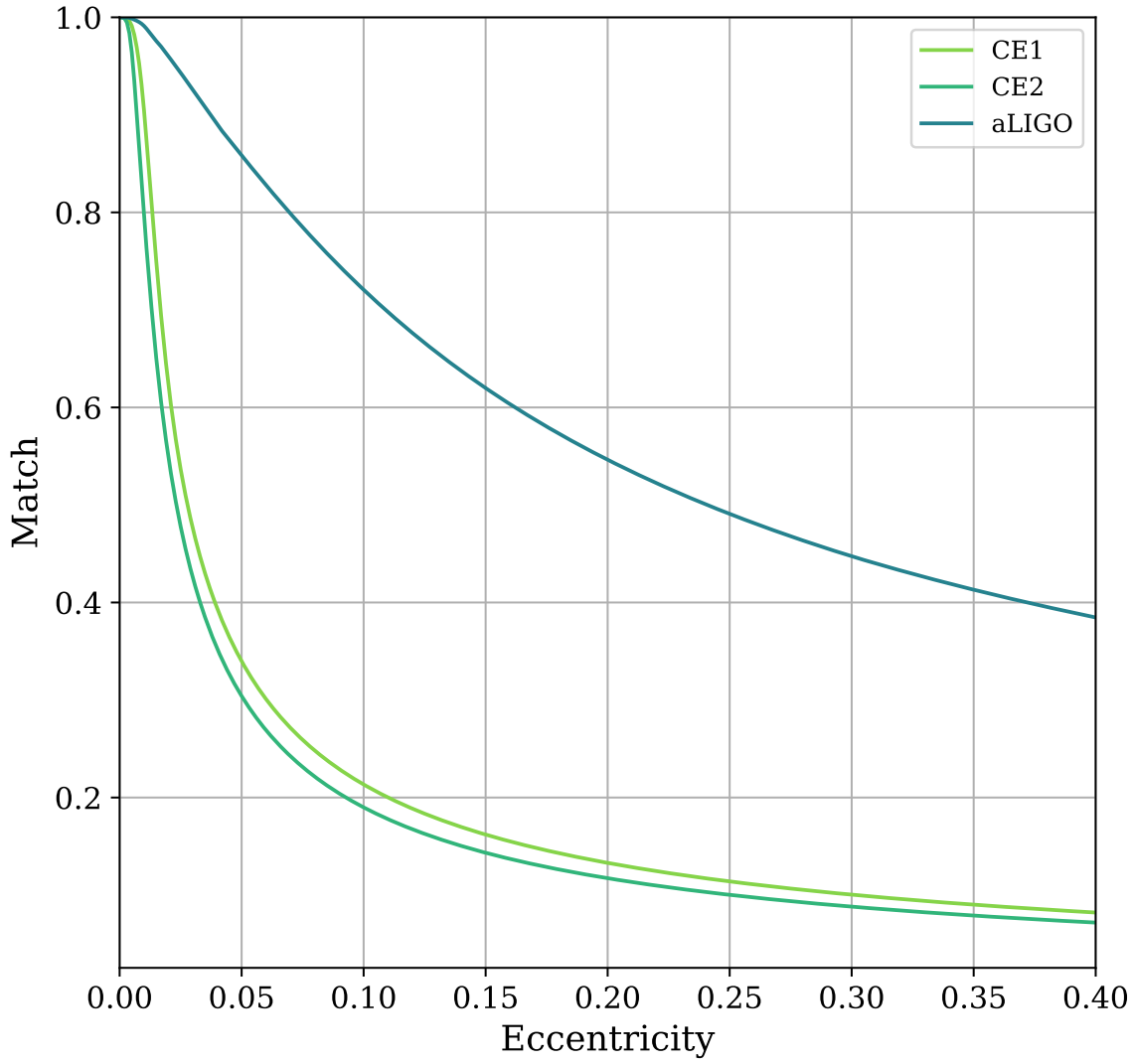

Figure 14: The match as a function of eccentricity for Cosmic Explorer (CE1/CE2) and Advanced LIGO (aLIGO). This gives a representation of the match between an circular waveform and an eccentric waveform for various eccentricities. The match for Cosmic Explorer at an eccentricity of 0.05 is about a factor of 3 smaller than that of Advanced LIGO.

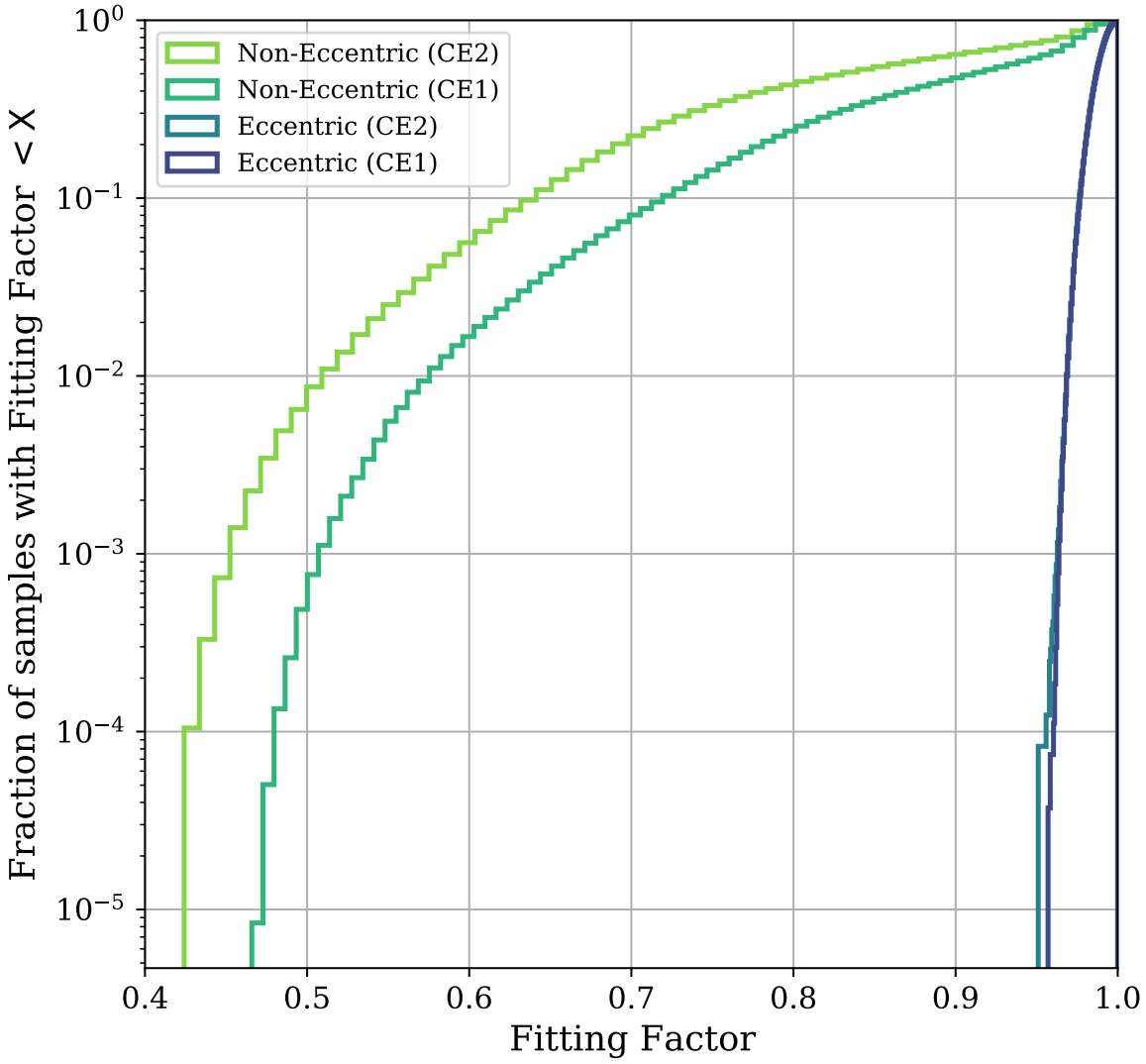

Figure 15: A cumulative histogram that shows the fraction of points where the fitting factor is less than the value on the x-axis for each template bank. Using the eccentric template bank, a majority of the samples are at a fitting factor $\gtrsim 95\%$. For our eccentricity range, the eccentric template banks appear to do a better job at detecting eccentric systems than the non-eccentric template banks.

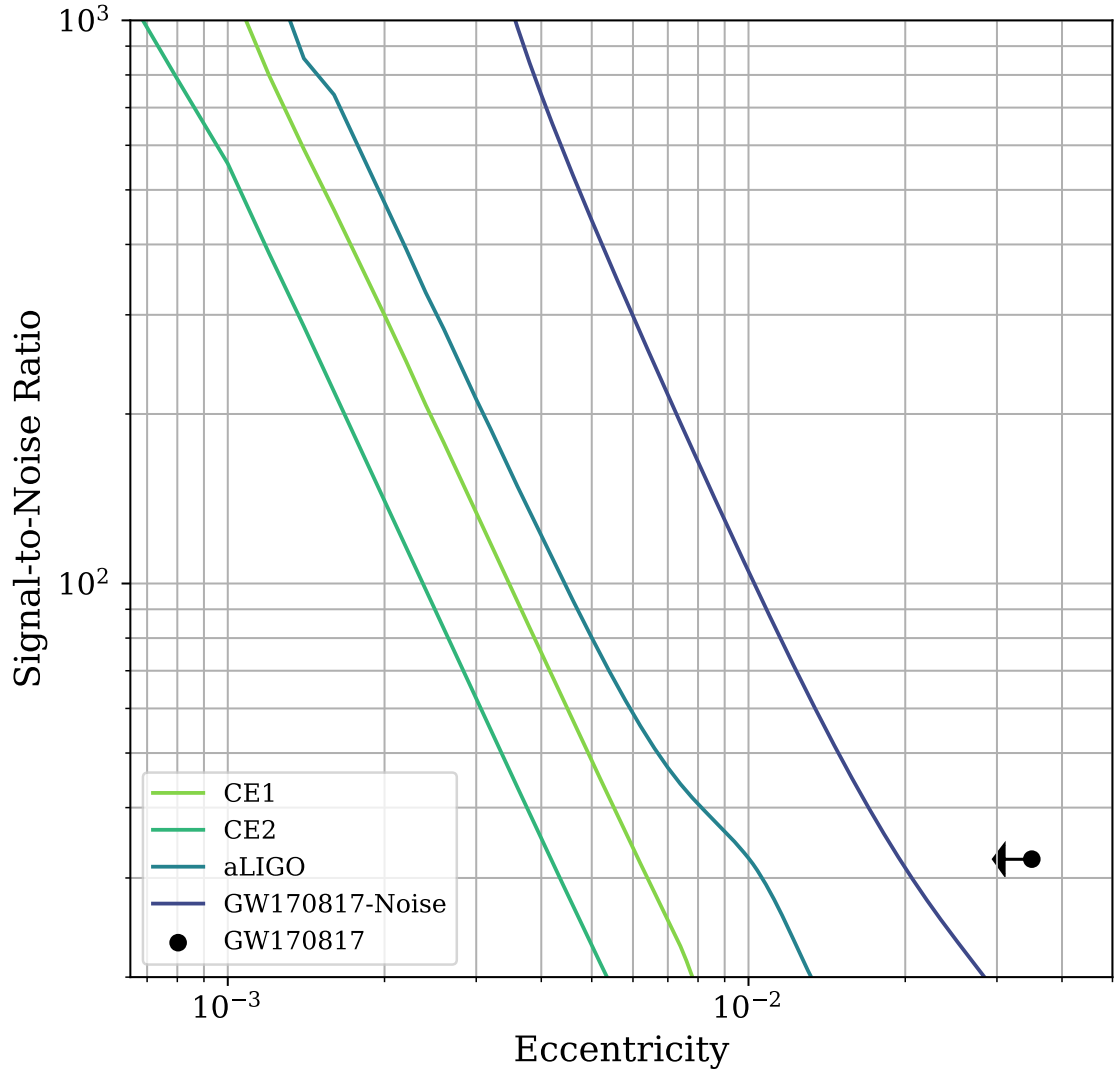

Figure 16: The signal-to-noise ratio as a function of eccentricity. The black dot is at a signal-to-noise ratio of 32.4 [4] and eccentricity of 0.035 at 90% confidence [5]. For each detector, we show the signal-to-noise ratio needed to resolve the signal with eccentricity on the eccentricity axis at 90% confidence. For $e \geq 5 \times 10^{-3}$, a signal-to-noise ratio of 20 would be needed to resolve the signal at 90% confidence in Cosmic Explorer. As the eccentricity decreases, the signal-to-noise ratio needed to resolve the signal increases.

Chapter 6

Conclusions

The multitude of gravitational-wave detections has created a thrilling era of astrophysics. With each detection and electromagnetic counterpart we have begun to answer many questions about the astrophysical compact objects. Currently binary black holes are routinely detected by the Advanced LIGO and Virgo detectors. The first two detections of binary neutron mergers provided so much insight into their physics, even though they were very different. We now understand that neutron star mergers can produce a gamma-ray bursts and provide us with the heavy elements in our universe as well as allowed us to explore the nuclear equation of state. With improvements to the detectors and the addition of third generation detectors the detection of binary neutron star mergers will also become routine. An increased number of detections will aid us in gaining new insights about the physics of compact objects and how binary these binaries form.

In this thesis, we used observations and modeling to study the eccentricity of binary neutron star systems. Specifically, the work in this thesis focuses on how we can extract information about the binary system through searches, parameter estimation, and future prospects in third generation detectors. We have used the Advanced LIGO and Virgo observations to search for eccentric binary systems and to measure their eccentricity, as well as determine the ability of a third generation detector to detect and measure eccentric binary systems.

We presented the form of the change in eccentricity and semi-major axis of an eccentric system as well as demonstrating the lifetime for a binary with a given eccentricity. We summarize the methods and algorithms used in the searches for

gravitational waves and the measurement of the parameters of the signals.

We conducted a search for eccentric binary neutron stars in Advanced LIGO's first and second observing runs and place an upper limit on their merger. While we did not find any other significant candidates, the limit we have placed aids in the understanding of how well we can detect these mergers with current detectors. We also determine how much data would be needed with A+ and with Cosmic Explorer to make a detection of a binary neutron star merger.

We provided estimates of the eccentricity of the two binary neutron star mergers detected in the first and second observing runs. Our analysis measured the eccentricity of GW170817 and GW190425 using a full parameter estimation analysis. We determined that there is a degeneracy between the eccentricity and chirp mass parameters. Previous works done to measure the eccentricity of GW190425 were done [3]. While our analysis was not in agreement with theirs, we determined that prior choice and full parameter estimation are important in accurately measuring parameters. The accurate measurement of the parameters is valuable as the eccentricity may provide valuable information about the binary. In the case of binary neutron stars, eccentric systems may have different electromagnetic emission than that of circular systems.

We determined the ability of a third generation detector, Cosmic Explorer, to detect eccentric binary neutron star mergers and to measure their eccentricity. Using template banks and simulations, we found what eccentricities a bank containing circular templates would be effectual at a gravitational-wave frequency of 7 Hz. We showed that a stochastic placement can be used to construct template banks that are effective. We also determined that the computational cost of a matched-filter search for both the quasi-circular and eccentric template banks is not significantly larger than that of Advanced LIGO. We calculated the approximate signal-to-noise ratio needed to distinguish the eccentricity of the binary.

As Advanced LIGO and Virgo continue to improve in sensitivity there will be more detections of gravitational waves from binary neutron star mergers. As third generation detectors are added to the detector network, the chance of detecting an eccentric gravitational wave from a binary neutron star system increases. With the detection of an eccentric binary neutron star merger we will be able to test the strong-field regime of general relativity, constrain the neutron star equation of state, and ascertain the formation channel of the binary.

Bibliography

[1] M. Punturo et al. The Einstein Telescope: A third-generation gravitational wave observatory. *Class. Quant. Grav.*, 27:194002, 2010.

[2] David Reitze et al. Cosmic Explorer: The U.S. Contribution to Gravitational-Wave Astronomy beyond LIGO. *Bull. Am. Astron. Soc.*, 51(7):035, 2019.

[3] Isobel M. Romero-Shaw, Nicholas Farrow, Simon Stevenson, Eric Thrane, and Xing-Jiang Zhu. On the origin of GW190425. *Mon. Not. Roy. Astron. Soc.*, 496(1):L64–L69, 2020.

[4] B.P. Abbott et al. GW170817: Observation of Gravitational Waves from a Binary Neutron Star Inspiral. *Phys. Rev. Lett.*, 119(16):161101, 2017.

[5] Amber K. Lenon, Alexander H. Nitz, and Duncan A. Brown. Measuring the eccentricity of GW170817 and GW190425. *Mon. Not. Roy. Astron. Soc.*, 497(2):1966–1971, 2020.

[6] R. A. Hulse and J. H. Taylor. Discovery of a pulsar in a binary system. *Astrophys. J. Lett.*, 195:L51–L53, 1975.

[7] Barry C. Barish and Rainer Weiss. Ligo and the detection of gravitational waves. *Physics Today*, 52(10):44–50, 1999.

[8] J. Aasi et al. Advanced LIGO. *Class. Quantum Grav.*, 32:074001, 2015.

[9] F. Acernese et al. Advanced Virgo: a second-generation interferometric gravitational wave detector. *Class. Quantum Grav.*, 32(2):024001, 2015.

[10] B. P. Abbott et al. Observation of Gravitational Waves from a Binary Black Hole Merger. *Phys. Rev. Lett.*, 116(6):061102, 2016.

[11] B. P. Abbott et al. Binary Black Hole Mergers in the first Advanced LIGO Observing Run. *Phys. Rev.*, X6(4):041015, 2016. [erratum: Phys. Rev.X8,no.3,039903(2018)].

[12] Alexander H. Nitz, Collin Capano, Alex B. Nielsen, Steven Reyes, Rebecca White, Duncan A. Brown, and Badri Krishnan. 1-OGC: The first open gravitational-wave catalog of binary mergers from analysis of public Advanced LIGO data. *Astrophys. J.*, 872(2):195, 2019.

[13] B. P. Abbott et al. Multi-messenger Observations of a Binary Neutron Star Merger. *Astrophys. J.*, 848(2):L12, 2017.

[14] B.. P.. Abbott et al. GW170608: Observation of a 19-solar-mass Binary Black Hole Coalescence. *Astrophys. J.*, 851(2):L35, 2017.

[15] B. P. Abbott et al. GW170814: A Three-Detector Observation of Gravitational Waves from a Binary Black Hole Coalescence. *Phys. Rev. Lett.*, 119(14):141101, 2017.

[16] Benjamin P. Abbott et al. GW170104: Observation of a 50-Solar-Mass Binary Black Hole Coalescence at Redshift 0.2. *Phys. Rev. Lett.*, 118(22):221101, 2017. [Erratum: Phys. Rev. Lett.121,no.12,129901(2018)].

[17] B. P. Abbott et al. GWTC-1: A Gravitational-Wave Transient Catalog of Compact Binary Mergers Observed by LIGO and Virgo during the First and Second Observing Runs. *Phys. Rev.*, X9(3):031040, 2019.

[18] R. Abbott et al. GWTC-2: Compact Binary Coalescences Observed by LIGO and Virgo During the First Half of the Third Observing Run. *ArXiv e-print*, 10 2020.

[19] B. P. Abbott et al. GW190425: Observation of a Compact Binary Coalescence with Total Mass $\sim 3.4 M_{\odot}$. *Astrophys. J. Lett.*, 892(1):L3, 2020.

[20] R. Abbott et al. GW190521: A Binary Black Hole Merger with a Total Mass of $150 M_{\odot}$. *Phys. Rev. Lett.*, 125(10):101102, 2020.

[21] R. Abbott et al. GW190412: Observation of a Binary-Black-Hole Coalescence with Asymmetric Masses. *ArXiv e-print*, 4 2020.

[22] R. Abbott et al. GW190814: Gravitational Waves from the Coalescence of a 23 Solar Mass Black Hole with a 2.6 Solar Mass Compact Object. *Astrophys. J. Lett.*, 896(2):L44, 2020.

[23] T. Buehrke. Nobel prize in physics 1993 for Russell A. Hulse and Joseph H. Taylor. (In German). *Phys. Unserer Zeit*, 24:253, 1993.

[24] P. C. Peters and J. Mathews. Gravitational radiation from point masses in a Keplerian orbit. *Phys. Rev.*, 131:435–439, 1963.

[25] P. C. Peters. Gravitational Radiation and the Motion of Two Point Masses. *Phys. Rev.*, 136:B1224–B1232, 1964.

[26] Joel M. Weisberg and Joseph H. Taylor. Relativistic binary pulsar B1913+16: Thirty years of observations and analysis. *ASP Conf. Ser.*, 328:25, 2005.

[27] J.G. Martinez, K. Stovall, P.C.C. Freire, J.S. Deneva, T.M. Tauris, A. Ridolfi, N. Wex, F.A. Jenet, M.A. McLaughlin, and M. Bagchi. Pulsar J1411+2551: A Low-mass Double Neutron Star System. *Astrophys. J. Lett.*, 851(2):L29, 2017.

[28] T.M. Tauris et al. Formation of Double Neutron Star Systems. *Astrophys. J.*, 846(2):170, 2017.

[29] A.D. Cameron et al. The High Time Resolution Universe Pulsar Survey – XIII. PSR J1757−1854, the most accelerated binary pulsar. *Mon. Not. Roy. Astron. Soc.*, 475(1):L57–L61, 2018.

[30] K. Stovall et al. PALFA Discovery of a Highly Relativistic Double Neutron Star Binary. *Astrophys. J. Lett.*, 854(2):L22, 2018.

[31] Ryan S. Lynch et al. The Green Bank North Celestial Cap Pulsar Survey III: 45 New Pulsar Timing Solutions. *Astrophys. J.*, 859(2):93, 2018.

[32] Xingjiang Zhu, Eric Thrane, Stefan Oslowski, Yuri Levin, and Paul D. Lasky. Inferring the population properties of binary neutron stars with gravitational-wave measurements of spin. *Phys. Rev.*, D98:043002, 2018.

[33] Jeff J. Andrews and Ilya Mandel. Double Neutron Star Populations and Formation Channels. *Astrophys. J.*, 880(1):L8, 2019.

[34] B.P. Flannery and E. P. J. van den Heuvel. On the origin of the binary pulsar PSR 1913+16. *Astron. and Astrophys.*, 39:61–67, Feb 1975.

[35] C. De Loore, J. P. De Greve, and J. P. de Cuyper. Evolution of Massive Close Binaries. II: The Post X-Ray Binary Stage: Origin of Run-away and Binary Pulsars. *Astronomy and Astrophysics, Supplement*, 36(1):219–225, Aug 1975.

[36] Benjamin P. Abbott et al. Sensitivity of the Advanced LIGO detectors at the beginning of gravitational wave astronomy. *Phys. Rev.*, D93(11):112004, 2016. [Addendum: Phys. Rev.D97,no.5,059901(2018)].

[37] B. J. Meers. Recycling in Laser Interferometric Gravitational Wave Detectors. *Phys. Rev. D*, 38:2317–2326, 1988.

[38] Lisa Barsotti, Lee McCuller, Matthew Evans, and Peter Fritschel. The A+ design curve. https://dcc.ligo.org/LIGO-T1800042/public.

[39] David Reitze et al. The US Program in Ground-Based Gravitational Wave Science: Contribution from the LIGO Laboratory. *Bull. Am. Astron. Soc.*, 51:141, 3 2019.

[40] B. P. Abbott et al. Prospects for Observing and Localizing Gravitational-Wave Transients with Advanced LIGO and Advanced Virgo. *Living Rev. Relat.*, 19:1, 2016.

[41] L. L. Smarr and R. Blandford. The binary pulsar: physical processes, possible companions, and evolutionary histories. *Astrophysical J.*, 207:574–588, July 1976.

[42] R. Canal, J. Isern, and J. Labay. The origin of neutron stars in binary systems. *Ann. Rev. Astron. Astrophys.*, 28:183–214, 1990.

[43] Simon F. Portegies Zwart and Lev R. Yungelson. Formation and evolution of binary neutron stars. *Astron. Astrophys.*, 332:173–188, 1998.

[44] K. Belczynski et al. Binary neutron star formation and the origin of GW170817. *ArXiv e-print*, 12 2018.

[45] Alejandro Vigna-Gómez et al. On the formation history of Galactic double neutron stars. *Mon. Not. Roy. Astron. Soc.*, 481(3):4009–4029, 2018.

[46] Nicola Giacobbo and Michela Mapelli. The progenitors of compact-object binaries: impact of metallicity, common envelope and natal kicks. *Mon. Not. Roy. Astron. Soc.*, 480(2):2011–2030, 2018.

[47] Michela Mapelli and Nicola Giacobbo. The cosmic merger rate of neutron stars and black holes. *Mon. Not. Roy. Astron. Soc.*, 479(4):4391–4398, 2018.

[48] Vassiliki Kalogera, K. Belczynski, C. Kim, Richard W. O'Shaughnessy, and B. Willems. Formation of Double Compact Objects. *Phys. Rept.*, 442:75–108, 2007.

[49] I. Kowalska, T. Bulik, K. Belczynski, M. Dominik, and D. Gondek-Rosinska. The eccentricity distribution of compact binaries. *Astron. Astrophys.*, 527:A70, 2011.

[50] Martyna Chruslinska, Krzysztof Belczynski, Jakub Klencki, and Matthew Benacquista. Double neutron stars: merger rates revisited. *Mon. Not. Roy. Astron. Soc.*, 474(3):2937–2958, 2018.

[51] D. C. Heggie. Binary evolution in stellar dynamics. *Mon. Not. Roy. Astron. Soc.*, 173:729–787, 1975.

[52] Jonathan Grindlay, Simon Portegies Zwart, and Stephen McMillan. Short gamma-ray bursts from binary neutron star mergers in globular clusters. *Nature Phys.*, 2:116, 2006.

[53] N. Ivanova, C. Heinke, F. A. Rasio, K. Belczynski, and J. Fregeau. Formation and evolution of compact binaries in globular clusters: II. Binaries with neutron stars. *Mon. Not. Roy. Astron. Soc.*, 386:553–576, 2008.

[54] Cristobal Petrovich and Fabio Antonini. Greatly enhanced merger rates of compact-object binaries in non-spherical nuclear star clusters. *Astrophys. J.*, 846(2):146, 2017.

[55] Steinn Sigurdsson and Lars Hernquist. Primordial black holes in globular clusters. *Nature*, 364:423–425, 1993.

[56] Simon F. Portegies Zwart and Stephen McMillan. Black hole mergers in the universe. *Astrophys. J.*, 528:L17, 2000.

[57] Ryan M. O'Leary, Bence Kocsis, and Abraham Loeb. Gravitational waves from scattering of stellar-mass black holes in galactic nuclei. *Mon. Not. Roy. Astron. Soc.*, 395(4):2127–2146, 2009.

[58] Fabio Antonini and Hagai B. Perets. Secular evolution of compact binaries near massive black holes: Gravitational wave sources and other exotica. *Astrophys. J.*, 757:27, 2012.

[59] C. L. Rodriguez, M. Morscher, B. Pattabiraman, S. Chatterjee, C.-J. Haster, and F. A. Rasio. Binary Black Hole Mergers from Globular Clusters: Implications for Advanced LIGO. *Physical Review Letters*, 115(5):051101, July 2015.

[60] C. L. Rodriguez, C.-J. Haster, S. Chatterjee, V. Kalogera, and F. A. Rasio. Dynamical Formation of the GW150914 Binary Black Hole. *ArXiv e-prints*, April 2016.

[61] C. L. Rodriguez, S. Chatterjee, and F. A. Rasio. Binary black hole mergers from globular clusters: Masses, merger rates, and the impact of stellar evolution. *Phys. Rev. D*, 93(8):084029, April 2016.

[62] Carl L. Rodriguez, Pau Amaro-Seoane, Sourav Chatterjee, Kyle Kremer, Frederic A. Rasio, Johan Samsing, Claire S. Ye, and Michael Zevin. Post-Newtonian Dynamics in Dense Star Clusters: Formation, Masses, and Merger Rates of Highly-Eccentric Black Hole Binaries. *Phys. Rev.*, D98(12):123005, 2018.

[63] Hang Yu, Sizheng Ma, Matthew Giesler, and Yanbei Chen. Spin and Eccentricity Evolution in Triple Systems: from the Lidov-Kozai Interaction to the Final Merger of the Inner Binary. *Phys. Rev. D*, 102:123009, 2020.

[64] Ian Hinder, Birjoo Vaishnav, Frank Herrmann, Deirdre Shoemaker, and Pablo Laguna. Universality and final spin in eccentric binary black hole inspirals. *Phys. Rev.*, D77:081502, 2008.

[65] Karl Martel and Eric Poisson. Gravitational waves from eccentric compact binaries: Reduction in signal-to-noise ratio due to nonoptimal signal processing. *Phys. Rev. D*, 60:124008, 1999.

[66] T. Cokelaer and D. Pathak. Searching for gravitational-wave signals emitted by eccentric compact binaries using a non-eccentric template bank: implications for ground-based detectors. *Class. Quantum Grav.*, 26:045013, 2009.

[67] Duncan A. Brown and Peter J. Zimmerman. The Effect of Eccentricity on Searches for Gravitational-Waves from Coalescing Compact Binaries in Ground-based Detectors. *Phys. Rev. D*, 81:024007, 2010.

[68] E. A. Huerta and Duncan A. Brown. Effect of eccentricity on binary neutron star searches in Advanced LIGO. *Phys. Rev.*, D87(12):127501, 2013.

[69] Konstantin Postnov and Lev Yungelson. The Evolution of Compact Binary Star Systems. *Living Rev. Rel.*, 9:6, 2006.

[70] N. Ivanova et al. Common Envelope Evolution: Where we stand and how we can move forward. *Astron. Astrophys. Rev.*, 21:59, 2013.

[71] Natalia Ivanova, C. O. Heinke, F. A. Rasio, R. E. Taam, K. Belczynski, and J. Fregeau. Formation and evolution of compact binaries in globular clusters: I.binaries with white dwarfs. *Mon. Not. Roy. Astron. Soc.*, 372:1043–1059, 2006.

[72] Douglas C. Heggie, Piet Hut, and Steven L. W. McMillan. Exchange cross-sections for hard binaries. *IAU Symp.*, 174:371, 1996.

[73] C. M. Biwer, Collin D. Capano, Soumi De, Miriam Cabero, Duncan A. Brown, Alexander H. Nitz, and V. Raymond. PyCBC Inference: A Python-based parameter estimation toolkit for compact binary coalescence signals. *Publ. Astron. Soc. Pac.*, 131(996):024503, 2019.

[74] K. Thorne C. Misner and J. Wheeler. *Gravitation.* WH Freeman & Co, 1973.

[75] Duncan A. Brown. Searching for gravitational radiation from binary black hole MACHOs in the galactic halo. Other thesis, The University of Wisconsin–Milwaukee, 12 2004.

[76] Thibault Damour, Achamveedu Gopakumar, and Bala R. Iyer. Phasing of gravitational waves from inspiralling eccentric binaries. *Phys. Rev. D*, 70:064028, 2004.

[77] E. A. Huerta, Prayush Kumar, Sean T. McWilliams, Richard O'Shaughnessy, and Nicolás Yunes. Accurate and efficient waveforms for compact binaries on eccentric orbits. *Phys. Rev.*, D90(8):084016, 2014.

[78] Sashwat Tanay, Maria Haney, and Achamveedu Gopakumar. Frequency and time domain inspiral templates for comparable mass compact binaries in eccentric orbits. *Phys. Rev. D*, 93(6):064031, 2016.

[79] Blake Moore, Marc Favata, K. G. Arun, and Chandra Kant Mishra. Gravitational-wave phasing for low-eccentricity inspiralling compact binaries to 3PN order. *Phys. Rev.*, D93(12):124061, 2016.

[80] E.A. Huerta et al. Complete waveform model for compact binaries on eccentric orbits. *Phys. Rev. D*, 95(2):024038, 2017.

[81] Zhoujian Cao and Wen-Biao Han. Waveform model for an eccentric binary black hole based on the effective-one-body-numerical-relativity formalism. *Phys. Rev.*, D96(4):044028, 2017.

[82] Ian Hinder, Lawrence E. Kidder, and Harald P. Pfeiffer. Eccentric binary black hole inspiral-merger-ringdown gravitational waveform model from numerical relativity and post-Newtonian theory. *Phys. Rev.*, D98(4):044015, 2018.

[83] Srishti Tiwari, Gopakumar Achamveedu, Maria Haney, and Phurailatapam Hemantakumar. Ready-to-use Fourier domain templates for compact binaries inspiraling along moderately eccentric orbits. *Phys. Rev. D*, 99(12):124008, 2019.

[84] Blake Moore and Nicolás Yunes. A 3PN Fourier Domain Waveform for Non-Spinning Binaries with Moderate Eccentricity. *Class. Quant. Grav.*, 36(18):185003, 2019.

[85] Nicolas Yunes, K. G. Arun, Emanuele Berti, and Clifford M. Will. Post-Circular Expansion of Eccentric Binary Inspirals: Fourier-Domain Waveforms in the

Stationary Phase Approximation. *Phys. Rev.*, D80(8):084001, 2009. [Erratum: Phys. Rev.D89,no.10,109901(2014)].

[86] Bruce Allen, Warren G. Anderson, Patrick R. Brady, Duncan A. Brown, and Jolien D. E. Creighton. FINDCHIRP: An Algorithm for detection of gravitational waves from inspiraling compact binaries. *Phys. Rev. D*, 85:122006, 2012.

[87] Bruce Allen. A chi**2 time-frequency discriminator for gravitational wave detection. *Phys. Rev. D*, 71:062001, 2005.

[88] Alexander H. Nitz, Thomas Dent, Tito Dal Canton, Stephen Fairhurst, and Duncan A. Brown. Detecting binary compact-object mergers with gravitational waves: Understanding and Improving the sensitivity of the PyCBC search. *Astrophys. J.*, 849(2):118, 2017.

[89] Tito Dal Canton et al. Implementing a search for aligned-spin neutron star-black hole systems with advanced ground based gravitational wave detectors. *Phys. Rev.*, D90(8):082004, 2014.

[90] Samantha A. Usman et al. The PyCBC search for gravitational waves from compact binary coalescence. *Class. Quant. Grav.*, 33(21):215004, 2016.

[91] Benjamin J. Owen. Search templates for gravitational waves from inspiraling binaries: Choice of template spacing. *Phys. Rev.*, D53:6749–6761, 1996.

[92] Benjamin J. Owen and B. S. Sathyaprakash. Matched filtering of gravitational waves from inspiraling compact binaries: Computational cost and template placement. *Phys. Rev. D*, 60:022002, 1999.

[93] Thomas Cokelaer. Gravitational waves from inspiralling compact binaries: Hexagonal template placement and its efficiency in detecting physical signals. *Phys. Rev. D*, 76:102004, 2007.

[94] Duncan A. Brown, Ian Harry, Andrew Lundgren, and Alexander H. Nitz. Detecting binary neutron star systems with spin in advanced gravitational-wave detectors. *Phys. Rev.*, D86:084017, 2012.

[95] Ian W. Harry, Bruce Allen, and B.S. Sathyaprakash. A Stochastic template placement algorithm for gravitational wave data analysis. *Phys. Rev. D*, 80:104014, 2009.

[96] Gian Mario Manca and Michele Vallisneri. Cover art: Issues in the metric-guided and metric-less placement of random and stochastic template banks. *Phys. Rev. D*, 81:024004, 2010.

[97] I.W. Harry, A.H. Nitz, Duncan A. Brown, A. Lundgren, Evan Ochsner, et al. Investigating the effect of precession on searches for neutron-star-black-hole binaries with Advanced LIGO. *Phys. Rev. D*, 89(2):024010, January 2014.

[98] J. Aasi et al. The characterization of Virgo data and its impact on gravitational-wave searches. *Class. Quantum Grav.*, 29:155002, 2012.

[99] J. Aasi et al. Characterization of the LIGO detectors during their sixth science run. *Class. Quant. Grav.*, 32(11):115012, 2015.

[100] L. K. Nuttall et al. Improving the Data Quality of Advanced LIGO Based on Early Engineering Run Results. *Class. Quantum Grav.*, 32(24):245005, 2015.

[101] S. Babak, R. Biswas, P.R. Brady, D.A. Brown, K. Cannon, et al. Searching for gravitational waves from binary coalescence. *Phys. Rev. D*, 87:024033, 2013.

[102] K S Thorne. Gravitational radiation. In S. W. Hawking and W. Israel, editors, *Three hundred years of gravitation*, chapter 9, pages 330–458. Cambridge University Press, Cambridge, 1987.

[103] Eanna E. Flanagan and Tanja Hinderer. Constraining neutron star tidal Love numbers with gravitational wave detectors. *Phys. Rev. D*, 77:021502, 2008.

[104] T. Hinderer, B. D. Lackey, R. N. Lang and J. S. Read. Tidal deformability of neutron stars with realistic equations of state and their gravitational wave signatures in binary inspiral. *Phys. Rev. D*, 81:123016, 2010.

[105] H. Wahlquist. The Doppler Response to Gravitational Waves From a Binary Star Source. *Gen. Rel. Grav.*, 19:1101–1113, 1987.

[106] LSC Algorithm Library Suite. https://git.ligo.org/lscsoft/lalsuite.

[107] L A Wainstein and V D Zubakov. *Extraction of signals from noise*. Prentice-Hall, Englewood Cliffs, NJ, 1962.

[108] Nelson Christensen and Renate Meyer. Using Markov chain Monte Carlo methods for estimating parameters with gravitational radiation data. *Phys.Rev.*, D64:022001, 2001.

[109] Daniel Foreman-Mackey, David W. Hogg, Dustin Lang, and Jonathan Goodman. emcee: The MCMC Hammer. *Publ. Astron. Soc. Pac.*, 125:306–312, 2013.

[110] W. D. Vousden, W. M. Farr, and I. Mandel. Dynamic temperature selection for parallel tempering in Markov chain Monte Carlo simulations. *Mon. Not. Roy. Astr. Soc.*, 455(2):1919–1937, January 2016.

[111] Joshua S. Speagle. dynesty: a dynamic nested sampling package for estimating Bayesian posteriors and evidences. *Mon. Not. Roy. Astron. Soc.*, 493(3):3132–3158, 2020.

[112] Nelson Christensen, Rejean J. Dupuis, Graham Woan, and Renate Meyer. A Metropolis-Hastings algorithm for extracting periodic gravitational wave signals from laser interferometric detector data. *Phys. Rev. D*, 70:022001, 2004.

[113] Neal Madras and Alan D. Sokal. The Pivot algorithm: a highly efficient Monte Carlo method for selfavoiding walk. *J. Statist. Phys.*, 50:109–186, 1988.

[114] Tejaswi Venumadhav, Barak Zackay, Javier Roulet, Liang Dai, and Matias Zaldarriaga. New search pipeline for compact binary mergers: Results for binary black holes in the first observing run of Advanced LIGO. *Phys. Rev.*, D100(2):023011, 2019.

[115] Tejaswi Venumadhav, Barak Zackay, Javier Roulet, Liang Dai, and Matias Zaldarriaga. New binary black hole mergers in the second observing run of Advanced LIGO and Advanced Virgo. *Phys. Rev. D*, 101(8):083030, 2020.

[116] Alexander H. Nitz, Thomas Dent, Gareth S. Davies, Sumit Kumar, Collin D. Capano, Ian Harry, Simone Mozzon, Laura Nuttall, Andrew Lundgren, and Márton Tápai. 2-OGC: Open Gravitational-wave Catalog of binary mergers from analysis of public Advanced LIGO and Virgo data. *Astrophys. J.*, 891:123, 3 2020.

[117] Isobel M. Romero-Shaw, Paul D. Lasky, and Eric Thrane. Searching for Eccentricity: Signatures of Dynamical Formation in the First Gravitational-Wave Transient Catalogue of LIGO and Virgo. *Mon. Not. Roy. Astron. Soc.*, 490(4):5210–5216, 2019.

[118] S. Klimenko et al. Coherent method for detection of gravitational wave bursts. *Class. Quantum Grav.*, 25:114029, 2008.

[119] S. Klimenko et al. Method for detection and reconstruction of gravitational wave transients with networks of advanced detectors. *Phys. Rev. D*, 93(4):042004, 2016.

[120] V. Tiwari et al. Proposed search for the detection of gravitational waves from eccentric binary black holes. *Phys. Rev.*, D93(4):043007, 2016.

[121] B. P. Abbott et al. Search for Eccentric Binary Black Hole Mergers with Advanced LIGO and Advanced Virgo during their First and Second Observing Runs. *Astrophys. J.*, 883(2):149, 2019.

[122] Tito Dal Canton and Ian W. Harry. Designing a template bank to observe compact binary coalescences in Advanced LIGO's second observing run. *Arxiv e-print*, 5 2017.

[123] E. A. Huerta et al. Eccentric, nonspinning, inspiral, Gaussian-process merger approximant for the detection and characterization of eccentric binary black hole mergers. *Phys. Rev.*, D97(2):024031, 2018.

[124] Tanja Hinderer and Stanislav Babak. Foundations of an effective-one-body model for coalescing binaries on eccentric orbits. *Phys. Rev.*, D96(10):104048, 2017.

[125] Brennan Ireland, Ofek Birnholtz, Hiroyuki Nakano, Eric West, and Manuela Campanelli. Eccentric Binary Black Holes with Spin via the Direct Integration of the Post-Newtonian Equations of Motion. *Phys. Rev.*, D100(2):024015, 2019.

[126] Blake Moore, Travis Robson, Nicholas Loutrel, and Nicolas Yunes. Towards a Fourier domain waveform for non-spinning binaries with arbitrary eccentricity. *Class. Quant. Grav.*, 35(23):235006, 2018.

[127] Jason W.T. Hessels, Scott M. Ransom, Ingrid H. Stairs, Paulo Cesar Carvalho Freire, Victoria M. Kaspi, et al. A radio pulsar spinning at 716-hz. *Science*, 311:1901–1904, 2006.

[128] Duncan A. Brown, Andrew Lundgren, and R. O'Shaughnessy. Nonspinning searches for spinning binaries in ground-based detector data: Amplitude and mismatch predictions in the constant precession cone approximation. *Phys. Rev. D*, 86:064020, 2012.

[129] Blake Moore and Nicolás Yunes. Data Analysis Implications of Moderately Eccentric Gravitational Waves. *Class. Quant. Grav.*, 37(22):225015, 2020.

[130] Michele Vallisneri, Jonah Kanner, Roy Williams, Alan Weinstein, and Branson Stephens. The LIGO Open Science Center. *J. Phys. Conf. Ser.*, 610(1):012021, 2015.

[131] Alexander Nitz, Amber Lenon, and Duncan Brown. gwastro/eccentric-bns-search: First Eccentric Binary Neutron Star Merger Catalog, December 2019.

[132] William H. Lee, Enrico Ramirez-Ruiz, and Glenn van de Ven. Short gamma-ray bursts from dynamically-assembled compact binaries in globular clusters: pathways, rates, hydrodynamics and cosmological setting. *Astrophys.J.*, 720:953–975, 2010.

[133] Claire S. Ye, Wen-fai Fong, Kyle Kremer, Carl L. Rodriguez, Sourav Chatterjee, Giacomo Fragione, and Frederic A. Rasio. On the Rate of Neutron Star Binary Mergers from Globular Clusters. *Astrophys. J. Lett.*, 888(1):L10, 2020.

[134] Alexander H. Nitz, Ian W. Harry, Joshua L. Willis, Christopher M. Biwer, Duncan A. Brown, Larne P. Pekowsky, T. Dal Canton, Andrew R. Williamson,

Thomas Dent, Collin D. Capano, Thomas J. Massinger, Amber K. Lenon, Alex B. Nielsen, and Miriam Cabero. gwastro/pycbc: Pycbc release v1.14.0, Jun 2019.

[135] Feryal Özel and Paulo Freire. Masses, Radii, and the Equation of State of Neutron Stars. *Ann. Rev. Astron. Astrophys.*, 54:401–440, 2016.

[136] Alexander Harvey Nitz. Distinguishing short duration noise transients in LIGO data to improve the PyCBC search for gravitational waves from high mass binary black hole mergers. *Class. Quant. Grav.*, 35(3):035016, 2018.

[137] B. P. Abbott et al. Characterization of transient noise in Advanced LIGO relevant to gravitational wave signal GW150914. *Class. Quant. Grav.*, 33(13):134001, 2016.

[138] B P Abbott et al. Effects of data quality vetoes on a search for compact binary coalescences in Advanced LIGO's first observing run. *Class. Quant. Grav.*, 35(6):065010, 2018.

[139] Alexander H. Nitz, Alex B. Nielsen, and Collin D. Capano. Potential Gravitational-wave and Gamma-ray Multi-messenger Candidate from 2015 October 30. *Astrophys. J. Lett.*, 876(1):L4, 2019. [Astrophys. J. Lett.876,L4(2019)].

[140] Patrick R. Brady, Jolien D. E. Creighton, and Alan G. Wiseman. Upper limits on gravitational-wave signals based on loudest events. *Class. Quant. Grav.*, 21:S1775–S1782, 2004.

[141] Andreas Bauswein, Oliver Just, Hans-Thomas Janka, and Nikolaos Stergioulas. Neutron-star radius constraints from GW170817 and future detections. *Astrophys. J. Lett.*, 850(2):L34, 2017.

[142] Eemeli Annala, Tyler Gorda, Aleksi Kurkela, and Aleksi Vuorinen. Gravitational-wave constraints on the neutron-star-matter Equation of State. *Phys. Rev. Lett.*, 120(17):172703, 2018.

[143] F.J. Fattoyev, J. Piekarewicz, and C.J. Horowitz. Neutron Skins and Neutron Stars in the Multimessenger Era. *Phys. Rev. Lett.*, 120(17):172702, 2018.

[144] Soumi De, Daniel Finstad, James M. Lattimer, Duncan A. Brown, Edo Berger, and Christopher M. Biwer. Tidal Deformabilities and Radii of Neutron Stars from the Observation of GW170817. *Phys. Rev. Lett.*, 121(9):091102, 2018. [Erratum: Phys.Rev.Lett. 121, 259902 (2018)].

[145] B.P. Abbott et al. GW170817: Measurements of neutron star radii and equation of state. *Phys. Rev. Lett.*, 121(16):161101, 2018.

[146] Collin D. Capano, Ingo Tews, Stephanie M. Brown, Ben Margalit, Soumi De, Sumit Kumar, Duncan A. Brown, Badri Krishnan, and Sanjay Reddy. Stringent constraints on neutron-star radii from multimessenger observations and nuclear theory. *Nature Astron.*, 4(6):625–632, 2020.

[147] I. Tews, J. Margueron, and S. Reddy. Critical examination of constraints on the equation of state of dense matter obtained from GW170817. *Phys. Rev. C*, 98(4):045804, 2018.

[148] Elias R. Most, Lukas R. Weih, Luciano Rezzolla, and Jürgen Schaffner-Bielich. New constraints on radii and tidal deformabilities of neutron stars from GW170817. *Phys. Rev. Lett.*, 120(26):261103, 2018.

[149] David Radice and Liang Dai. Multimessenger Parameter Estimation of GW170817. *Eur. Phys. J. A*, 55(4):50, 2019.

[150] Michael W. Coughlin, Tim Dietrich, Ben Margalit, and Brian D. Metzger. Multimessenger Bayesian parameter inference of a binary neutron star merger. *Mon. Not. Roy. Astron. Soc.*, 489(1):L91–L96, 2019.

[151] Michael McNeil Forbes, Sukanta Bose, Sanjay Reddy, Dake Zhou, Arunava Mukherjee, and Soumi De. Constraining the neutron-matter equation of state with gravitational waves. *Phys. Rev. D*, 100(8):083010, 2019.

[152] B.P. Abbott et al. Tests of General Relativity with GW170817. *Phys. Rev. Lett.*, 123(1):011102, 2019.

[153] Alexander H. Nitz, Amber Lenon, and Duncan A. Brown. Search for Eccentric Binary Neutron Star Mergers in the first and second observing runs of Advanced LIGO. *Astrophys. J.*, 890:1, 12 2019.

[154] David Radice, Filippo Galeazzi, Jonas Lippuner, Luke F. Roberts, Christian D. Ott, and Luciano Rezzolla. Dynamical Mass Ejection from Binary Neutron Star Mergers. *Mon. Not. Roy. Astron. Soc.*, 460(3):3255–3271, 2016.

[155] Swami Vivekanandji Chaurasia, Tim Dietrich, Nathan K. Johnson-McDaniel, Maximiliano Ujevic, Wolfgang Tichy, and Bernd Brügmann. Gravitational waves and mass ejecta from binary neutron star mergers: Effect of large eccentricities. *Phys. Rev. D*, 98(10):104005, 2018.

[156] Lee Samuel Finn. Aperture synthesis for gravitational-wave data analysis: Deterministic sources. *Phys. Rev. D*, 63:102001, 2001.

[157] Christian Rover, Renate Meyer, and Nelson Christensen. Bayesian inference on compact binary inspiral gravitational radiation signals in interferometric data. *Class. Quantum Grav.*, 23:4895–4906, 2006.

[158] K. Blackburn, A. Weinstein, J. Kanner, and E. Chassande-Mottin. Losc cln data products for gw170817, 2017.

[159] B. P. Abbott et al. Glitch model for gw190425, 2020.

[160] Alex Nitz, Ian Harry, Duncan Brown, Christopher M. Biwer, Josh Willis, Tito Dal Canton, Collin Capano, Larne Pekowsky, Thomas Dent, Andrew R. Williamson, Soumi De, Gareth Davies, Miriam Cabero, Duncan Macleod, Bernd Machenschalk, Steven Reyes, Prayush Kumar, Thomas Massinger, Francesco Pannarale, dfinstad, Márton Tápai, Stephen Fairhurst, Sebastian Khan, Leo Singer, Sumit Kumar, Alex Nielsen, shasvath, idorrington92, Amber Lenon, and Hunter Gabbard. gwastro/pycbc: Pycbc release v1.15.4, January 2020.

[161] Michele Cantiello et al. A Precise Distance to the Host Galaxy of the Binary Neutron Star Merger GW170817 Using Surface Brightness Fluctuations. *Astrophys. J. Lett.*, 854(2):L31, 2018.

[162] J. C. Driggers et al. Improving astrophysical parameter estimation via offline noise subtraction for Advanced LIGO. *Phys. Rev.*, D99(4):042001, 2019.

[163] Alessandra Buonanno, Bala R. Iyer, Evan Ochsner, Yi Pan, and B. S. Sathyaprakash. Comparison of post-Newtonian templates for compact binary inspiral signals in gravitational-wave detectors. *Phys.Rev.*, D80:084043, 2009.

[164] Alejandro Bohé, Sylvain Marsat, and Luc Blanchet. Next-to-next-to-leading order spin–orbit effects in the gravitational wave flux and orbital phasing of compact binaries. *Class. Quant. Grav.*, 30:135009, 2013.

[165] Balazs Mikoczi, Matyas Vasuth, and Laszlo A. Gergely. Self-interaction spin effects in inspiralling compact binaries. *Phys. Rev.*, D71:124043, 2005.

[166] K.G. Arun, Alessandra Buonanno, Guillaume Faye, and Evan Ochsner. Higher-order spin effects in the amplitude and phase of gravitational waveforms emitted by inspiraling compact binaries: Ready-to-use gravitational waveforms. *Phys. Rev. D*, 79:104023, 2009.

[167] Emily Baird, Stephen Fairhurst, Mark Hannam, and Patricia Murphy. Degeneracy between mass and spin in black-hole-binary waveforms. *Phys. Rev.*, D87(2):024035, 2013.

[168] Mohammadtaher Safarzadeh, Will M. Farr, and Enrico Ramirez-Ruiz. A trend in the effective spin distribution of LIGO binary black holes with mass. *Astrophys. J.*, 894(2):129, 2020.

[169] János Takátsy, Bence Bécsy, and Peter Raffai. Eccentricity distributions of eccentric binary black holes in galactic nuclei. *Mon. Not. Roy. Astron. Soc.*, 486(1):570–581, 2019.

[170] D. A. Coulter et al. Swope Supernova Survey 2017a (SSS17a), the Optical Counterpart to a Gravitational Wave Source. *Science*, 2017. [Science358,1556(2017)].

[171] M. Soares-Santos et al. The Electromagnetic Counterpart of the Binary Neutron Star Merger LIGO/Virgo GW170817. I. Discovery of the Optical Counterpart Using the Dark Energy Camera. *Astrophys. J.*, 848(2):L16, 2017.

[172] Hsin-Yu Chen, Daniel E. Holz, John Miller, Matthew Evans, Salvatore Vitale, and Jolien Creighton. Distance measures in gravitational-wave astrophysics and cosmology. *Class. Quant. Grav.*, 38(5):055010, 2021.

[173] Paz Beniamini and Tsvi Piran. Formation of Double Neutron Star systems as implied by observations. *Mon. Not. Roy. Astron. Soc.*, 456(4):4089–4099, 2016.

[174] A. Palmese et al. Evidence for Dynamically Driven Formation of the GW170817 Neutron Star Binary in NGC 4993. *Astrophys. J. Lett.*, 849(2):L34, 2017.

[175] Surabhi Sachdev et al. The GstLAL Search Analysis Methods for Compact Binary Mergers in Advanced LIGO's Second and Advanced Virgo's First Observing Runs. *ArXiv e-print*, 1 2019.

[176] Kipp Cannon et al. GstLAL: A software framework for gravitational wave discovery. *ArXiv e-print*, 10 2020.

[177] Gareth S. Davies, Thomas Dent, Márton Tápai, Ian Harry, Connor McIsaac, and Alexander H. Nitz. Extending the PyCBC search for gravitational waves from compact binary mergers to a global network. *Phys. Rev. D*, 102(2):022004, 2020.

[178] Tito Dal Canton, Alexander H. Nitz, Bhooshan Gadre, Gareth S. Davies, Veronica Villa-Ortega, Thomas Dent, Ian Harry, and Liting Xiao. Realtime search for compact binary mergers in Advanced LIGO and Virgo's third observing run using PyCBC Live. *ArXiv e-print*, 8 2020.

[179] Kevin Kuns, Evan Hall, Joshua Smith, Matthew Evans, Peter Fritschel, Christopher Wipf, and Stefan Ballmer. Cosmic explorer sensitivity curves, 2020.

[180] T. Adams, D. Buskulic, V. Germain, G. M. Guidi, F. Marion, M. Montani, B. Mours, F. Piergiovanni, and G. Wang. Low-latency analysis pipeline for compact binary coalescences in the advanced gravitational wave detector era. *Class. Quant. Grav.*, 33(17):175012, 2016.

[181] Michele Maggiore et al. Science Case for the Einstein Telescope. *JCAP*, 03:050, 2020.

[182] T. A. Apostolatos. Search templates for gravitational waves from precessing, inspiraling binaries. *Phys. Rev. D*, 52:605–620, 1995.

[183] Alexander Harvey Nitz and Yi-Fan Wang. Search for Gravitational Waves from High-Mass-Ratio Compact-Binary Mergers of Stellar Mass and Subsolar Mass Black Holes. *Phys. Rev. Lett.*, 126(2):021103, 2021.

[184] Alexander H. Nitz and Yi-Fan Wang. Search for gravitational waves from the coalescence of sub-solar mass and eccentric compact binaries. *ArXiv e-print*, 2 2021.

[185] Marcus E. Lower, Eric Thrane, Paul D. Lasky, and Rory Smith. Measuring eccentricity in binary black hole inspirals with gravitational waves. *Phys. Rev. D*, 98(8):083028, 2018.

Amber K. **Lenon**

518-307-2748 | amberklenon@gmail.com | lenona | amberklenon | 0000-0001-8429-2458

Education

Syracuse University — *Syracuse, NY*
PhD in Physics — *Jan 2020 - May 2021*

West Virginia University — *Morgantown, WV*
MS in Physics — *Aug 2016 - Dec 2019*

Syracuse University — *Syracuse, NY*
BS in Physics — *Aug 2013 - May 2016*

Awards

PAARE Fellowship, Syracuse University — *2020-2021*

CGR Oral Award, Outstanding Graduate Oral Presentation – National Society of Black Physicists — *2019*

Chancellor's Scholars Fellow, West Virginia University — *2019*

W.E.B Du Bois Fellowship, West Virginia University — *2016-2019*

Publications

Short Author – Refereed and Preprints:

4. **Amber K Lenon**, Duncan A Brown, Alexander H Nitz, *Eccentric Binary Neutron Star Search Prospects for Cosmic Explorer*, arXiv:2103.14088, (2021), Submitted to Phys. Rev. D.
3. Kenneth Herner, James Annis, Alyssa Garcia, Marcelle Soares-Santos, Dillon Brout, Noemi Glaeser, Nora Sherman, Richard Kessler, Robert Morgan, Antonella Palmese, Francisco Paz-Chinchon, **Amber Lenon**, and Tristan Bachmann, *The updated DESGW processing pipeline for the third LIGO/VIRGO observing run*, EDP Sciences, 245, 01008, (2020).
2. **Amber K Lenon**, Alexander H Nitz, Duncan A Brown, *Measuring the eccentricity of GW170817 and GW190425*, Mon. Not. R. Astron Soc., Volume 497, Issue 2, September 2020, Pages 1966–1971.
1. Alexander H Nitz, **Amber K Lenon**, Duncan A Brown, *Search for Eccentric Binary Neutron Star Mergers in the first and second observing runs of Advanced LIGO* , Astrophys. J., Volume 890, Number 1, 2020 February 6

LIGO Scientific Collaboration Publications:

Following are publications that I contributed to as a member of the collaboration:

3. B. P. Abbott et al., *GW151226: Observation of Gravitational Waves from a 22-Solar-Mass Binary Black Hole Coalescence*, Phys. Rev. Lett., 116, 241103 (2016).
2. B. P. Abbott et al., *GW150914: First Results from the Search for Binary Black Hole Coalescence with Advanced LIGO*, Phys. Rev. D 93, 122003 (2016).
1. B. P. Abbott et al., *Observation of Gravitational Waves from a Binary Black Hole Merger*, Phys. Rev. Lett., 116, 061102 (2016).

Presentations

Contributed Talks:

- Measuring the Eccentricity of GW170817 and GW190425, *National Society of Black Physicists*, November 2020, Virtual due to COVID-19
- Measuring the Eccentricity of GW170817 and GW190425, *Society for Advancement of Chicanos/Hispanics and Native Americans in Science*, October 2020, Virtual due to COVID-19
- Searching for Gravitational Waves from Eccentric Binary Neutron Stars, *National Society of Black Physicists*, November 2019
- Improving LIGO Sensitivity to Eccentric Searches, *National Society of Black Physicists*, November 2018

Invited Speaker:

- Astronomy II: Talk with Gravitational Wave Physicists, *Columbus, OH*, April 2020

Professional Development

Research Scientist — *Internship*
Fermi National Accelerator Laboratory — *May 2018 – Aug 2018*

Southern Data Science Conference — *Conference*
Virtual Due to COVID-19 — *Aug 2020*

Southern Data Science Conference — *Conference*
Orlando, FL — *Oct 2018*

Skills

Languages	Python (Numpy, H5py, Pandas, Matplotlib, Scipy), Jupyter Notebook, Bash, git, HTCondor, MySQL
Statistical Modeling	Bayesian Inference, Matched Filtering